

# 1. Theory & Background

This simulation basically replicates Mike Tarbutt's [simulations](#). However, I found the explanation in his papers a little confusing (it's really just that some of the formulas seem to come out of nowhere, probably because the whole derivation isn't really suitable for a paper), and it's written in a way that seems to encourage what is effectively 'element-by-element' summing of terms as opposed to matrix multiplication. To that end, I've written a more detailed summary below of what the code is attempting to accomplish:

## 1.1. The Master Equation

The evolution of a density matrix coupled to an open-system through spontaneous emission can be expressed through the master equation (NOTE: This actually simplifies the situation quite a bit, as we have implicitly assumed that there are no coherences between different system-reservoir terms, see discussion here ([M. Lukin Textbook](#)) on page 57. I'll discuss this in greater detail later on when I discuss the last two terms in Sec. 1.5).

$$\frac{\partial \rho}{\partial t} = \frac{1}{i\hbar} [H_{AL}, \rho] - \left[ \sum_p \frac{\gamma_p}{2} (S_p^\dagger S_p \rho - S_p \rho S_p^\dagger) + h.c. \right] \quad (1)$$

where  $H_{AL}$  is the 'atom-light + B-Field mixing' Hamiltonian and  $S_p$  represent terms coupling excited states to ground states (e.g.  $S_{p=1}$  takes the form  $= |g_1\rangle\langle e_1|$ ,  $S_{p=2} = |g_2\rangle\langle e_2|$ , etc.), which decay at a rate  $\gamma_p$ .

To solve for the time evolution of  $\rho$  we need to determine the diagonal and off-diagonal elements of  $H_{AL}$ . For molecules in a combined electronic and magnetic field, the hamiltonian becomes:

$$H_{AL} = -\vec{D} \cdot \vec{E} - \vec{\mu} \cdot \vec{B} \quad (2)$$

where  $E$  is the electronic field created by the interfering light and  $B$  is typically a magnetic quadrupole field. Let's take these terms one-by-one:

## 1.2. Relevant States

First, we will find it helpful to define the states we are considering in this problem. For simplicity, I will only consider  $v = 0$  vibrational states. We are coupling the  $N = 1$  rotational level of the  $X^2\Sigma$  electronic level to the  $A\Pi_{1/2}^+$  state. We will be considering alkaline-halogen molecules (specifically SrF, but the discussion here should also work for CaF, BaF, etc. as long as the alkaline element has no hyperfine structure). First, we use John Barry's correction to Eq. 6.149 of Brown+Carrington to write the X states (normally in the case (b) basis, which I'll express as  $|N, J\rangle$  (other quantum numbers are same for all in the  $X\Sigma$  manifold ( $S=1/2, I=1/2, \Lambda = 0$ )) in the case (a) basis:

$$|X^2\Sigma\rangle = |\Lambda = 0; N = 1, S, J\rangle = \sum_{\Omega=-1/2}^{1/2} \sum_{\Sigma=-1/2}^{1/2} \begin{pmatrix} S & N & J \\ \Sigma & \Lambda & -\Omega \end{pmatrix} |\Lambda, \Sigma, \Omega\rangle \quad (3)$$

The states we are considering, in the b basis (now with hyperfine considered, so I'll express these as  $|F, \tilde{J}\rangle$  since  $m_F$  does not matter for this stage.  $\tilde{J}$  indicates that  $J$  is only an approximately good number, as was shown in HW 7.5 of Dave DeMille's molecule class, hyperfine interactions mix states with the same  $F$  but different  $J$ , in this case  $|F = 1, J = 3/2\rangle$  and  $|F = 1, J = 1/2\rangle$ ) are:

- $|F = 2, \tilde{J} = 3/2\rangle = |F = 2, J = 3/2\rangle$
- $|F = 1, \tilde{J} = 3/2\rangle = a|F = 1, J = 3/2\rangle + b|F = 1, J = 1/2\rangle$
- $|F = 1, \tilde{J} = 1/2\rangle = -b|F = 1, J = 3/2\rangle + a|F = 1, J = 1/2\rangle$
- $|F = 0, \tilde{J} = 1/2\rangle = |F = 0, J = 1/2\rangle$

where, for SrF,  $a=0.888$  and  $b=0.4598$ . Using Eq. 3, we express these states in the case (a) basis  $|\Sigma, \Omega, F, J\rangle$ :

- $|F = 2, \tilde{J} = 3/2\rangle = \frac{1}{\sqrt{2}} [|1/2, 1/2, 2, 3/2\rangle + |-1/2, -1/2, 2, 3/2\rangle]$
- $|F = 1, \tilde{J} = 1/2\rangle = \frac{1}{\sqrt{2}} [a(|1/2, 1/2, 1, 3/2\rangle + |-1/2, -1/2, 1, 3/2\rangle) + b(-|1/2, 1/2, 1, 1/2\rangle + |-1/2, -1/2, 1, 1/2\rangle)]$
- $|F = 1, \tilde{J} = 1/2\rangle = \frac{1}{\sqrt{2}} [-b(|1/2, 1/2, 1, 3/2\rangle + |-1/2, -1/2, 1, 3/2\rangle) + a(-|1/2, 1/2, 1, 1/2\rangle + |-1/2, -1/2, 1, 1/2\rangle)]$
- $|F = 0, \tilde{J} = 1/2\rangle = \frac{1}{\sqrt{2}} [-|1/2, 1/2, 0, 1/2\rangle + |-1/2, -1/2, 0, 1/2\rangle]$

Finally, the A state that we are electronically coupling the X state to is a  $^2\Pi_{1/2}^+$  state, which is written as:

$$|A^2\Pi_{1/2}^+\rangle = \frac{1}{\sqrt{2}} [|1/2, -1/2, F\rangle + |-1/2, 1/2, F\rangle] \quad (4)$$

where  $F$  can be 1 or 0 and  $J = 1/2$  always, so I've omitted it from the wavefunction labeling.

### 1.3. The atom/molecule-light interaction (Calculating $\langle \vec{D} \cdot \vec{E} \rangle$ )

We will be considering terms like  $\langle \Lambda, F, J, \Omega, M_F | \vec{D} \cdot \vec{E} | \Lambda', F', J', \Omega', M'_F \rangle$  (note:  $\Sigma$  can't change due to E1 transitions so I won't list it here). We start with:

$$\langle \vec{D} \cdot \vec{E} \rangle = \exp[iE_{F,J,\Lambda}t] \exp[-iE_{F',J',\Lambda'}t] \sum_{p=-1}^1 (-1)^p E_p D_{-p} \quad (5)$$

where  $p$  refers to the vector component in real space ( $p = -1 = -\hat{x} + i\hat{y}$ , etc.) and I have included the phases that accrue in the heisenberg picture (I will temporarily drop these in subsequent steps, and re-introduce them again in the discussion following Eq. 21). Since we are dealing with molecules, the 'real' space component of  $D$  is not well

specified: only its components in the molecular frame are. To rotate from the molecular frame to the real space frame, we apply a rotation matrix, and thus find:

$$\langle \vec{D} \cdot \vec{E} \rangle = \sum_{q,p} (-1)^p E_p \langle \Lambda | T_q^1(D) | \Lambda' \rangle \langle F, J, \Omega, M_F | D_{-pq}^1(\omega)^* | F', J', \Omega', M'_F \rangle \quad (6)$$

First, let's consider the latter term. We use Eq 5.184 of Brown and Carrington to write:

$$\langle F, J, \Omega, M_F | D_{-pq}^1(\omega)^* | F', J', \Omega', M'_F \rangle = (-1)^{F-M} \begin{pmatrix} F & 1 & F' \\ -M_F & -p & M'_F \end{pmatrix} \langle F, J, \Omega | D_{-q}^1(\omega)^* | F', J', \Omega' \rangle \quad (7)$$

$D_{-q}^1(\omega)^*$  only acts on the  $J$  part of the coupled angular momentum  $F = J + I$ , thus, we can use Eq 5.174 of Brown and Carrington (note: inserted  $I=1/2$ ):

$$\langle F, J, \Omega | D_{-q}^1(\omega)^* | F', J', \Omega' \rangle = (-1)^{F'+J+1+1/2} \sqrt{(2F+1)(2F'+1)} \left\{ \begin{matrix} J' & F' & 1/2 \\ F & J & 1 \end{matrix} \right\} \langle J, \Omega | D_{-q}^1(\omega)^* | J', \Omega' \rangle \quad (8)$$

we then use the Wigner-Echart theorem to get:

$$\langle J, \Omega | D_{-q}^1(\omega)^* | J', \Omega' \rangle = (-1)^{J-\Omega} \sqrt{(2J+1)(2J'+1)} \begin{pmatrix} J & 1 & J' \\ -\Omega & q & \Omega' \end{pmatrix} \quad (9)$$

Putting it all together, we get:

$$\langle D_{-pq}^1(\omega)^* \rangle = (-1)^{F-M_F+F'+J+3/2+J-\Omega} \sqrt{(2F+1)(2F'+1)(2J+1)(2J'+1)} \begin{pmatrix} F & 1 & F' \\ -M_F & -p & M'_F \end{pmatrix} \left\{ \begin{matrix} J' & F' & 1/2 \\ F & J & 1 \end{matrix} \right\} \begin{pmatrix} J & 1 & J' \\ -\Omega & q & \Omega' \end{pmatrix} \quad (10)$$

Let's return to Eq. 6 Since  $\Sigma$  cannot change, it is clear on inspection of the coupled states that  $\Omega$  must change (X and A states of like  $\Sigma$  have unlike  $\Omega$ ). Thus,  $q = 0$  terms do not contribute. It is apparently true that:  $\langle \Lambda | T_{+1}^1 | \Lambda' \rangle = \langle \Lambda | T_{-1}^1 | \Lambda' \rangle$ . This term is referred to as  $d_{\perp}$ . So, this term goes outside of the summation (this term basically gives you the oscillator strength coupling the two states, similar to the  $\langle L | T^1(er) | L \rangle$  term that shows up in atomic physics calculations). Ultimately, this means that the  $p$  component of  $\langle \vec{D} \cdot \vec{E} \rangle$  can be expressed as

$$\langle \vec{D} \cdot \vec{E} \rangle_p = d_{\perp} E_p (-1)^p \sum_q \langle F, J, \Omega, M_F | D_{-pq}^1(\omega)^* | F', J', \Omega', M'_F \rangle \quad (11)$$

where the diagonal (which are all zero) and off-diagonal elements of  $\langle F, J, \Omega, M_F | D_{-pq}^1(\omega)^* | F', J', \Omega', M'_F \rangle$  can be calculated using Eq. 10. These correspond to 3 16X16 matrices. We will write these in the following way: the first 3 columns correspond to  $|X^2\Sigma_{1/2}, F = 1, \tilde{J} = 1/2, m_F = -1, 0, 1\rangle$ , the next is  $|X^2\Sigma_{1/2}, F = 0\rangle$ , the next 3 correspond to  $|X^2\Sigma_{1/2}, F = 1/2, m_F = -1, 0, 1\rangle$

$1, \tilde{J} = 3/2, m_F = -1, 0, 1\rangle$ , the next 5 to  $|X^2\Sigma_{1/2}, F = 1, \tilde{J} = 2, m_F = -2, -1, 0, 1, 2\rangle$ , the next 3 to  $|A^2\Pi_{1/2}, F = 1, m_F = -1, 0, 1\rangle$  and the last to  $|A^2\Pi_{1/2}, F = 0\rangle$ . Since these matrices are really large, I will use the shorthand  $\langle C \rangle_p = \frac{\langle \vec{D} \cdot \vec{E} \rangle_p}{E_p d_\perp}$

$$C_{-1} = \begin{pmatrix} 0 & 0 & 0 & 0 & 0 & 0 & 0 & 0 & 0 & 0 & 0 & 0 & .342 & 0 & .572 \\ 0 & 0 & 0 & 0 & 0 & 0 & 0 & 0 & 0 & 0 & 0 & 0 & 0 & .342 & 0 \\ 0 & 0 & 0 & 0 & 0 & 0 & 0 & 0 & 0 & 0 & 0 & 0 & 0 & 0 & 0 \\ 0 & 0 & 0 & 0 & 0 & 0 & 0 & 0 & 0 & 0 & 0 & 0 & 0 & -\frac{\sqrt{2}}{3} & 0 \\ 0 & 0 & 0 & 0 & 0 & 0 & 0 & 0 & 0 & 0 & 0 & 0 & .365 & 0 & -.080 \\ 0 & 0 & 0 & 0 & 0 & 0 & 0 & 0 & 0 & 0 & 0 & 0 & 0 & 0 & 0 \\ 0 & 0 & 0 & 0 & 0 & 0 & 0 & 0 & 0 & 0 & 0 & 0 & 0 & .365 & 0 \\ 0 & 0 & 0 & 0 & 0 & 0 & 0 & 0 & 0 & 0 & 0 & 0 & 0 & 0 & 0 \\ 0 & 0 & 0 & 0 & 0 & 0 & 0 & 0 & 0 & 0 & 0 & 0 & 0 & 0 & 0 \\ 0 & 0 & 0 & 0 & 0 & 0 & 0 & 0 & 0 & 0 & 0 & 0 & -\frac{1}{\sqrt{6}} & 0 & 0 \\ 0 & 0 & 0 & 0 & 0 & 0 & 0 & 0 & 0 & 0 & 0 & 0 & -\frac{1}{2\sqrt{3}} & 0 & 0 \\ 0 & 0 & 0 & 0 & 0 & 0 & 0 & 0 & 0 & 0 & 0 & 0 & 0 & 0 & -\frac{1}{6} \\ 0 & 0 & 0 & 0 & 0 & 0 & 0 & 0 & 0 & 0 & 0 & 0 & 0 & 0 & 0 \\ 0 & 0 & 0 & 0 & 0 & 0 & 0 & 0 & 0 & 0 & 0 & 0 & 0 & 0 & 0 \\ 0 & 0 & 0 & 0 & 0 & 0 & 0 & 0 & 0 & 0 & 0 & 0 & 0 & 0 & 0 \\ .342 & 0 & 0 & 0 & .365 & 0 & 0 & 0 & -\frac{1}{2\sqrt{3}} & 0 & 0 & 0 & 0 & 0 & 0 \\ 0 & .342 & 0 & -\frac{\sqrt{2}}{3} & 0 & .365 & 0 & 0 & 0 & -\frac{1}{6} & 0 & 0 & 0 & 0 & 0 \\ .572 & 0 & 0 & 0 & -.080 & 0 & 0 & 0 & 0 & 0 & 0 & 0 & 0 & 0 & 0 \end{pmatrix} \quad (12)$$

$$C_0 = \begin{pmatrix} 0 & 0 & 0 & 0 & 0 & 0 & 0 & 0 & 0 & 0 & 0 & 0 & -.342 & 0 & 0 & 0 \\ 0 & 0 & 0 & 0 & 0 & 0 & 0 & 0 & 0 & 0 & 0 & 0 & 0 & 0 & 0 & .572 \\ 0 & 0 & 0 & 0 & 0 & 0 & 0 & 0 & 0 & 0 & 0 & 0 & 0 & 0 & .342 & 0 \\ 0 & 0 & 0 & 0 & 0 & 0 & 0 & 0 & 0 & 0 & 0 & 0 & 0 & \frac{\sqrt{2}}{3} & 0 & 0 \\ 0 & 0 & 0 & 0 & 0 & 0 & 0 & 0 & 0 & 0 & 0 & 0 & -.365 & 0 & 0 & 0 \\ 0 & 0 & 0 & 0 & 0 & 0 & 0 & 0 & 0 & 0 & 0 & 0 & 0 & 0 & 0 & -.080 \\ 0 & 0 & 0 & 0 & 0 & 0 & 0 & 0 & 0 & 0 & 0 & 0 & 0 & 0 & .365 & 0 \\ 0 & 0 & 0 & 0 & 0 & 0 & 0 & 0 & 0 & 0 & 0 & 0 & 0 & 0 & 0 & 0 \\ 0 & 0 & 0 & 0 & 0 & 0 & 0 & 0 & 0 & 0 & 0 & 0 & 0 & -\frac{1}{2\sqrt{3}} & 0 & 0 \\ 0 & 0 & 0 & 0 & 0 & 0 & 0 & 0 & 0 & 0 & 0 & 0 & 0 & 0 & -\frac{1}{3} & 0 \\ 0 & 0 & 0 & 0 & 0 & 0 & 0 & 0 & 0 & 0 & 0 & 0 & 0 & 0 & -\frac{1}{2\sqrt{3}} & 0 \\ 0 & 0 & 0 & 0 & 0 & 0 & 0 & 0 & 0 & 0 & 0 & 0 & 0 & 0 & 0 & 0 \\ -.342 & 0 & 0 & 0 & -.365 & 0 & 0 & 0 & -\frac{1}{2\sqrt{3}} & 0 & 0 & 0 & 0 & 0 & 0 & 0 \\ 0 & 0 & 0 & \frac{\sqrt{2}}{3} & 0 & 0 & 0 & 0 & -\frac{1}{3} & 0 & 0 & 0 & 0 & 0 & 0 & 0 \\ 0 & 0 & .342 & 0 & 0 & 0 & .365 & 0 & 0 & 0 & -\frac{1}{2\sqrt{3}} & 0 & 0 & 0 & 0 & 0 \\ 0 & .572 & 0 & 0 & 0 & -.080 & 0 & 0 & 0 & 0 & 0 & 0 & 0 & 0 & 0 & 0 \end{pmatrix} \quad (13)$$

The next step is to figure out what  $E_p$  is. Since we will primarily be considering cases where the molecules are in a ‘Magneto-Optical Trap’ configuration, we will have one pair of counterpropagating, cross polarized, beams with opposite polarity relative to the other two pairs of counter-propagating cross-polarized beams. E.g., I will have, say,  $\sigma^+$  coming from  $-x$  and  $-y$ , which means I must have  $\sigma^-$  coming from  $-z$  (here  $z$  is the quadrupole ‘strong’ axis with oppositely signed gradient with respect to the two weak axes). From Eq. 2.4 of [this Cohen-Tannoudji & Dalibard paper](#), we get:

- $E_{xBeams} = -\sqrt{2}i\mathcal{E}_0 [\hat{y} \sin kx + \hat{z} \cos kx] \exp[-i\omega_L t] + c.c$
  - $E_{yBeams} = -\sqrt{2}i\mathcal{E}_0 [\hat{z} \sin ky + \hat{x} \cos ky] \exp[-i\omega_L t] + c.c$
  - $E_{zBeams} = -\sqrt{2}i\mathcal{E}_0 [-\hat{x} \sin kz + \hat{y} \cos kz] \exp[-i\omega_L t] + c.c$

where  $\mathcal{E}_0$  is the magnitude of the electric field component of one of the lasers. We see that the effect of  $z$  having relative reversed polarity is observed in the sign of the  $\sin kz$  component. Putting it all together, we get:

$$E_{total} = -\sqrt{2}\mathcal{E}_0 i [(\cos ky - \sin kz) \hat{x} + (\cos kz + \sin kx) \hat{y} + (\cos kx + \sin ky) \hat{z}] \exp[-i\omega_L t] + c.c. \quad (15)$$

We ultimately want the  $\pm 1, 0$  components of  $E$ . The total field can be expressed in terms of these components as:

$$E_{total} = \frac{E_1}{\sqrt{2}}(-\hat{x} - i\hat{y}) + E_0\hat{z} + \frac{E_{-1}}{\sqrt{2}}[\hat{x} - i\hat{y}] = \frac{E_{-1} - E_1}{\sqrt{2}}\hat{x} + \frac{i(-E_1 - E_{-1})}{\sqrt{2}}\hat{y} + E_0\hat{z} \quad (16)$$

Comparing the two Eqs above, one can show:

- $\tilde{E}_{-1}(a) = \frac{E_{-1}}{\mathcal{E}_0} = [\cos kz + a \sin kz + i(a \sin kz - \cos ky)] \exp[-i\omega_L t] + c.c.$
- $\tilde{E}_0(a) = \frac{E_0}{\mathcal{E}_0} = -\sqrt{2}i [\cos kz + a \sin ky] \exp[-i\omega_L t] + c.c.$
- $\tilde{E}_1(a) = \frac{E_1}{\mathcal{E}_0} = [\cos kz + a \sin kz - i(a \sin kz - \cos ky)] \exp[-i\omega_L t] + c.c.$

where I have added a term  $a = \pm 1$  indicating the polarity of the laser (this is necessary for molecules because one of the hyperfine levels requires the opposite polarization of the others, both for DC (in which case it's  $F = 2$ ) and rf (in which case it's  $F = 1, J = 1/2$ )).

Finally, we also would like to put everything in normalized units. For the Hamiltonian, this will involve dividing by  $\hbar\Gamma$  where  $\Gamma$  is the decay rate from the  $A$  state into the  $X$  state. Thus, we have:

$$\langle \vec{D} \cdot \vec{E} \rangle_{norm} = \frac{\mathcal{E}_0 d_\perp}{\hbar\Gamma} \sum_p \tilde{E}_p C_p \quad (17)$$

The final step will be to express  $\mathcal{E}_0 d_\perp / (\hbar\Gamma)$  in terms of the saturation parameter for this transition, which is defined as  $I_{sat} = \hbar c \Gamma \omega^3 / (4\pi \times 3c^3)$ . From atomic physics theory, we have:

$$\Gamma = \frac{4}{3\hbar} \frac{1}{4\pi\epsilon_0} \frac{\omega^3}{c^3} d_\perp^2 \quad (18)$$

and so:

$$\left( \frac{\mathcal{E}_0 d_\perp}{\hbar\Gamma} \right)^2 = \frac{3\hbar}{4} 4\pi\epsilon_0 \frac{c^3}{\omega^3} \Gamma \frac{\mathcal{E}_0^2}{\hbar^2\Gamma^2} \quad (19)$$

The electric field  $\mathcal{E}_0$  can be expressed in terms of the intensity of one laser  $\mathcal{E}_0^2 = I/(2c\epsilon_0)$  (**NOTE**: This might look different than the ‘standard’ expression of  $I = c\epsilon_0 E^2/2$ . This is because the way that Dalibard+Cohen-Tannoudji defined their field. The ‘standard’ expression results from assuming  $E = E_0 \cos(\omega t) \rightarrow \frac{E_0}{2} [e^{i\omega t} + e^{-i\omega t}]$ . In other words, the field they defined is roughly 1/2 of the ‘standard’ field expression). Doing so yields:

$$\left( \frac{\mathcal{E}_0 d_\perp}{\hbar\Gamma} \right)^2 = \frac{3\hbar}{4} 4\pi\epsilon_0 \frac{c^3}{\omega^3} \Gamma \frac{1}{\hbar^2\Gamma^2} \frac{I}{2c\epsilon_0} = 3 \times 4\pi \frac{1}{c\hbar\Gamma} \frac{c^3}{\omega^3} \frac{I}{8} = \frac{I}{8I_{sat}} \quad (20)$$

Thus, we have, in ‘simulation units’ (energy normalized by  $\hbar\Gamma$ ), the  $-\vec{D} \cdot \vec{E}$  term due to the interaction with *one laser*:

$$-\vec{D} \cdot \vec{E} = \frac{1}{2} \sqrt{\frac{s_0}{2}} \sum_p (-C_p) (\tilde{E}_p(a) \exp[-i\omega_L t] + c.c.) \quad (21)$$

Of course, we will almost always (except for when considering single frequency cooling) need multiple lasers. Let’s take care of this now, **and also bring back the phase evolutions from earlier**. In other words, the  $\langle \vec{d} \cdot \vec{E} \rangle_{mn}$ , term, where  $m$  and  $n$  refer a ground and an excited state, respectively, will accrue a phase of  $\exp[\frac{iE_{gmt}}{\hbar}] \exp[-\frac{iE_{ent}}{\hbar}]$ .

To simplify things, we wrap up this term into the laser frequency term (this can be thought of as ‘our version’ of the rotating wave approximation, except here there are multiple lasers coupling multiple ground states to multiple excited states, so there is no way to move to a frame that eliminates all of the phase evolution).

Here’s a concrete example. Consider the ‘row 1, column 13’ term. This winds up being non-zero for  $C_0$  (see Eq. 13), and corresponds to the laser-induced coupling between  $|X\Sigma, F = 1, \tilde{J} = 1/2, m_F = -1\rangle$  and  $|A\Pi, F = 1, m_F = -1\rangle$ . Further, to keep things simple, let’s express  $\tilde{E}_0 = A \exp[-i\omega_L t] + A^* \exp[i\omega_L t]$ . The time-evolution term will be multiplied by the following ‘phase terms’, in addition to whatever the value of  $C_0(1,13)$  is:  $A(\exp[-i\omega_L t] * \exp[i(\omega_{E_{\Sigma,F=1,J=1/2}} - \omega_{E_{\Pi,F=1}})t]) + A^*(\exp[i\omega_L t] * \exp[i(\omega_{E_{\Sigma,F=1,J=1/2}} - \omega_{E_{\Pi,F=1}})t])$ , where I’ve defined  $\omega_E = E/\hbar$ . The energy difference  $\omega_{E_{\Pi,F=1}} - \omega_{E_{\Sigma,F=1,J=1/2}}$  is of the order  $\omega_L$ . So, the term with the  $A$  coefficient oscillates very rapidly, and we assume it averages to zero over relevant timescales, of order  $\Gamma$  (basically assumes  $2\omega_L \gg \Gamma$ , which is a very good approximation). The total relevant phase oscillation term is then given by  $A^* \exp[i(\omega_L - \omega_{\Pi,F=1,\Sigma,F=1,J=1/2})t]$  where  $\omega_{\Pi,F=1,\Sigma,F=1,J=1/2} = \omega_{E_{\Pi,F=1}} - \omega_{E_{\Sigma,F=1,J=1/2}}$ .

A similar analysis of the ‘row 13 column 1’ term would yield a term  $A \exp[-i(\omega_L - \omega_{e,F=1,g,F=1,J=1/2})t]$ . It is clear then that the phase multiplication part for the interaction of this laser with our atomic system is given by:

$$\begin{aligned} L_{mn,p} &= A_p^*(\exp[i(\omega_L - \omega_{en,gm})t]) = A_p^*(\exp[i((\omega_L - (\omega_{en} - \omega_{F=1\downarrow})) + (\omega_{gm} - \omega_{F=1\downarrow}))t]) \{m = X\Sigma, n = A\Pi\} \\ L_{mn,p} &= L_{nm}^* \{m = A\Pi, n = X\Sigma\} \\ L_{mn,p} &= 0 \{m = n = \text{ground}, m = n = \text{excited}\} \end{aligned} \quad (22)$$

where  $A_p$  is given by the coefficient in the definition of  $\tilde{E}_p$  (below Eq. 16) and, in the second equality for the  $\{m = X\Sigma, n = A\Pi\}$  case, I’ve added the  $\omega_{F=1\downarrow}$  ( $\downarrow$  indicating that this is the lower  $F = 1$  term associated with  $J = 1/2$  primarily) terms because, in the matlab code, I index all ground state energies relative to that state (e.g, if  $m$  corresponds to a  $F = 1 \downarrow$  term, its ‘energy’ is 0, if it corresponds to  $1 \uparrow$ , its energy is  $19.6\Gamma$ , etc.) and all laser energies relative to the energy difference between the  $A\Pi$  level and the  $X_{F=1\downarrow}$  level (e.g., the ‘laser energy’ for a laser resonant with  $F = 1 \downarrow$  to  $A\Pi$  is zero, for  $F = 1 \uparrow$  to  $A\Pi$  it is  $-19.6\Gamma$ , etc.). See the quantities ‘groundEnergies’ and ‘laserEnergies’ in my matlab code.

**Finally, we can write the full, simplified expression for  $-\langle \vec{D} \cdot \vec{E} \rangle$ , in ‘normalized’ units, as:**

$$\tilde{H}_{-\vec{D} \cdot \vec{E}} = -\langle \vec{D} \cdot \vec{E} \rangle = \sum_{kp} \frac{1}{2} \sqrt{\frac{s_{0,k}}{2}} \tilde{L}_{k,p} * \tilde{E}_p(a_k) * (-C_p) \quad (23)$$

where, as in matlab, the  $.*$  term indicates *element-wise* multiplication of matrices,  $C_p$  is what I calculated in Eqs 12-14 (I call it the ‘coupling’ matrix hence ‘C’),  $k$  refers

to the  $k$ th frequency component (call this  $\omega_{L,k}$ ),  $a_k$  refers to the polarization of that component,  $\tilde{L}_p = L_p/A^*$  and, in order to keep consistent with the definition of  $L_{mn}$ ,  $E_p(a_k)$  is now a matrix where  $E_{p,mn}(a_k)$  is given by the coefficient that corresponds to  $\exp(i\omega_{L,k}t)$  in the series below Eq. 16 for  $m < n$ , and, for  $m > n$ , it is given by the conjugate component (that corresponds to  $\exp(-i\omega_{L,k}t)$ ).

The change in  $\rho$  due to this term is easily calculated in matlab:

$$\frac{d\rho}{dt}_{-\vec{D}\cdot\vec{E}} = i(\rho(\tilde{H}_{-\vec{D}\cdot\vec{E}}) - (\tilde{H}_{-\vec{D}\cdot\vec{E}})\rho) \quad (24)$$

#### 1.4. The atom/molecule-Bfield interaction (Calculating $\langle \vec{\mu} \cdot \vec{B} \rangle$ )

Here I'll assume we are using the same relative states (good for a MOT, probably not so good for a high B-Field Type-II Zeeman slower).

This will go down similarly to how we calculated  $\langle \vec{D} \cdot \vec{E} \rangle$ . In this case, we will only be coupling states within the same  $F$  manifold ( $F$  cannot change due to this interaction, and neither can the electronic state). I will also be using the effective  $g_{g/e,F,J}$  factors (such that  $H_{-\vec{\mu}\cdot\vec{B}} = g_{g/e,F,J}\vec{B}\cdot\vec{F}$ , where the first subscript is  $g$  for the X state and  $e$  for the A state). From John Barry's thesis, the values for these factors in the  $X$  state are:

- $g_{g,2,3/2}=0.5$
- $g_{g,1,3/2} = 0.97$
- $g_{g,1,1/2} = -0.47$

(note: from here on I'm dropping the tildes on the J. Just assume that I am always referring to the properly mixed states for  $F = 1, J$  states). For the excited state, we have  $g_{e,1,1/2} = -0.083$ .

We write the dot product in the normal way:

$$g_{F,J}\langle \vec{B} \cdot \vec{F} \rangle = g_{F,J}\mu_B \sum_{p=-1}^1 (-1)^p B_p T_{-p}^1(F) \quad (25)$$

Here I'll note that there are no additional phase terms here since the magnetic fields only couple states within the same  $F, J$  manifold within a given electronic state, and thus the phase terms will cancel ( $E_{\Lambda,F,J} - E_{\Lambda,F,J} = 0$ ). Using the Wigner-Eckart theorem, we get:

$$g_{F,J}\langle \vec{B} \cdot \vec{F} \rangle = g_{F,J}\mu_B \sum_{p=-1}^1 (-1)^p B_p (-1)^{F-m_F} \begin{pmatrix} F & 1 & F \\ -m_F & -p & m'_F \end{pmatrix} \sqrt{F(F+1)(2F+1)} \quad (26)$$

Similarly to the electric field case, I find it useful to define a term  $\langle C_{p,B} \rangle = g_{F,J} \langle \vec{B} \cdot \vec{F} \rangle_p / (B_p \mu_B)$  (can call this the ‘Bfield coupling matrix’ or ‘zeeman coupling matrix’). For molecules with an ‘SrF like’ structure, these are:

And so we are left with:

$$H_{-\vec{\mu} \cdot \vec{B}} = \mu_B \sum_{p=-1}^1 B_p C_{p,B} \quad (30)$$

All that's left is to determine what  $B_p$  are and what the 'normalized' version of  $H$  looks like (e.g. what happens when we divide by  $\hbar\Gamma$ ?). First, let's consider the field due to a pair of anti-Helmholtz coils:

$$B_{quad} = \frac{b(t)}{k} (kx\hat{x} + ky\hat{y} - 2kz\hat{z}) = \frac{b(t)}{k} (\tilde{x}\hat{x} + \tilde{y}\hat{y} - 2\tilde{z}\hat{z}) \quad (31)$$

where  $b(t)$  is the field gradient and can, in principle, be time dependent (for example if you are simulating an rfMOT), and I've explicitly put in the  $k$  that are needed to go to normalized units (with tildes). One can show then that the  $B_p$  are:

- $\tilde{B}_{-1} = B_{-1}/(b/k) = \frac{1}{\sqrt{2}} (\tilde{x} + i\tilde{y})$
- $\tilde{B}_0 = B_0/(b/k) = -2\tilde{z}$
- $\tilde{B}_1 = B_1/(b/k) = \frac{1}{\sqrt{2}} (-\tilde{x} + i\tilde{y})$

So, finally, in normalized units, we have:

$$\tilde{H}_{-\vec{\mu} \cdot \vec{B}} = \frac{\mu_B}{\hbar\Gamma} \frac{b}{k} \sum_{p=-1}^1 \tilde{B}_p C_{p,B} \quad (32)$$

and the change in  $\rho$  due to this term is easily calculated in matlab:

$$\frac{d\rho}{dt}_{-\vec{\mu} \cdot \vec{B}} = i(\rho(\tilde{H}_{-\vec{\mu} \cdot \vec{B}}) - (\tilde{H}_{-\vec{\mu} \cdot \vec{B}})\rho) \quad (33)$$

For the SrF  $X \rightarrow A$  transition, we have  $\mu_B/\hbar\Gamma = 0.2114 \text{ Gauss}^{-1}$  and  $b/k \sim 10^{-5} \times b(\text{Gauss/cm})$ .

## 1.5. Calculating $\sum_p -\frac{\gamma}{2} (S_p^\dagger S_p \rho - S_p \rho S_p^\dagger + h.c.)$

It actually turns out that the term above is not quite right for our system. This is because it assumes that there are no coherences between different system-reservoir terms, or, if there are, they are rotating fast enough to not matter. This isn't the case here since our hyperfine levels are so close together. In this case, you can have coherent phase differences between, say, terms relating to the decay of  $|A\Pi, F=1\rangle$  to  $|X\Sigma, F=2\rangle$  and terms relating to the decay of  $|A\Pi, F=1\rangle$   $|X\Sigma, F=0\rangle$  (the phase that accrues between these terms will look something like  $\pm i(\omega_{\Pi,F=1,\Sigma,F=2} - \omega_{\Pi,F=1,\Sigma,F=0})t$ ).

In this case, then, the system-reservoir coupling takes the following form:

$$-\frac{1}{2} \sum_{g',e',g'',e''} \left( R_{g',e'}^\dagger R_{g'',e''} \rho - R_{g',e'} \rho R_{g'',e''}^\dagger + h.c. \right) \quad (34)$$

where  $R_{p'} = \sqrt{\Gamma} \sum_{q=-1}^1 (\sum_{g',e'} |g'\rangle\langle e'|) \langle e' | C_q | g' \rangle$ , and  $|g'\rangle$  must be a ground (e.g.  $\Sigma$ ) state while  $|e'\rangle$  must be an excited ( $\Pi$ ) state. To make sense of this, recall that this is the coupling that comes from ‘trading photons with’ the vacuum. These ‘trades’ can only convert you from an excited state to a ground state ( $R$ , for when you ‘give’ a photon) or from a ground to excited state ( $R^\dagger$ , for when you ‘take’ a photon). The likelihood of the trade will be proportional to the dipole-dipole matrix element, hence the  $\sqrt{\Gamma}C$  prefactor.

### 1.5.1. The $M = -\frac{1}{2} \sum_{g',e',g'',e''} R_{g',e'}^\dagger R_{g'',e''} \rho$ term

We want to know the  $m, n$ th element of this matrix. We start with:

$$M_{mn} = -\frac{\Gamma}{2} \left( \sum_{g',e',g'',e'',q} \langle m | \langle g' | C_q | e' \rangle | e' \rangle \langle g' | g'' \rangle \langle e'' | \langle e'' | C_q | g'' \rangle \rho | n \rangle \right) \quad (35)$$

Here, we see that  $m = e'$  (and thus that  $m$  must correspond to an *excited* state) and  $g' = g''$ , and so we get:

$$M_{mn} = -\frac{\Gamma}{2} \left( \sum_{g',e'',q} \langle g' | C_q | m \rangle \langle e'' | C_q | g' \rangle \langle e'' | \rho | n \rangle \right) \quad (36)$$

we know that  $m$  and  $e''$  must be excited states and, further, that both  $C_q$  terms can only be non-zero simultaneously if  $|m\rangle = |e''\rangle$  (the same  $q$  cannot connect the ground state  $|g'\rangle$  to two different excited states simultaneously). Thus, we can further simplify:

$$M_{mn} = -\frac{\Gamma}{2} \left( \sum_{g',q} |\langle g' | C_q | m \rangle|^2 \langle m | \rho | n \rangle \right) \quad (37)$$

We can go even further. We know that, for a given excited state  $m$  that, the sum of all branching ratios into all ground states  $|g'\rangle$  summed also over all polarizations  $q$  must equal 1. We know that  $|\langle g' | C_q | m \rangle|^2$  is itself the branching ratio from state  $m$  into state  $g'$  and thus this summation over  $g'$  and  $q$  must yield one. Thus, finally, we get

$$\tilde{M}_{mn} = -\frac{1}{2} \rho_{mn} \quad (38)$$

where  $m$  must be an excited state while  $n$  can be either an excited state or a ground state and here I’ve added the  $\sim$  to indicate I’ve gone to normalized units (recall,  $M$  corresponded to a time derivative term of form  $d\rho/dt$  and so I’ve just divided by  $\Gamma$  to normalize it)

We still need to add the hermitian conjugate to this term. Ultimately, it’s clear that the density matrix time derivative contributions due to this term are:

$$\begin{aligned}
\frac{d\rho_{mn}}{dt}_{\tilde{M}+h.c.} &= -\rho_{mn} (\text{m, n both correspond to excited states}) \\
&= -\frac{1}{2}\rho_{mn} (\text{either m is ground and m is excited or vice versa}) \\
&= 0 (\text{m,n both ground})
\end{aligned} \tag{39}$$

### 1.5.2. The $N = \frac{1}{2} \sum_{g',e',g'',e''} R_{g',e'} \rho R_{g'',e''}^\dagger$ term

Let's proceed in the same way. We have:

$$N_{mn} = \frac{\Gamma}{2} \left( \sum_{g',e',g'',e'',q} \langle e' | C_q | g' \rangle \langle g'' | C_q | e'' \rangle \langle m | g' \rangle \langle e' | \rho | e'' \rangle \langle g'' | n \rangle \right) \tag{40}$$

So,  $g'' = n$  and  $g' = m$ . Thus, both  $m$  and  $n$  must be *ground states* for this term to be non-zero. Simplifying, we get:

$$N_{mn} = \frac{\Gamma}{2} \left( \sum_{e',e'',q} \langle e' | C_q | m \rangle \langle n | C_q | e'' \rangle \langle e' | \rho | e'' \rangle \right) \tag{41}$$

Here, since we have two different  $C_q$  terms to consider, we must also add in the phases (these phases have always been present, as per the discussion in the  $\vec{D} \cdot \vec{E}$  calculation, but they just happened to cancel for the previous term since we wound up with  $|\langle m | C_q | n \rangle|^2$ ). Thus, we actually have:

$$\tilde{N}_{mn} = \frac{1}{2} \left( \sum_{e',e'',q} \exp[i(\omega_{e',m} - \omega_{e'',n})t] \langle e' | C_q | m \rangle \langle n | C_q | e'' \rangle \langle e' | \rho | e'' \rangle \right) \tag{42}$$

where  $\omega_{e,m} = \omega_e - \omega_m$  and now the  $C_q$  refer to just the ‘phaseless, real’ terms in Eqs 12-14. To get the full effect of the term, we must also add the hermitian conjugate of  $N$ , which takes the form:

$$\tilde{N}_{mn}^\dagger = \frac{1}{2} \left( \sum_{e',e'',q} \exp[-i(\omega_{e',m} - \omega_{e'',n})t] \langle m | C_q | e' \rangle \langle e'' | C_q | n \rangle \langle e'' | \rho | e' \rangle \right) \tag{43}$$

where I have used the fact that  $C$  and  $\rho$  are both hermitian. On inspection, it is obvious that this is the same term as the equation above but with  $e'$  and  $e''$  flipped. Since we are summing over both of these variables, we may as well ‘switch’ them back, in which case the we find  $N_{mn} = N_{mn}^\dagger$  and thus the total effect on  $d\rho/dt$  from this term is:

$$\begin{aligned} \frac{d\rho_{mn}}{dt}_{\tilde{N}+h.c.} &= \sum_{e',e'',q} \exp[i(\omega_{e',m} - \omega_{e'',n})t] \langle e' | C_q | m \rangle \langle n | C_q | e'' \rangle \langle e' | \rho | e'' \rangle \\ &\quad (\text{m, n both correspond to ground states}) \\ &= 0(\text{otherwise}) \end{aligned} \tag{44}$$

On initial glance, this seems like a problem, as it involves a term-by-term sum, which is very time consuming in matlab. We want to convert this to a matrix multiplication like all the other terms. On inspection, it's clear that this basically has the form of a matrix multiplication:

$$\frac{d\rho_{mn}}{dt}_{\tilde{N}+h.c.} = \sum_q C_{eff,q} \rho_{eff} C_{eff,q}^\dagger \tag{45}$$

where:

- $\rho_{eff,mn} = \rho_{mn}$  if  $m, n$  both correspond to excited states (e.g., bottom right corner) and 0 if not.
- $C_{eff,q,mn} = C_{q,mn} \exp[i\omega_{nm}t]$  if  $n$  is an excited state and  $m$  is an ground state, 0 if not.

### 1.5.3. Summary of additional terms resulting from coupling to the vacuum field

In addition to the two contributions to  $d\rho/dt$  from  $i[\rho, -\vec{D} \cdot \vec{E}]$  (Eq. 23&24) and  $i[\rho, -\vec{\mu} \cdot \vec{B}]$  (Eq. 32&33), which were calculated in sections 1.2 and 1.3, there are two more terms that arise due to coupling to the vacuum electro-magnetic field. These terms sum to give the following additional contributions:

$$\begin{aligned} \frac{d\rho_{mn}}{dt}_{vacCoup} &= -\rho_{mn} (\text{m, n both correspond to excited states}) \\ &= -\frac{1}{2}\rho_{mn} (\text{either m is ground and m is excited or vice versa}) \\ &= \sum_q C_{eff,q} \rho_{eff} C_{eff,q}^\dagger (\text{m, n both correspond to ground states}) \end{aligned} \tag{46}$$

## 1.6. Calculating forces

The central application of this simulation is to determine the force felt by a molecule/atom given its position, velocity, etc. in a given magnetic field + laser field configuration. So far, I have written about how we can determine the evolution of  $\rho(t)$ . Once  $\rho(t)$  is calculated over all times of interest (typically one period of the hamiltonian after steady-state is achieved. I round frequencies to either  $0.1\Gamma$  or  $0.01\Gamma$  depending on what I am simulating, so this is either  $20\pi$  or  $200\pi$  in normalized time units), we will then want to

determine what the average force felt by the particle was.

Given a density matrix  $\rho$ , the force can be calculated using the heisenberg picture time derivative:

$$\frac{d\tilde{p}}{dt} = i[\tilde{H}, -i\nabla] = [\tilde{H}, \nabla] \quad (47)$$

Let's consider what this operator does to a wavefunction  $|\psi\rangle$ . The definition of the base-kets is not spatially dependent (e.g. whether the particle is at  $r_1$  or  $r_2$  the definition of  $|F, m_F\rangle$  means the same thing), and so the  $H\nabla$  term goes to zero (this is sometimes a point of confusion for me. This derivative is with respect to the coordinate of the molecule/atom center, NOT the electron position itself, for which the  $\nabla$  term is obviously not zero, and so it is the base-ket dependence on  $r$  (or lack there-of) that determines the derivative, and not the actual electron cloud). The  $\nabla H$  term, however, is not zero. We have:

$$\frac{dp_i}{dt} = -\frac{\partial}{\partial \tilde{r}_i} H = \frac{1}{2} \sqrt{\frac{s_0}{2}} \sum_{p,k} \frac{\partial \tilde{E}_p(a_k)}{\partial \tilde{r}_i} * L_{k,p} * C_p \quad (48)$$

This is fairly straightforward to calculate in matlab. To get the average force over the density matrix, you simply take:

$$\left[ \frac{\partial p_i}{dt} \right]_{ensemble} = Tr \left[ \rho \frac{\partial p_i}{\partial t} \right] \quad (49)$$

## 2. Simple code example

Throughout this writeup I will refer to a ‘simple’ example of how this works in practice. For this, I choose to use a model  $J' = 1 \rightarrow J = 1$  system, where  $I = 0$  and thus there’s no hyperfine terms (I choose this because I find it useful to benchmark my results against Mike’s here <https://arxiv.org/pdf/1608.04645.pdf>). This is visualized in Fig. 1 below. The full system is simulated in ‘runObeSolverParallel.m’

### 2.1. Simple concrete example of what the $\langle -\vec{D} \cdot \vec{E} \rangle$ term looks like in code

Since this is a ‘simple’ atomic system, the term is a bit simpler:

$$\langle \vec{D} \cdot \vec{E} \rangle = \sum_{p=-1}^1 (-1)^p E_p D_{-p} = \sum_{p=-1}^1 E_p (-1)^p \langle J, m_J | T_{-p}^1(er) | J', m'_J \rangle \quad (50)$$

The second term, corresponding roughly to the  $C_p$  term in Eq. 23 (it’s not exact since I haven’t divided out the  $d_\perp$ -like term yet), is, as usual, calculated using the Wigner-Eckhart theorem:

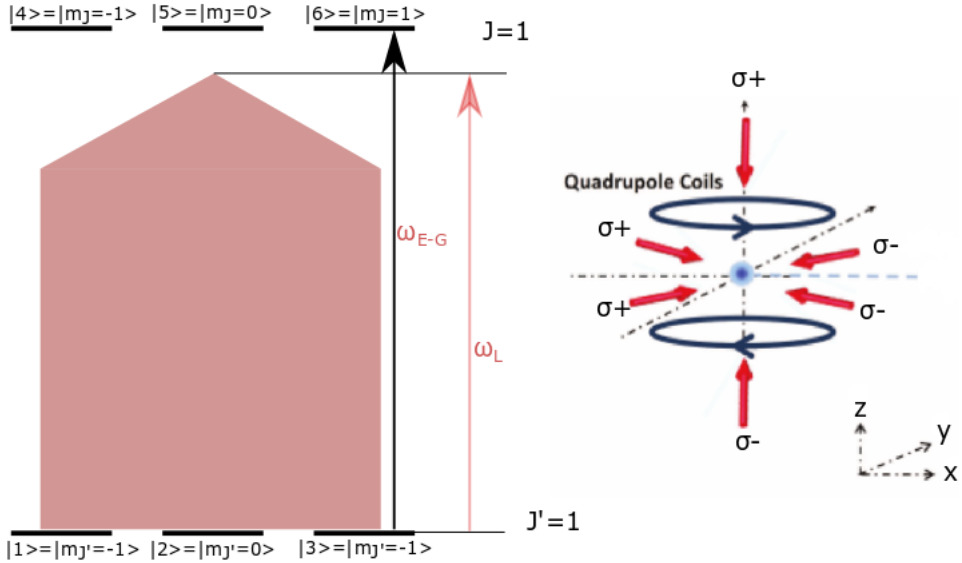


Figure 1: Sketch of model system

$$\langle J, m_J | T_{-p}^1(er) | J', m'_J \rangle = (-1)^{J-m_J+p} \begin{pmatrix} J & 1 & J' \\ -m_J & -p & m'_J \end{pmatrix} \langle J | T^1(er) | J \rangle \quad (51)$$

where the last term is equivalent to  $d_{\perp}$  from before and can be combined with the term for the field in terms of intensity  $I$  and normalization factors to get  $\sqrt{s_0}/2/2$ . We find that (NOTE: for some reason I need to multiply by  $\sqrt{2J+1} = \sqrt{3}$  to make this work out correctly (where transition rates sum to 1 from a given excited state)...I think this is due to going from a ‘clebsch-gordan’ to a 3-j symbol, but that begs the question of why I didn’t need to add a similar factor in the molecule picture. I’m just going to move on from now though with this problem left unsolved.):

$$C_{-1} = \begin{pmatrix} 0 & 0 & 0 & 0 & \frac{1}{\sqrt{2}} & 0 \\ 0 & 0 & 0 & 0 & 0 & \frac{1}{\sqrt{2}} \\ 0 & 0 & 0 & 0 & 0 & 0 \\ 0 & 0 & 0 & 0 & 0 & 0 \\ \frac{1}{\sqrt{2}} & 0 & 0 & 0 & 0 & 0 \\ 0 & \frac{1}{\sqrt{2}} & 0 & 0 & 0 & 0 \end{pmatrix} \quad (52)$$

$$C_0 = \begin{pmatrix} 0 & 0 & 0 & -\frac{1}{\sqrt{2}} & 0 & 0 \\ 0 & 0 & 0 & 0 & 0 & 0 \\ 0 & 0 & 0 & 0 & 0 & \frac{1}{\sqrt{2}} \\ -\frac{1}{\sqrt{2}} & 0 & 0 & 0 & 0 & 0 \\ 0 & 0 & 0 & 0 & 0 & 0 \\ 0 & 0 & \frac{1}{\sqrt{2}} & 0 & 0 & 0 \end{pmatrix} \quad (53)$$

$$C_1 = \begin{pmatrix} 0 & 0 & 0 & 0 & 0 & 0 \\ 0 & 0 & 0 & -\frac{1}{\sqrt{2}} & 0 & 0 \\ 0 & 0 & 0 & 0 & -\frac{1}{\sqrt{2}} & 0 \\ 0 & -\frac{1}{\sqrt{2}} & 0 & 0 & 0 & 0 \\ 0 & 0 & -\frac{1}{\sqrt{2}} & 0 & 0 & 0 \\ 0 & 0 & 0 & 0 & 0 & 0 \end{pmatrix} \quad (54)$$

The other relevant matrices in Eq. 23 become:

$$L_k = \begin{pmatrix} 0 & e^{i\omega_L t} \\ e^{-i\omega_L t} & 0 & e^{i\omega_L t} & e^{i\omega_L t} & e^{i\omega_L t} & e^{i\omega_L t} \\ e^{-i\omega_L t} & e^{-i\omega_L t} & 0 & e^{i\omega_L t} & e^{i\omega_L t} & e^{i\omega_L t} \\ e^{-i\omega_L t} & e^{-i\omega_L t} & e^{-i\omega_L t} & 0 & e^{i\omega_L t} & e^{i\omega_L t} \\ e^{-i\omega_L t} & e^{-i\omega_L t} & e^{-i\omega_L t} & e^{-i\omega_L t} & 0 & e^{i\omega_L t} \\ e^{-i\omega_L t} & 0 \end{pmatrix} \quad (55)$$

$$\tilde{E}_p = \begin{pmatrix} 0 & A_p^* & A_p^* & A_p^* & A_p^* & A_p^* \\ A_p & 0 & A_p^* & A_p^* & A_p^* & A_p^* \\ A_p & A_p & 0 & A_p^* & A_p^* & A_p^* \\ A_p & A_p & A_p & 0 & A_p^* & A_p^* \\ A_p & A_p & A_p & A_p & 0 & A_p^* \\ A_p & A_p & A_p & A_p & A_p & 0 \end{pmatrix} \quad (56)$$

where  $A_p$  is taken from the coefficients in the expressions written below Eq. 16 (e.g.:  $A_{-1} = [\cos kz + a \sin kz + i(a \sin kz - \cos ky)]$ , etc.). This term, along with the magnetic field discusses later, are the only places where the molecular position  $r$  actually matters.

## 2.2. Simple concrete example of what the $\langle -\vec{\mu} \cdot \vec{B} \rangle$ term looks like in code

Again, we will be working with our model  $J' = 1 \rightarrow J = 1$  system. In this system, the  $C_{B,p}$  terms become:

$$C_{-1,B} = \begin{pmatrix} 0 & 0 & 0 & 0 & 0 & 0 \\ g_g & 0 & 0 & 0 & 0 & 0 \\ 0 & g_g & 0 & 0 & 0 & 0 \\ 0 & 0 & 0 & 0 & 0 & 0 \\ 0 & 0 & 0 & g_e & 0 & 0 \\ 0 & 0 & 0 & 0 & g_e & 0 \end{pmatrix} \quad (57)$$

$$C_{0,B} = \begin{pmatrix} -g_g & 0 & 0 & 0 & 0 & 0 \\ 0 & 0 & 0 & 0 & 0 & 0 \\ 0 & 0 & g_g & 0 & 0 & 0 \\ 0 & 0 & 0 & -g_e & 0 & 0 \\ 0 & 0 & 0 & 0 & 0 & 0 \\ 0 & 0 & 0 & 0 & 0 & g_e \end{pmatrix} \quad (58)$$

$$C_{1,B} = \begin{pmatrix} 0 & -g_g & 0 & 0 & 0 & 0 \\ 0 & 0 & -g_g & 0 & 0 & 0 \\ 0 & 0 & 0 & 0 & 0 & 0 \\ 0 & 0 & 0 & 0 & -g_e & 0 \\ 0 & 0 & 0 & 0 & 0 & -g_e \\ 0 & 0 & 0 & 0 & 0 & 0 \end{pmatrix} \quad (59)$$

All of the other terms in Eq. 32 are just pre-factors that we've already defined:  $(\mu_B/(\hbar\Gamma)) = 0.2114$ ,  $b/k = 10^{-4}$  (for a 10 G/cm gradient), and  $\tilde{B}_p$  depend on the specific field, and are defined for a quadrupole field in the discussion just above Eq. 32).

### 2.3. Simple concrete example of what the reservoir coupling term looks like in code

Again, we consider the model  $J' = 1 \rightarrow J = 1$  system. In this system, there are no phase terms in  $C_{eff}$ , as all excited states have the same energy, as do all ground states. Thus, the last term in Eq. 46 becomes:

$$\frac{d\rho_{mn}}{dt} = \sum_q C_{eff,q} \rho_{eff} C_{eff,q} (m, n \text{ both correspond to ground states}) \quad (60)$$

I usually don't hard code this in (infact, for SrF you can't really do this due to the time dependent phase factors), but instead just have matlab calculate it at each time step. But, you can hard code it if you want. For this example, you get:

$$\frac{d\rho_{mn}}{dt}_{vacCoup,ground-ground} = \begin{pmatrix} \frac{\rho_{44} + \rho_{55}}{2} & \frac{\rho_{56}}{2} & -\frac{\rho_{46}}{2} & 0 & 0 & 0 \\ \frac{\rho_{65}}{2} & \frac{\rho_{44} + \rho_{66}}{2} & \frac{\rho_{45}}{2} & 0 & 0 & 0 \\ -\frac{\rho_{64}}{2} & \frac{\rho_{54}}{2} & \frac{\rho_{55} + \rho_{66}}{2} & 0 & 0 & 0 \\ 0 & 0 & 0 & 0 & 0 & 0 \\ 0 & 0 & 0 & 0 & 0 & 0 \\ 0 & 0 & 0 & 0 & 0 & 0 \end{pmatrix} \quad (61)$$

To this, we add the other terms:

$$\frac{d\rho_{mn}}{dt}_{vacCoup,g-e \text{ and } e-e} = \rho \cdot * \begin{pmatrix} 0 & 0 & 0 & -\frac{1}{2} & -\frac{1}{2} & -\frac{1}{2} \\ 0 & 0 & 0 & -\frac{1}{2} & -\frac{1}{2} & -\frac{1}{2} \\ 0 & 0 & 0 & -\frac{1}{2} & -\frac{1}{2} & -\frac{1}{2} \\ -\frac{1}{2} & -\frac{1}{2} & -\frac{1}{2} & -1 & -1 & -1 \\ -\frac{1}{2} & -\frac{1}{2} & -\frac{1}{2} & -1 & -1 & -1 \\ -\frac{1}{2} & -\frac{1}{2} & -\frac{1}{2} & -1 & -1 & -1 \end{pmatrix} \quad (62)$$

where, as before,  $\cdot *$  refers to element-wise multiplication.

## 2.4. A Note on $\rho$ and $r$ evolution in matlab

**In the code**, we must propagate both  $\rho$  and  $r$ . This means we must record  $N_e \times N_g + 3$  variables, where  $N_e$  and  $N_g$  are the number of electronic excited and ground states. In this example, this is 36+3, where the 3 tacked on at the end are the position components of the molecule. The  $\rho$  propagation, once all the matrices above are calculated, is easily calculated in matlab:

$$\frac{d\rho}{dt} = i(\rho(-\vec{D} \cdot \vec{E}) - (-\vec{D} \cdot \vec{E})\rho) + i(\rho(-\vec{\mu} \cdot \vec{B}) - (-\vec{\mu} \cdot \vec{B})\rho) + \frac{d\rho}{dt}_{vacCoup} \quad (63)$$

All that's left is to step the positions as well. To do this, we just define the initial position (*note: in most cases, you will want to run for a few different initial positions. In normalized units ( $\tilde{x} = kx$ ), the Hamiltonian repeats every  $2\pi$  (not strictly true when there is a spatially dependent  $B$  field, but in practice the field varies slowly over one wavelength, so there's not much difference between, say, 1 mm off trap center and 1 mm+ $\lambda$  off the trap center), so you just pick either a series of random values for  $x, y, z$  between 0 and  $2\pi$  (plus whatever your displacement is if you are trying to do MOT simulations) and average until it converges or else sample a fine enough 'grid' of points such that the average value of whatever you are calculating (say,  $F(v)$ , the damping force as a function of velocity) converges with respect to 'grid-fineness') and initial velocity (these don't need to be random or finely gridded, but instead you pick based on what you are trying to calculate).*

One more matlab detail I will point out here: the ode solver in matlab wants a column vector of the variables you are evolving. Ideally, we'd be able to just feed it two terms, a 6x6 matrix for  $d\rho/dt$  in this case, and a 3x1 vector for  $dr/dt$ . But, since we can't, what we do is give it a 39X1 column vector with the first 36 elements from  $\rho$  and the last 3 dealing with the position. I still want the functions that I actually use to operate with a density matrix and a position vector separately, so I create a function below that 'converts' between the two:

```
diffEqColumns = @(t,p) [reshape(densityMatrixChangeTerms(t,reshape(p(1:length(p)-3),6,6),p((length(p)-2):end)),36,1);vx;vy;vz];
```

where ‘densityMatrixChangeTerms( $t, \rho, r$ )’ returns the  $d\rho/dt$  terms (in the form of a 6x6 matrix) for a given value of  $\rho$  and  $r$  (e.g., it performs the calculation in Eq. 60).  $p$  in this case is our 39X1 vector recording the values of  $\rho$  and  $r$  for a given  $t$ . So, in the call to ‘densityMatrixChangeTerms’, I reshape the first 36 terms into a 6x6 density matrix to form the  $\rho$  that the function actually uses, and I just read the last 3 terms (the ‘ $p((length(p)-2):end))$ ’) to give it the  $r$  that the function uses. Since the output of this function is the 6x6 matrix form of  $d\rho/dt$ , I reshape it into a 36X1 matrix (this is the outer ‘reshape’ term) to which I add the terms corresponding to the position evolution ( $vx$ ,  $vy$ ,  $vz$ ) to get the 39x1 matrix that goes into the matlab ode solver, which is called using:

```
[ts1,ps] = ode45(diffEqColumns,[0 1000],[pStart(:);rxInit;ryInit;rzInit]);
```

The code corresponding to this example is ‘runObeSolverParallel.m’. I won’t go over too many other gory details in this manual, but I’ve commented the code itself, so read through that and let me know if you have any questions.

## 2.5. Comparing results to Mike Tarbutt

**NOTE:** For some reason it seems like I have a sign error somewhere, either in this derivation or in the code somewhere. I’ve spent the better part of a day tracking it down to no avail. Basically: the velocity damping works as expected, however, the relative field orientation vs polarization setup needed for trapping is the opposite of what I would’ve expected. The magnitude seems exactly right though so I’m chalking it up to a sign error somewhere as opposed to a serious problem. If you find one in either my derivation or the code, please let me know...

I replicated two of the plots in Mike’s paper (<https://arxiv.org/pdf/1608.04645.pdf>). The results are in Figs. 2 and 3. The code contains scripts to reproduce this data.

### 2.5.1. Results for other ‘two zeeman manifold’ systems

I wrote a separate code that works for configurations involving two zeeman manifolds, which can be useful for a few applications (e.g.,  $F' = 2$  and  $F = 3$  for Rb...ignoring repumping). Instead of hardcoding the values of  $C_p$ ,  $C_{p,B}$ , they are calculated within the program using 3j symbols. The script for this code is including in the same folder as this writeup: ‘runObeSolverParallelWithTimeDepFlexibleLevels.m’ (you’ll see that, in the first few lines of the script you set  $F$  and  $F'$ , the excited and ground state angular momenta, respectively). Below I’ve included comparisons between my results from this program and the results from the Tarbutt group.

(quick note: In order to do this relatively quickly I ran fewer trials than the tarbutt group for each data point. For example, in the ‘force vs speed’ plots I ran 50 trials (randomized position and velocity direction) while the tarbutt group ran 500-5000 trials.

**Damping Force vs vx,  $\Delta = -2.5$   $s_0 = 0.5$  (2 in mike tarbutt units)**

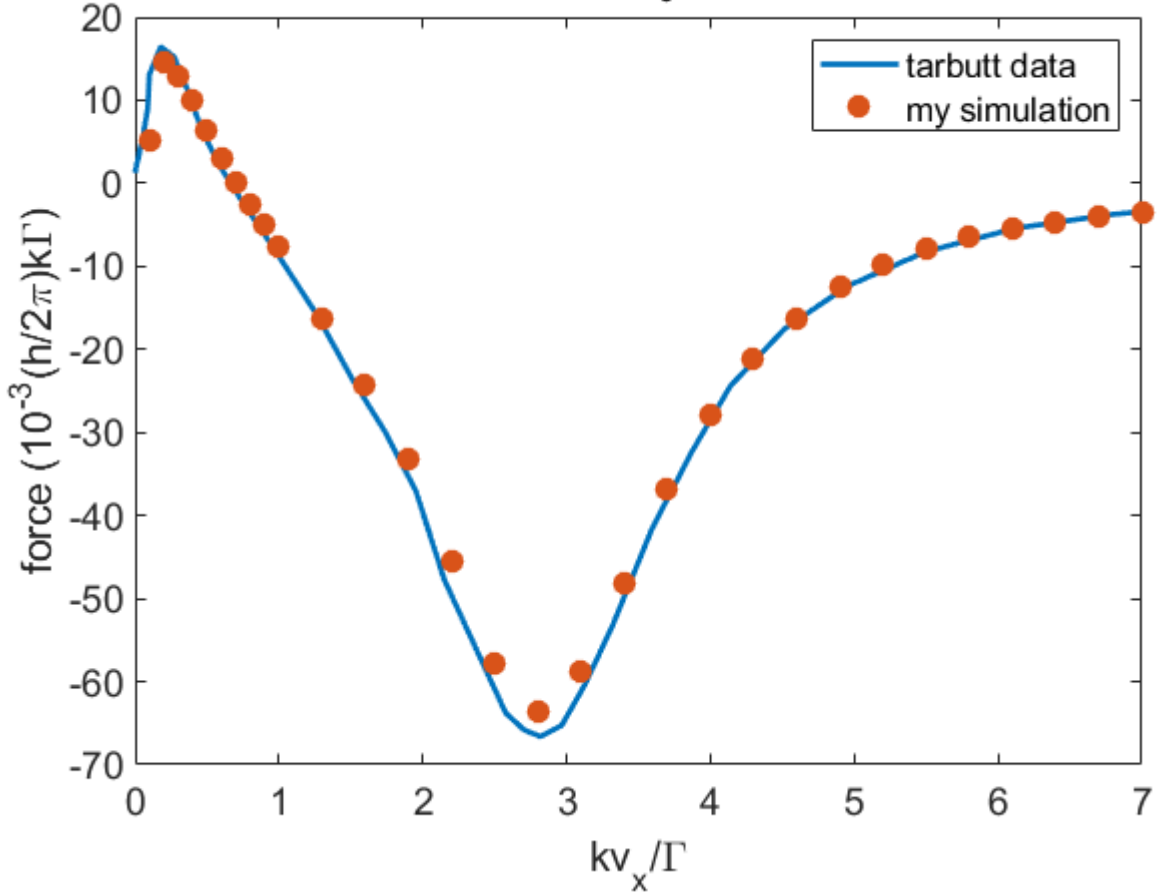


Figure 2: Comparison of velocity damping simulation to M. Tarbutt's work (Fig. 3 of <https://arxiv.org/pdf/1608.04645.pdf>)

This, I assume, is why my data is a little noisier. The error bars come from standard error from the 50 trials. For the field simulation I did a 4x4x4 grid of initial positions (e.g. points spaced apart by 1/4 wavelength), and 1 trial at each point with a random velocity. Really I should do more trials for this, but I think for the purposes of benchmarking these results are fine, as the simulations here are quite time consuming.)

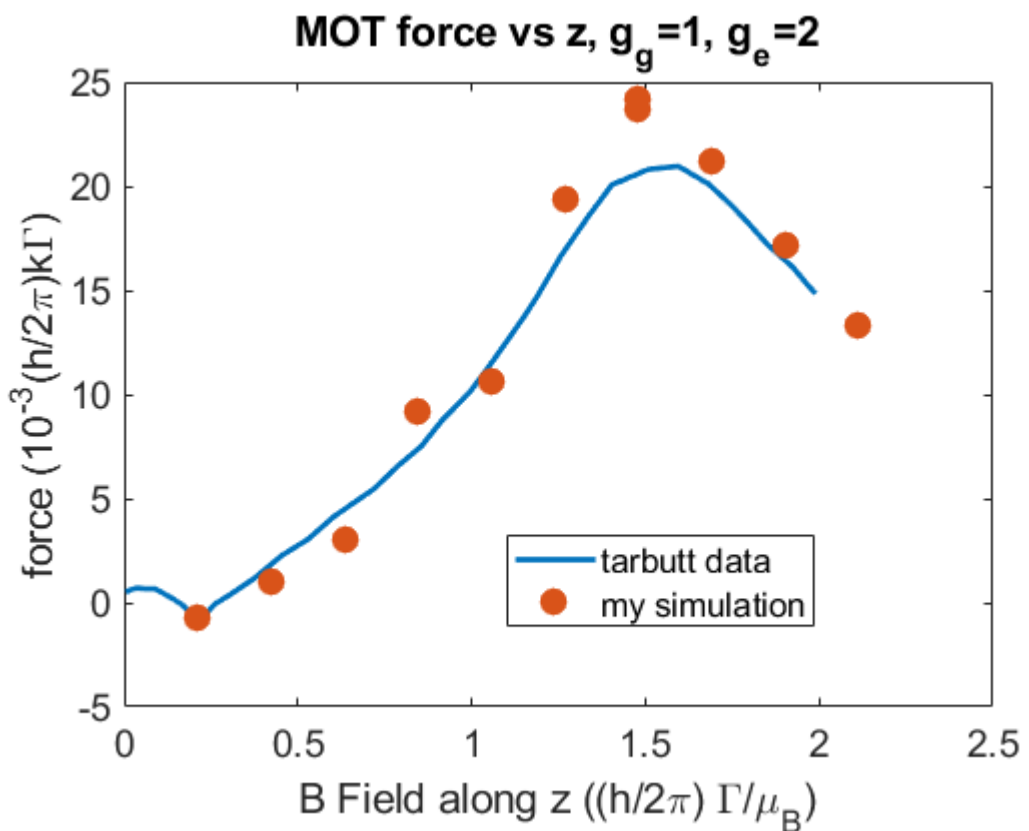


Figure 3: Comparison of MOT simulation to M. Tarbutt's work (Fig. 7 of <https://arxiv.org/pdf/1608.04645.pdf>)

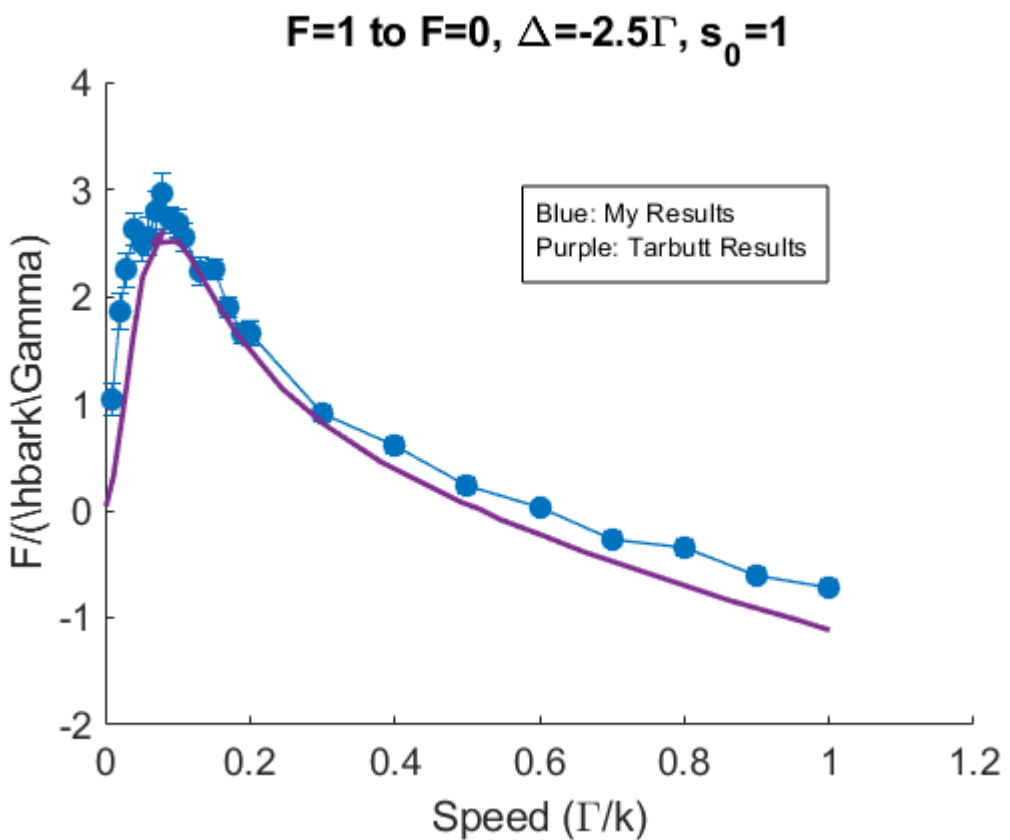


Figure 4: Comparison between my simulation and the Tarbutt results for force vs speed for  $F' = 1$  to  $F = 0$  molasses. (Fig. 4 of <https://arxiv.org/pdf/1608.04645.pdf>)

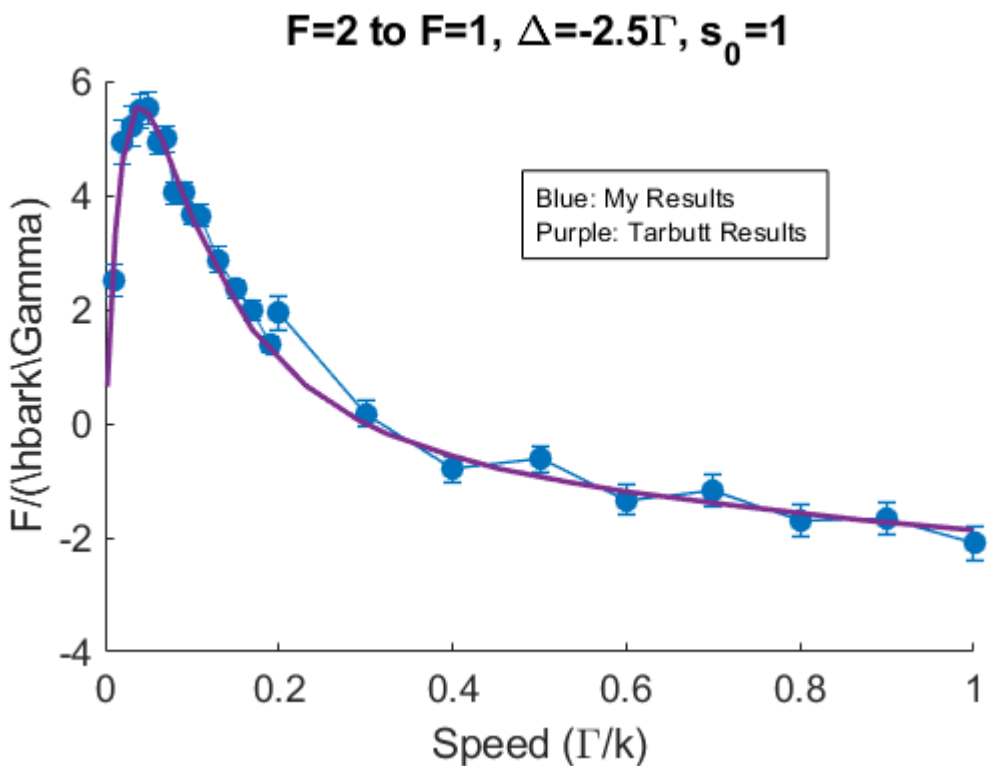


Figure 5: Comparison between my simulation and the Tarbutt results for force vs speed for  $F' = 2$  to  $F = 1$  molasses. (Fig. 4 of <https://arxiv.org/pdf/1608.04645.pdf>)

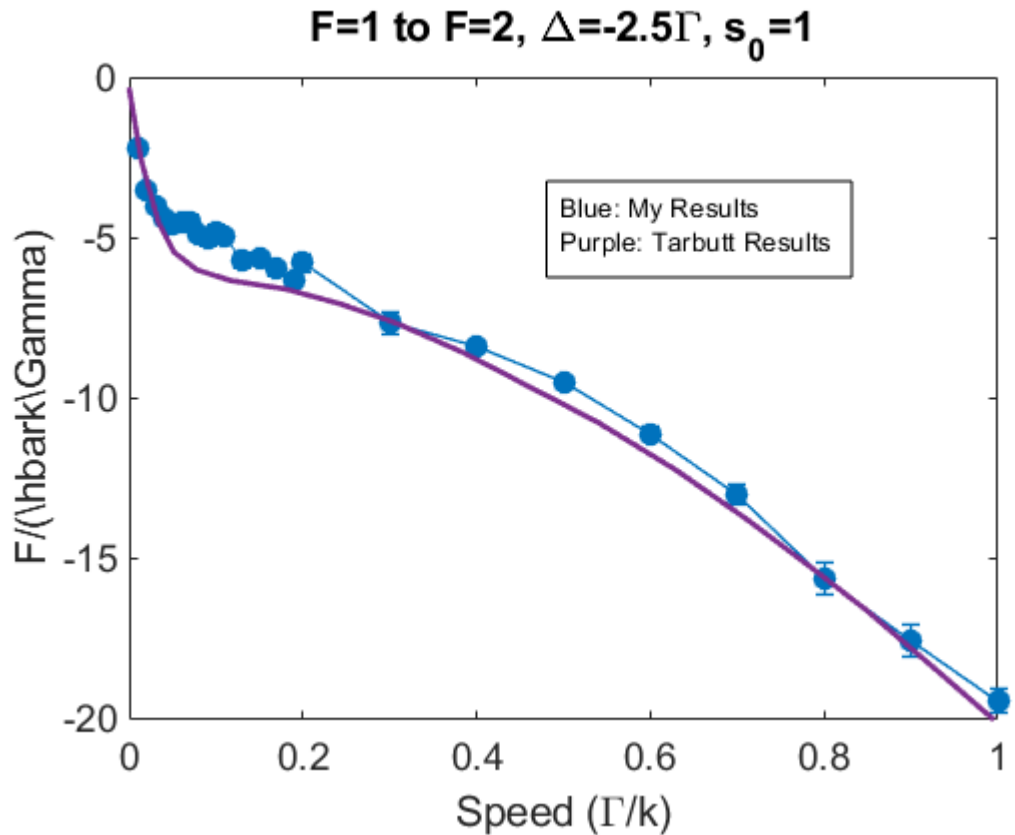


Figure 6: Comparison between my simulation and the Tarbutt results for force vs speed for  $F' = 1$  to  $F = 2$  molasses. (Fig. 4 of <https://arxiv.org/pdf/1608.04645.pdf>)

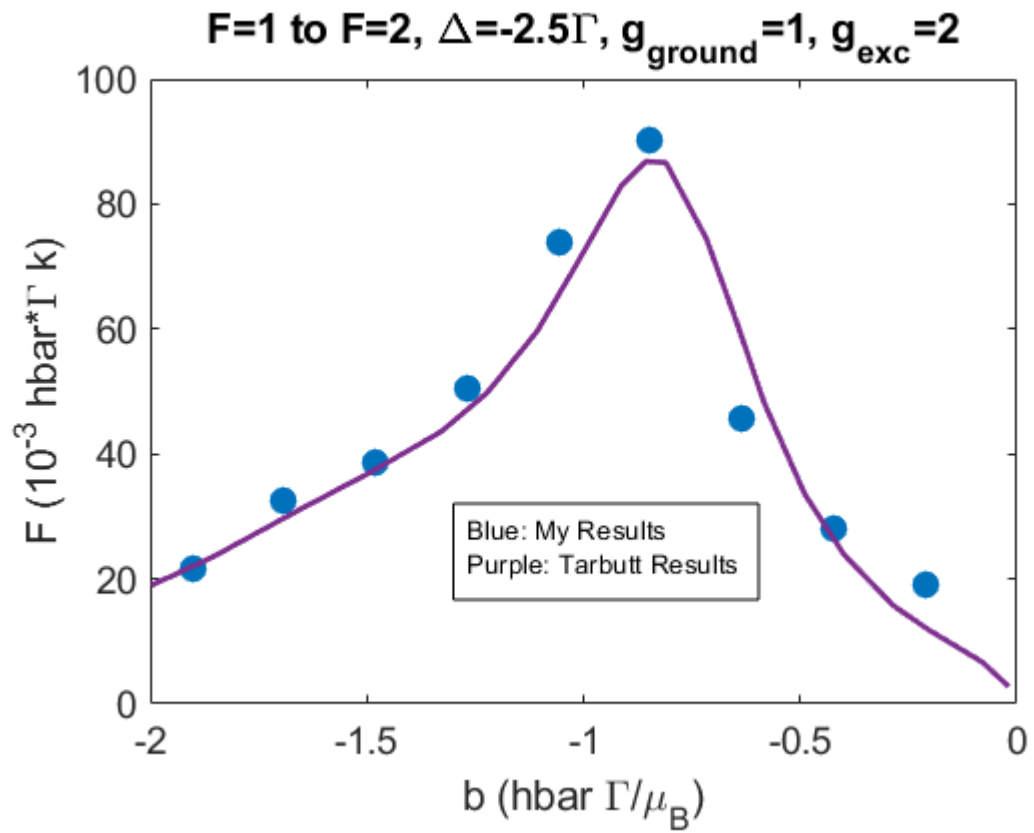


Figure 7: Comparison between my simulation and the Tarbutt results for force vs field for  $F' = 1$  to  $F = 2$  MOT configuration. (Fig. 7 of <https://arxiv.org/pdf/1608.04645.pdf>)

## 2.6. Results for Field Dependence of Doppler + Sub-Doppler Forces

In Type-I MOTs, one often implements a period of optical molasses after trapping, in order to further cool the atoms using the sub-Doppler sisyphus type force. Since sub-Doppler cooling for Type-I systems works for red-detuning, and the MOT itself was already operating using red-detuning, naively one would think that this stage shouldn't be necessary since the sisyphus force should already be felt within the MOT. However, this is not the case, since it turns out that the sisyphus mechanism does not work in the presence of even small magnetic fields (see Fig. 8)

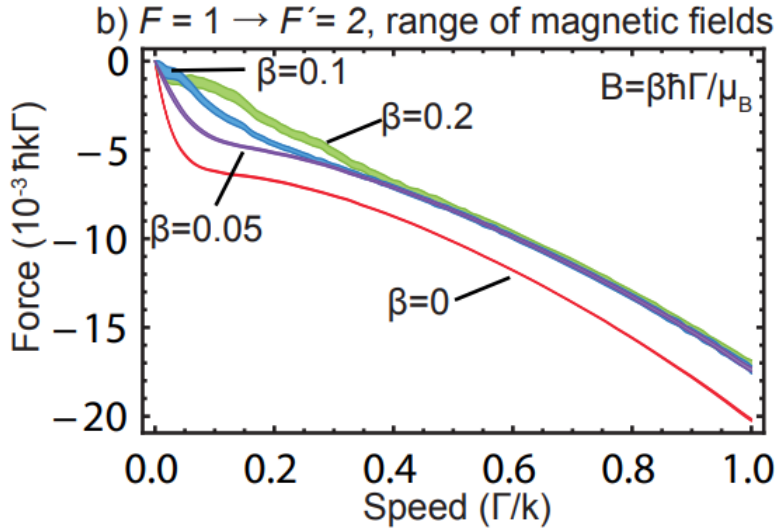


Figure 8: The Sisyphus force in Type-I systems is strongly diminished even for  $\beta \sim 0.05$ . (Fig. 6 of <https://arxiv.org/pdf/1608.04645.pdf>). For context:  $\beta = 0.05$  corresponds to roughly 0.2 Gauss for most alkali transitions ( $\Gamma \sim 2\pi \times 10^6 \text{ s}^{-1}$ ). 20 G/cm is a pretty common gradient, and so this corresponds to a 0.1 mm displacement from the trap center. Most Rb MOTs are at least a couple 100  $\mu\text{m}$ , and so most atoms in a MOT are not experiencing a sisyphus force while the field is active, hence why an optical molasses step is deployed.

For Type-II systems, it turns out that the Sisyphus force is much more robust to magnetic fields. Unfortunately, the Sisyphus force winds up *heating* the molecules when the lasers are red-detuned. This can be seen in Fig. 9 and 10. It dies out a little bit faster for rf fields (Fig. 10), which may be one reason why the so-called 'rf MOT' performs better (we will investigate this in the next section).

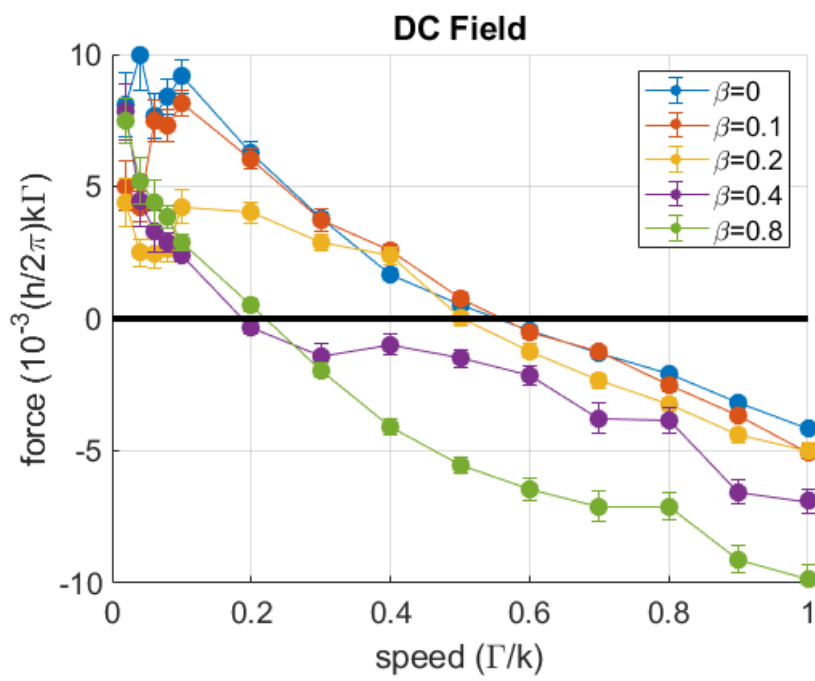


Figure 9: F vs Speed for different fields  $\beta = \mu_B B / (\hbar \Gamma)$  for a  $F = 1 \rightarrow F' = 1$  transition in a DC field. The sisyphus force is fairly robust to magnetic fields, potentially allowing for a ‘blue-MOT’ operating on the Sisyphus force, discussed later on.

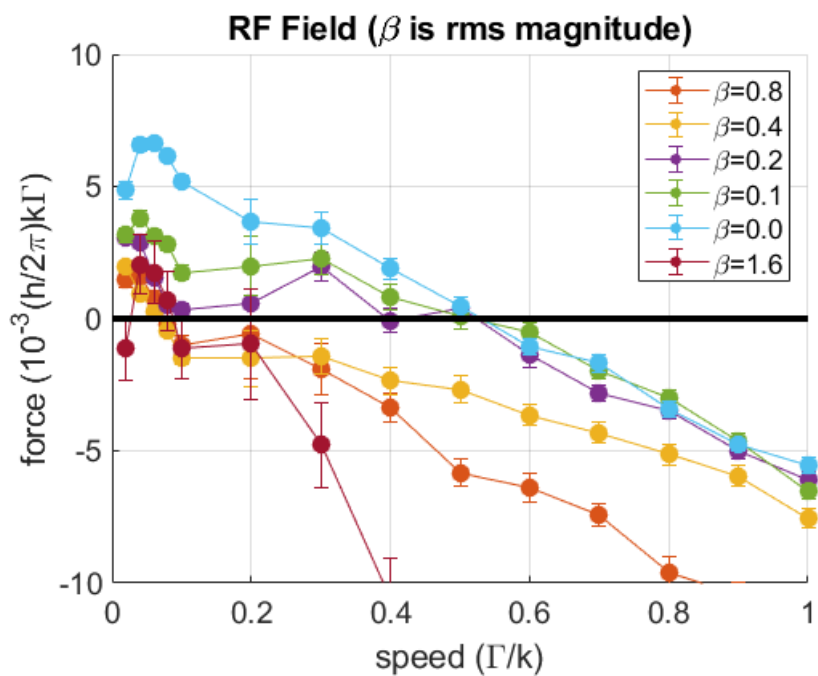


Figure 10: F vs Speed for different fields  $\beta = \mu_B B / (\hbar\Gamma)$  for a  $F = 1 \rightarrow F' = 1$  transition in an RF field (with synchronous polarization switching). The force seems to die out a lot quicker with an increasing RF field than for a DC field.

### 3. Results of SrF Simulations

In this section, I will summarize the results of my simulations for the SrF Magneto-Optical Trap.

#### 3.1. Capture Velocity of Various MOTs

Here I will consider MOTs for molecules which have a level diagram like the one in Fig. 11. For both SrF and CaF, it turns out that the 4 hyperfine levels in the X state are separated by anywhere between  $3\Gamma$  and  $12\Gamma$ , i.e., just far enough apart that they must be addressed by individual lasers (in practice, by sidebands of the same laser), but not so far apart that we can ignore off-resonant scattering events from a laser addressing a ‘different’ level. This is the sort of situation that requires the multi-laser multi-level simulation described in Sec. 1.

The first thing that I wanted to look into is if the simulations could predict a reasonable value for the MOT capture velocity. This has been determined to be on the order of 5 m/s (for SrF rfMOT, see [M. Steinecker thesis](#)) through a measurement involving applying a pulse of light to accelerate the trapped molecules and seeing how many are ‘recaptured’ for a given pulse length (longer pulse = higher velocity molecules). For a CaF dcMOT, a similar measurement yielded 11 m/s ([H. Williams thesis](#), Tarbutt group).

I also wanted to do this measurement in order to determine what the capture velocity of various SrF dcMOT configurations can be (see Fig. 11). In particular, I want to benchmark the two ‘5-laser’ dcMOTs performances (note: we have never tried the 5-laser dcMOTs in the lab) vs the rfMOT performance. The ‘5-laser’ dcMOTs attempt to take advantage of the dual-frequency properties that make the CaF dcMOTs effective. For CaF, the top two hyperfine states ( $|F = 2\rangle$  and  $|F = 1, \tilde{J} = 3/2\rangle$ ) are only separated by  $3\Gamma$ . Thus, a laser that is  $-1\Gamma$  detuned from  $|F = 1, \tilde{J} = 3/2\rangle$  is  $+2\Gamma$  detuned from  $|F = 2\rangle$ . This laser is also the opposite polarization of the laser that is red-detuned from  $|F = 2\rangle$ . The effect of this is to eliminate the main problem with ‘Type-II’ MOTs, namely, that you can wind up in a stretched Zeeman state that can only possibly scatter light from the ‘wrong’ beam (this is the main motivation for using an rfMOT, in which one synchronously switches both the laser polarization and the B-field such that the state that is ‘dark’ for a  $b_{grad} > 0$  becomes ‘bright’ for  $b_{grad} < 0$ ). This is illustrated in Fig. 12.

In SrF, these levels are separated by  $6.3\Gamma$ , which is likely too far apart for the dual-frequency mechanism to help all that much. Therefore, if we want to try a dual frequency MOT, we would need to add another laser (‘blue’ lasers in Fig. 11).

To determine the capture velocity, I used the simulation to obtain  $F$  (or  $a$ , where  $a$  is acceleration) vs  $v$  curves for the case where  $v$  is along  $\hat{d} = (\hat{x} + \hat{y})/\sqrt{2}$  for various  $d$  along that same axis. This is the direction in which the slowed molecular beam travels in a coordinate system where the (x,y,z) axes are defined by the MOT laser propagation

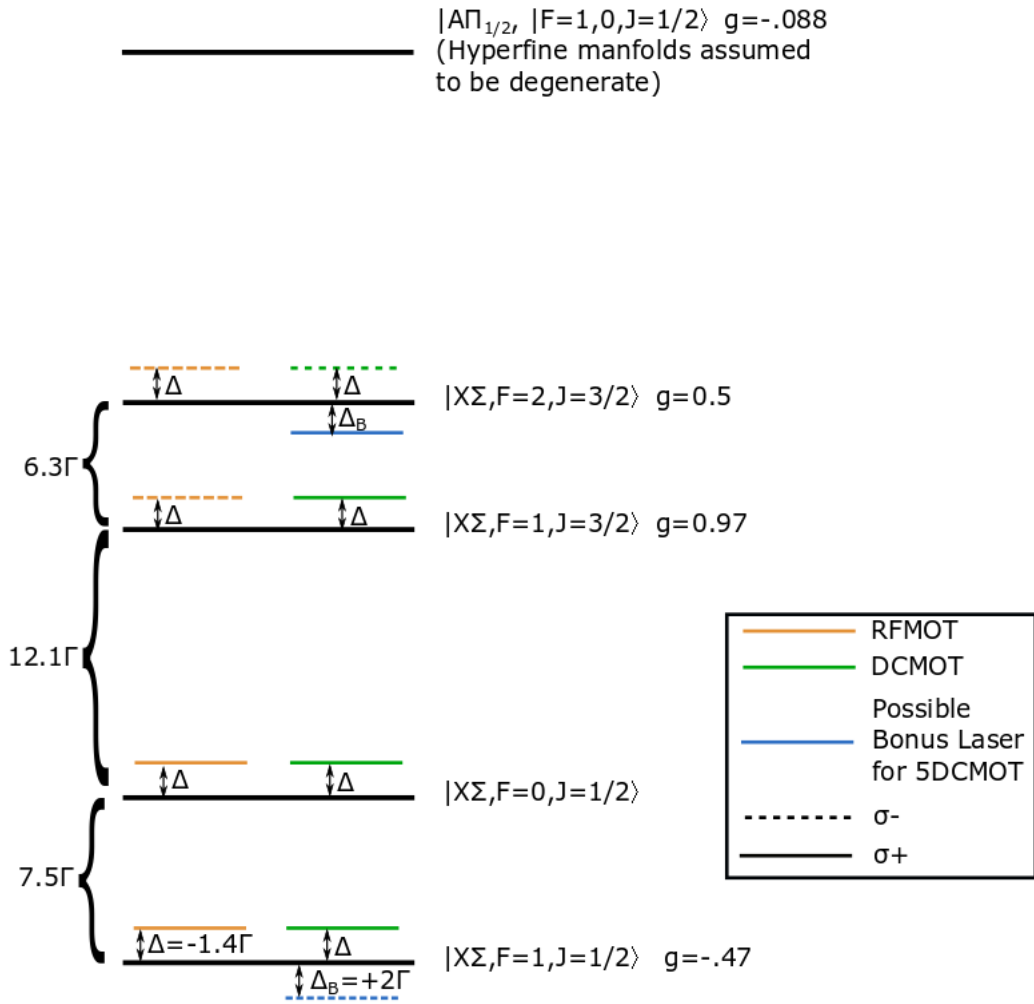


Figure 11: SrF Level diagram, along with the laser configurations used in molecular MOTs.

directions (see Fig. 13). The relevant parameters for this simulation are:

- $b_{grad} = 12.5 \text{ G/cm}$  (weak axis gradient)
- $\Delta = -1.4\Gamma$
- $\Delta_{blue} = 2\Gamma$  (for the ‘bonus’ laser in 5-laser MOT schemes)
- $w_{beam} = 7 \text{ mm}$  ( $e^2$  radius)
- $r_{beamAperture} = 12.7 \text{ mm}$  (MOT beams are apertured with a 1” diameter blackened copper gasket attachment)
- $s_0 = 14$  (all beams)

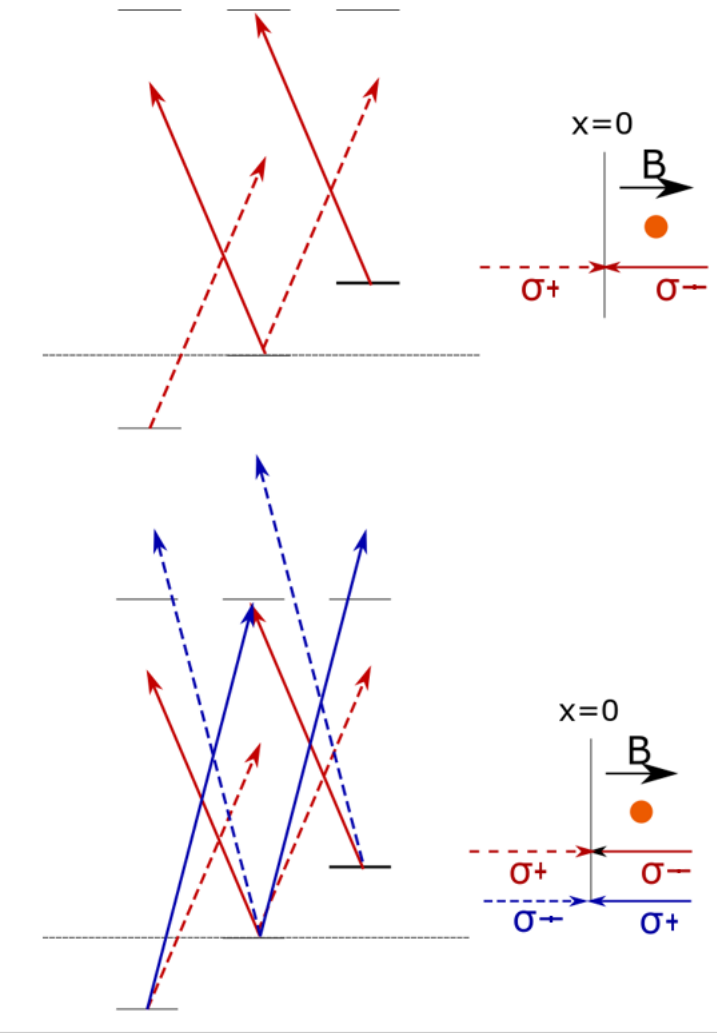


Figure 12: Top: Single frequency dcMOT schematic (upper state assumed to have no magnetic moment). The molecule (on the right hand side of the trap) is likely to absorb from the ‘correct’ beam if it is in the  $m = 1$  state. However, there is nothing stopping the molecule from decaying to the  $m = -1$  state after a few scatters, at which point it *has to* absorb light from the ‘anti-confining’ beam. This trap will therefore be somewhere between weak and non-existent (as we now know, it is in fact possible to have a weak Type II dcMOT trap). Bottom: Dual frequency schematic. We see here that now the molecule is likely to absorb from a beam pointing in the correct direction if it is in either  $m = 1$  or  $m = -1$ . The cost is that you will lose velocity damping, since the extra laser must be blue detuned.

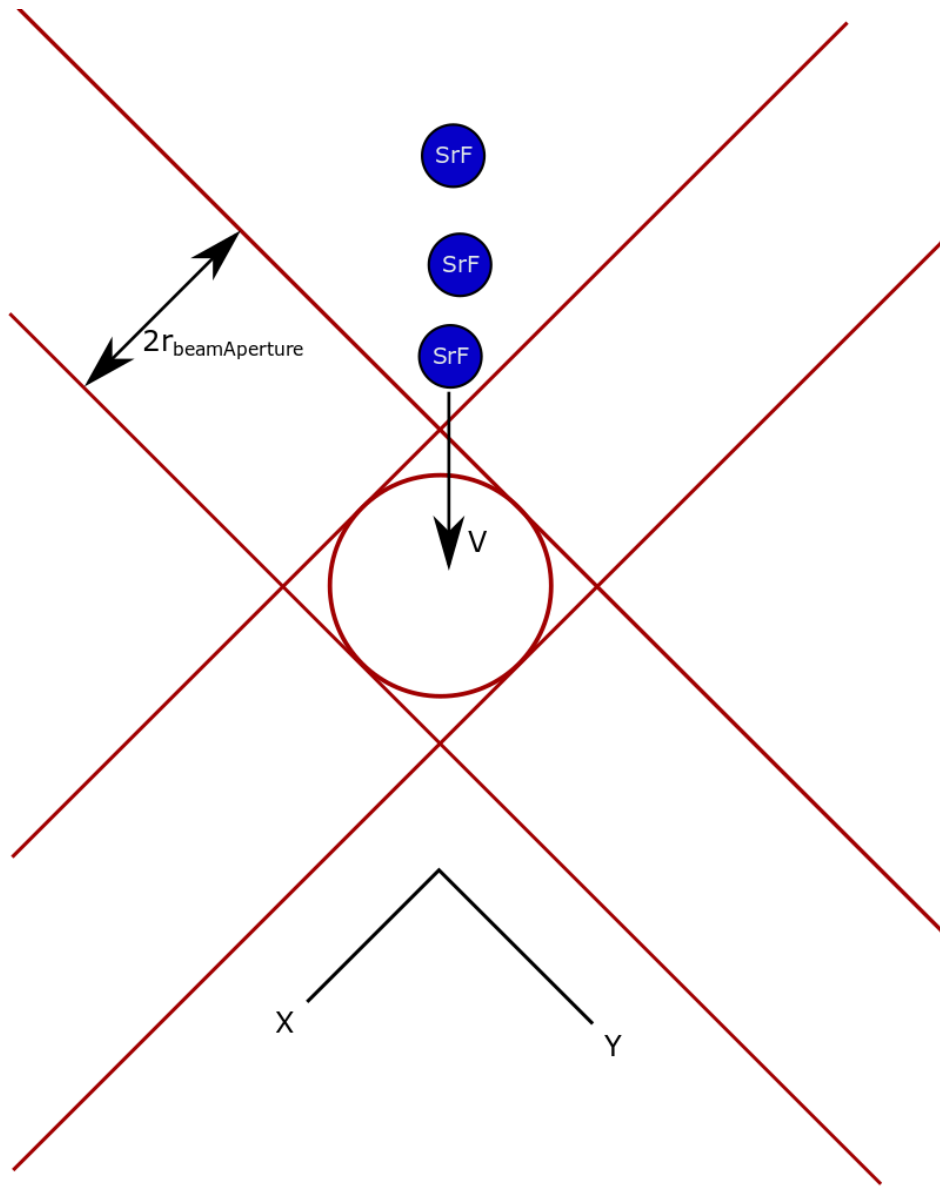


Figure 13: The SrF molecular source is ‘upstream’ in the  $(-\hat{x} - \hat{y})/\sqrt{2}$  direction. A molecule with  $v < v_{capture}$  will turn around before it reaches  $d = 2\sqrt{2}r_{beamAperture}$ . Lasers are indicated by red-lines (the circle in the middle indicates the lasers in the  $\pm z$  direction)

These parameters (roughly) replicate the ones used in our SrF apparatus during the initial trapping stage. In principle, one may be able to do better by picking a  $\Delta$  which changes for each hyperfine level, or an  $s_0$  that changes with hyperfine level.

The  $a(d, v)$  mapping for the rfMOT is shown in Fig. 14. There are a few important features to point out. First: we can clearly see that, for  $d = 0$  there is a substantial sisyphus heating force that dissipates for  $d \pm 7$  mm (this is because the sisyphus force eventually disappears as a result of a magnetic field + polarization switching, see Fig. 10). Second: The force is positive for  $v = 0$  for the  $d = -7$  mm curve and negative for the  $d = +7$  mm curve. This reflects the fact that the MOT force is a restoring force.

Once the  $a(d, v)$  curve is obtained, the capture velocity can be obtained by solving (note: to actually solve the equations I linearly interpolate  $a(d, v)$  via matlab's interp2 function.) for  $v(t)$  and  $d(t)$  for  $v(0) = v_{start}$  and  $d = -\sqrt{2}r_{beamAperture}$ . A molecule with  $v(0) = v_{start}$  is ‘captured’ if it ‘turns around’ before  $d > \sqrt{2}r_{beamAperture}$ . The capture velocity is the maximum velocity for which the molecule is captured. In Fig. 15 I show the  $a(d, v)$  maps for the various MOT configurations while in Fig. 16 I show phase plots for the various MOT configurations described above.

Unfortunately, this is not the full story. For SrF (and I believe all CaF MOTs made thus far), the  $v=1$  repump laser couples  $|X\Sigma, v = 1\rangle$  to  $|\Lambda\Pi_{1/2}, v = 0\rangle$ . This forms a  $\Lambda$  system, reducing the scattering rates (and thus forces) that can be achieved. In the simulation, we observe a 10% population in the excited state, whereas in the experiment we measure a scattering rate of  $R_{scat} \sim 3.5 \times 10^6 \text{ s}^{-1}$  ( $R_{sc}/\Gamma \sim 0.075$ ). Thus, we can expect all forces to be reduced by a factor of roughly 3/4 (I decided to overestimate this effect and reduce them by 2/3 for the following plots). In Fig. 17 I show phase plots for the MOT configurations with forces multiplied by 2/3.

**(Speculation):** We clearly see that, in this case, the capture velocity of the 4-laser dcMOT goes to zero. Since we have made this work in the past (albeit very poorly), this is a little perplexing. One thing that we have yet to consider is that clearly the molecules are traversing over a wide range of positions ( $r_{capture} \sim r_{beamAperture}$ ). In this limit, the force along  $\hat{d}$  is substantially different than the force along  $\hat{x}$ , for example. Due to the pluming of the SrF beam + random scattering events in the MOT, it is probably possible for the molecules to veer off the  $\hat{d}$  axis substantially, even in the first pass through the trapping region, which would bring their path of travel closer to being along a beam axis. If this happens, then the molecules will experience a stronger restoring force, as no matter how far they travel from the trap center, there will still be substantial beam intensity from the restoring lasers. I redid the simulations for displacements along the  $\hat{x}$  axis instead of the  $\hat{d}$  axis: resulting phase plots are in Fig. 18. (side note: this sort of asymmetry is not normally something people worry about in MOTs since the atoms/molecules are typically confined to a region  $\sigma \ll r_{aperture}$ . For Type-II MOTs, the sisyphus heating force experienced preferentially for  $r = 0$  makes particles spend more time at trap extremes). It is possible that the molecules that are captured in this MOT are those that veer off course in this manner.

There are other imperfections in the experimental MOT that we do not take into ac-

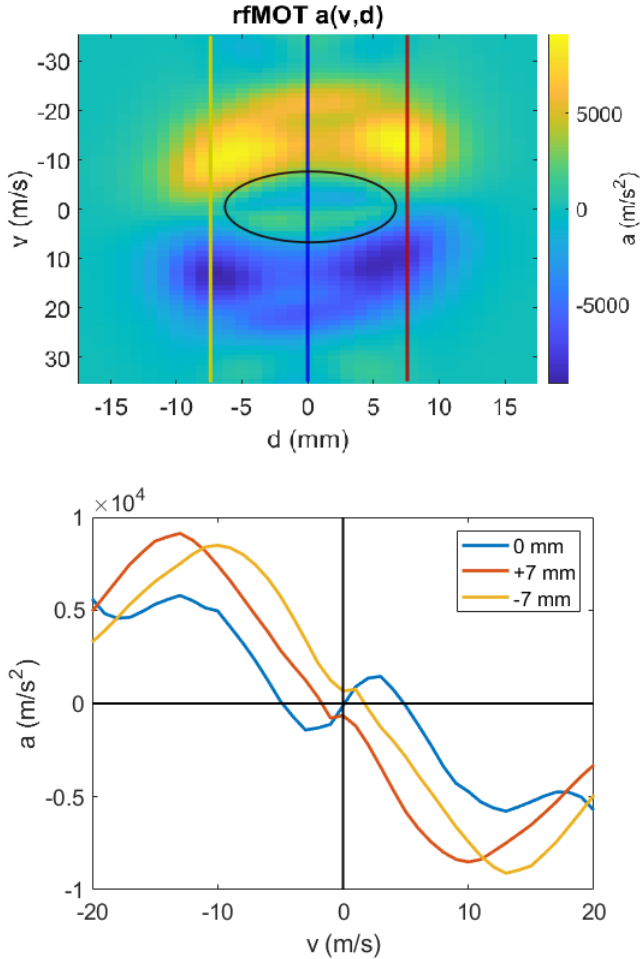


Figure 14: Top:  $a(v,d)$  for the SrF rfMOT, determined by the simulation. Yellow, Blue, Red vertical lines correspond to  $F$  vs.  $v$  transects plotted in the bottom figure. The black circle indicates the region where the Sisyphus force dominates over the Doppler force; it is clear from the figure that, for sufficiently large  $d$ , the sisyphus force dissipates entirely. Bottom:  $F$  vs.  $v$  for different positions. We see that the  $+7\text{ mm}$  curve is left-shifted with respect to the  $-7\text{ mm}$  curve. The effect of this is to make the force in the region of  $v = 0$  a restoring force (positive for  $d = -7\text{ mm}$ , negative for  $d = 7\text{ mm}$ ). We also clearly see here that the sisyphus force has mostly disappeared for the  $d \neq 0$  curves.

count here. The most important difference is that the beam waist and intensity profile are different for each beam pass in the experiment: since the MOT requires a lot of power, we use just one beam that we ‘wrap’ through the chamber 6 times. Since this beam goes through many optical surfaces, power is lost from the beam. We therefore make the beam weakly converging, such that the intensity in the center of the beam

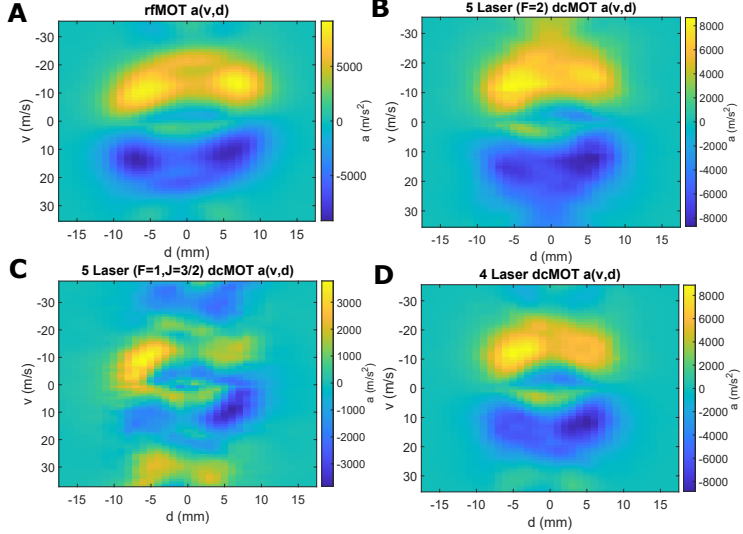


Figure 15:  $a(d, v)$  plots. {A,B,C,D}: {RFMOT, 5-laser DC MOT ( $F=2$ ), 5-laser DC MOT ( $|F = 1, J = 1/2\rangle$ ), 4-laser DC MOT}. If you look closely at the regions of high  $|a|$ , you can see a slight tilt in the upper-right direction (particularly for A+B): this is a signature of the restoring nature of the force: for  $d < 0$  the positive force portion is more prominent for lower velocities and vice versa for  $d > 0$ .

is the same for each pass. We are not modeling this change in size or intensity profile. Other imperfections include: possible field imperfections (e.g. not a perfect quadrupole), molecular pluming (for each case here I have considered only travel directly along  $\hat{d}$  or  $\hat{x}$ ), etc. Some combination of these factors may be responsible for why, in the experiment, the rfMOT capture velocity was measured to be 6,m/s instead of  $\geq 10$  m/s. In any event, though the simulations cannot incorporate every aspect of the experiment, I think that the main conclusion that we can draw from them, which is that the rfMOT>5-laser dcMOT>4-laser dcMOT, is valid, though it would be nice to test the 5-laser system experimentally whenever we get the chance.

A common thing people like to plot are  $F$  vs  $V$  and  $F$  vs  $X$  curves (See Sec. 2). Since the nature of the  $F$  vs  $V$  curve depends on  $X$  (and vice versa) for these Type-II MOTs, it's not really intuitive how to do this. What I decided to do is just plot  $a(v) = \int_{-7\text{mm}}^{7\text{mm}} dx a(d, v)$  and  $a(x) = \int_{-4\text{m/s}}^{4\text{m/s}} dv a(d, v)$ , where I've chosen to average over the (rough) range of velocities and positions that the molecule experiences in its phase evolution. These are plotted in Fig. 20 and Fig. 19. These plots make it fairly obvious why the 5-laser  $|F = 1, J = 3/2\rangle$  MOT wasn't very effective: adding that extra blue laser to  $|F = 1, J = 1/2\rangle$  somehow totally kills the velocity damping.

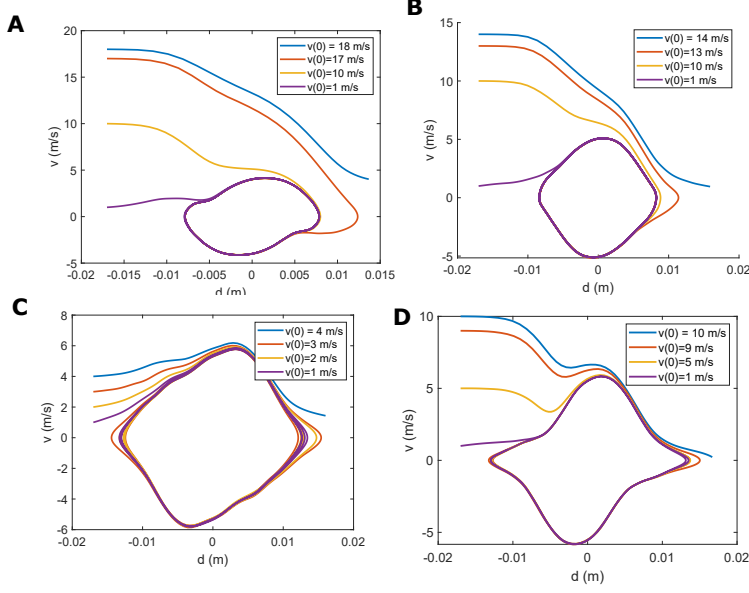


Figure 16: Phase plots under the assumption that the  $\Lambda$  system does not affect the MOT behavior. {A,B,C,D}: {RFMOT, 5-laser DC MOT ( $F=2$ ), 5-laser DC MOT ( $|F=1, J=1/2\rangle$ ), 4-laser DC MOT}. We see here that the capture velocity is maximized for the rfMOT, but is not too bad for the 5-laser  $F=2$  dcMOT.

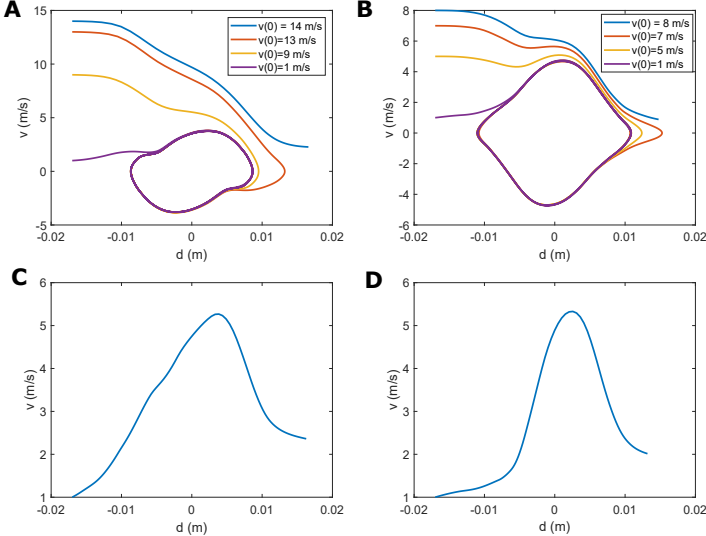


Figure 17: Phase plots under the assumption that the  $\Lambda$  system causes the force to be multiplied by  $2/3$ . {A,B,C,D}: {RFMOT, 5-laser DC MOT ( $F=2$ ), 5-laser DC MOT ( $|F=1, J=1/2\rangle$ ), 4-laser DC MOT}. The capture velocities are all reduced relative to those in Fig. 16. Further, the dcMOT does not seem to capture any molecules (here I've only included the phase plot for  $v(0) = 1 \text{ m/s}$ ).

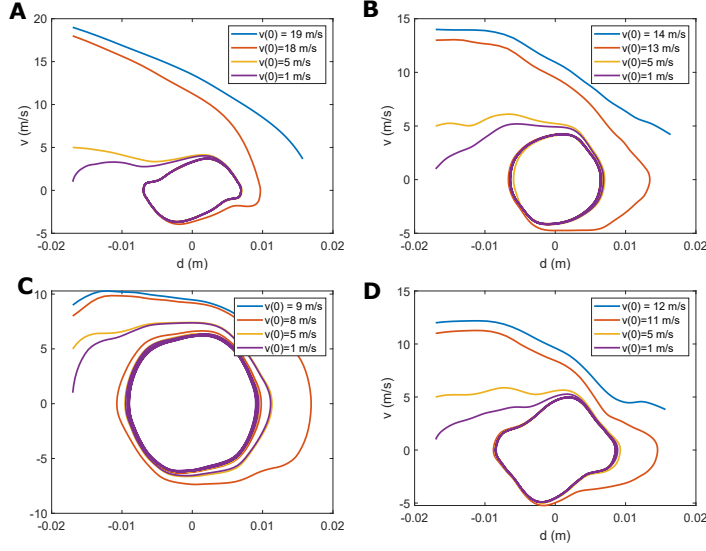


Figure 18: Phase plots under the assumption that the  $\Lambda$  system causes the force to be multiplied by  $2/3$ , for  $\hat{d} = \hat{x}$  (e.g., the molecules feel strong restoring forces even for large  $d$ ). {A,B,C,D}: {RFMOT, 5-laser DC MOT ( $F=2$ ), 5-laser DC MOT ( $|F=1, J=1/2\rangle$ ), 4-laser DC MOT}. We see here that, even with the reduced power, the dc MOT will trap molecules displaced along this axis, unlike for when  $\hat{d} = (1/\sqrt{2})(\hat{x} + \hat{y})$  (Fig. 17)

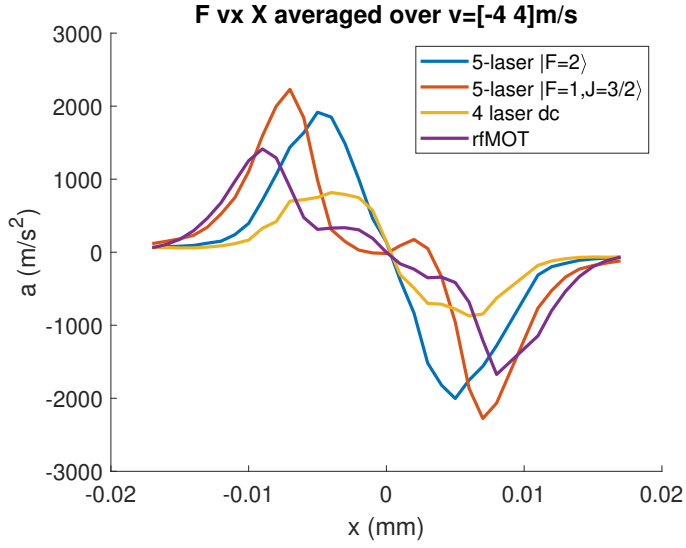


Figure 19: A Vs X for relevant MOT configurations.

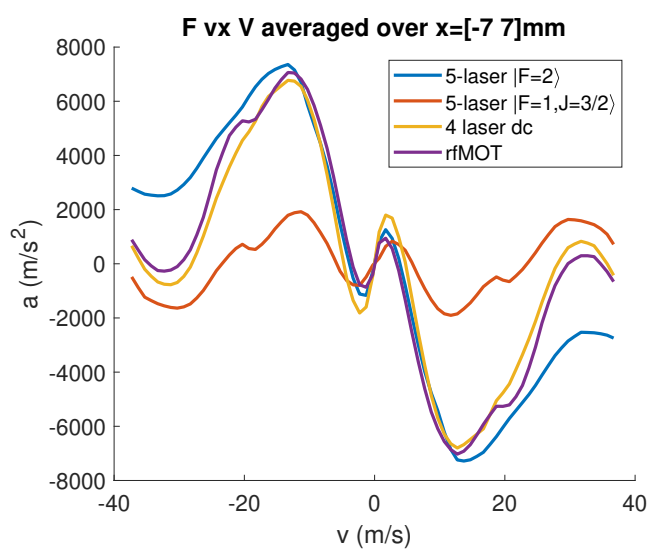


Figure 20: A Vs V for relevant MOT configurations.

### 3.1.1. Special case: dual frequency MOT operating on $|F = 1, J = 3/2\rangle$

For completeness, I also decided to simulate a dual frequency MOT operating on the  $|F = 1, J = 3/2\rangle$  state (initially I didn't simulate this because the Tarbutt group [paper](#) specifically only simulated dual frequency MOTs for the  $|F = 2\rangle$  and  $|F = 1, J = 3/2\rangle$  states. This is because of the special circumstances for CaF that I discussed above regarding the spacing of only  $3\Gamma$  between the top two hyperfine levels).

Naively, I assumed that the optimal polarizations for the dual frequency MOT would match the ones used for the dcMOT (e.g., the red detuned laser would retain the same polarization as the dcMOT while the ‘bonus’ blue detuned laser would have opposite polarization, see Fig. 21). When I ran my simulation for this configuration, curiously I found that the  $F$  vs  $X$  force was even weaker than that of the 4-laser dcMOT: adding the dual frequency scheme had somehow made things worse (Fig. 22)!

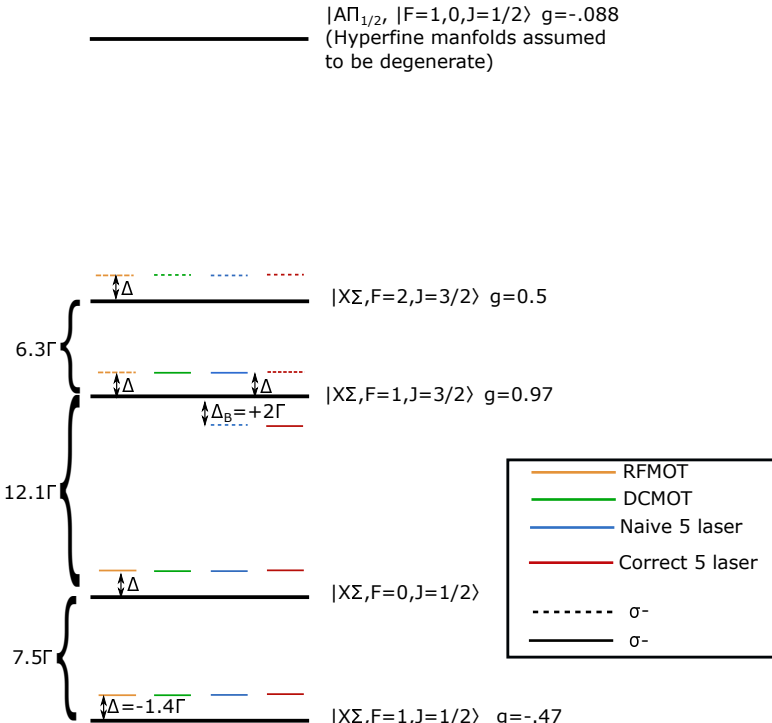


Figure 21: MOT configurations for 5-laser MOT with dual-freq scheme operating on  $|F = 1, J = 3/2\rangle$

I eventually realized that my choice for polarization here was likely incorrect. While the choice of polarization for a dcMOT depends solely on the sign of the upper state  $g_{\text{factor}}$  and whether  $F_{\text{Excite}} > F_{\text{ground}}$  (if  $F_{\text{ground}} > F_{\text{excite}}$ , the polarization is reversed, see Mike Tarbutt's [NJP paper](#)), the dual-frequency MOT mechanism relies on the *ground state* g-factor. So, if the dual-frequency scheme is ‘more-impactful’ than the single-laser

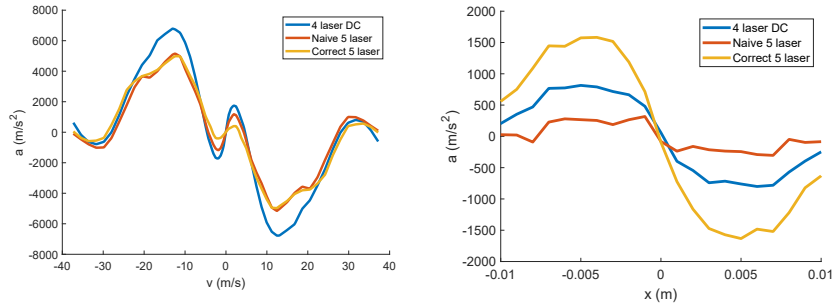


Figure 22: Comparison of  $F(v)$  and  $F(x)$  for  $|F = 1, J = 3/2\rangle$  dual-frequency MOTs. Clearly we see that the ‘naive’ choice (Fig. 21) actually weakens the trapping.

dc scheme (which we would expect for situations like SrF where  $g_{\text{ground}} \gg g_{\text{excite}}$ ), we should choose the polarizations based on this ground-state factor. This is also what drove the choice of polarization in the rfMOT, and so the red-detuned polarization should match what it is in the rfMOT.

I decided to test this in a simple system first: just a  $F = 1 \rightarrow F' = 1$ . Sure enough, the correct  $\Delta < 0$  polarization is reversed relative to the case in the dcMOT. Furthermore, I also simulated the case where there is no excited state  $g$ , and saw that there was little difference between that and the results for  $g = -0.088$ , further demonstrating that the dual-frequency force results from the ground state  $g$ -factor (Fig. 23).

In Fig. 24 I plot  $a(x, v)$  and phase plots for the ‘correct’ 5-laser dual frequency  $|F = 1, J = 3/2\rangle$  configuration. Here we see that the performance is comparable to the 5-laser dc  $|F = 2\rangle$  case.

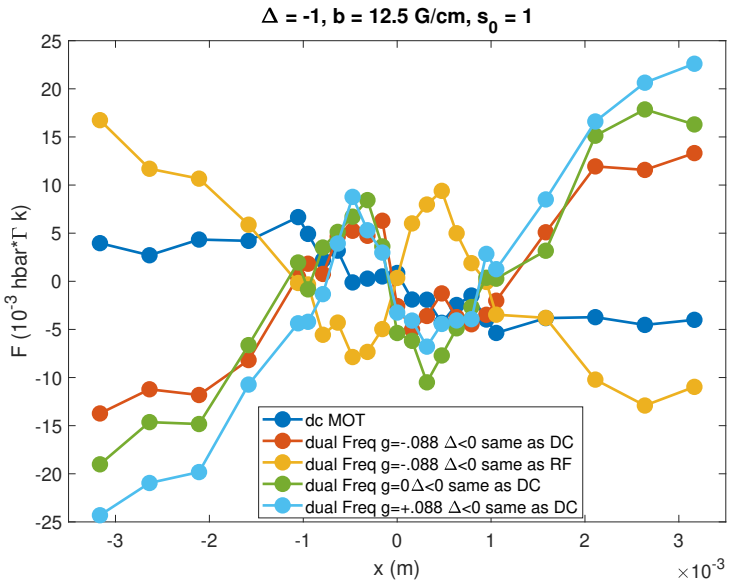


Figure 23: Comparison of  $F(x)$  for various MOT configs and  $g_{upper}$  values for a  $F = 1$  to  $F' = 1$  system. We see that, for  $|x| > 1$  mm, the dual frequency MOT with the same trapping polarization for red-detuning as the dcMOT becomes *anti-trapping* even though the dcMOT is trapping at these positions. This is true regardless of the sign of  $g_{upper}$ . If the polarization is reversed (e.g. matching the rfMOT), the force again becomes trapping (for  $|x| > 1$  mm...it seems like there's some sort of 'positional sisyphus' type thing happening for low  $|x|$  in the dual frequency case) in the dual frequency case (yellow curve).

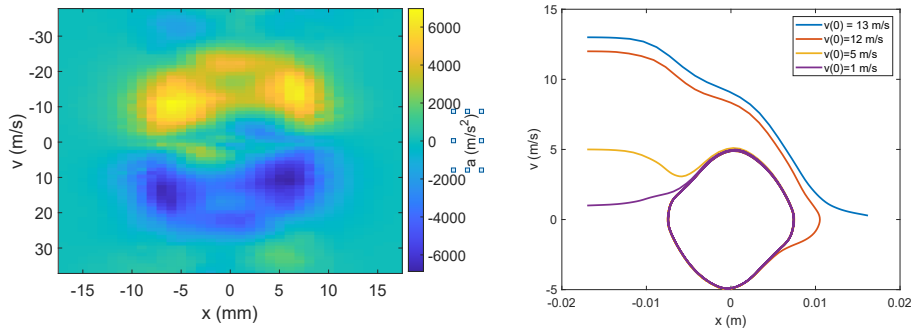


Figure 24:  $a(d, v)$  and phase plot for  $v_{capture}$  for  $|F = 1, J = 3/2\rangle$  dual frequency trapping MOT. Performance is comparable to the  $|F = 2\rangle$  MOT (See Figs. 15- 16).

### 3.1.2. Trap Stability

Once we have the  $a(d, v)$  map, along with a reasonable estimate of the scattering rate, it's relatively easy to setup a stochastic evolution that takes into account photon scatters. To keep things simple, I focus on 1D trapping (the OBEs themselves are 3D by necessity, but here I am assuming that the only relevant force, velocity, position, etc. is along the  $\hat{d}$  axis.), where we have the  $a(v, d)$  map along with a scattering rate  $R_s$ , which I assume for simplicity does not depend on  $v$  or  $d$  (it does, a little bit, but it's really only for  $\Lambda$ -cooling that it varies significantly enough to worry about).

Since the matlab documentation on stochastic OBEs is inscrutable to me (it seems to exist only for financial applications and uses very unfamiliar terminology), and the application is simple, I decided to do a very basic Eulerian simulation:

- Define  $R_s$  (scattering rate). Start at some reasonable position and velocity (say, 1 mm, 1 m/s) for  $t = 0$  (e.g., assume a trapped molecule). Define  $t_{Step} = 1/(R_s)$  (e.g., take a time step such that 1 scatter occurs). Define  $v_{kick} = \hbar k/m$ .
- Step  $x_{n+1} = x_n + v_n t_{Step}$
- Roll for two angles  $\phi_1$  and  $\phi_2$ . These determine the direction of each photon kick (I'm assuming we need to account for an 'absorption' kick and an 'emission' kick) with respect to the  $\hat{d}$  axis.
- Step  $v_{n+1} = v_n + v_{kick} \times (\cos \phi_2 + \cos \phi_1) + a(x, v) t_{Step}$
- Step  $t_{n+1} = t_n + t_{Step}$
- repeat until  $t = t_{max}$  (100 ms should be fine).

In Fig. 25 I plot the phase evolution in the 5-laser  $|F = 2\rangle$  dcMOT with and without this scattering term (choose  $R_s = 0.1\Gamma$ ). Here we see that the molecule trapping is robust to photon scatters (in principle, if there are enough scatters and the forces are weak enough, molecules could become un-trapped via scattering). This will become more important when we talk about low power MOTs.

### 3.1.3. Dependence on $\Delta, s_0$

Thus far I have only discussed simulations conducted for  $\Delta = -1.4\Gamma$  and  $s_0 = 14$ . I know that the latter is indeed what we have in the experiment while the former is taken from the magnetic quadrupole PRL. It is entirely possible that these are sub-optimal values: the Tarbutt group runs with  $\Delta = -0.75\Gamma$  (infact, they observe terrible trapping for  $-1.4\Gamma$  for their dcMOTs) and the Doyle group operates at around  $-1\Gamma$ . It's also possible that the optimal values are different for dc and rfMOTs. To that end, I tried two other simulations:  $\Delta = -0.75\Gamma$  (for both) and  $s_0 = \{7, 14\}$ . The results for  $F$  vs  $x, v$  (Fig. 26) and the capture velocity (Fig. 27) are below, for the rfMOT and for a 5-laser dcMOT operating on  $|F = 2\rangle$  (results are similar for  $|F = 1, J = 3/2\rangle$ ).

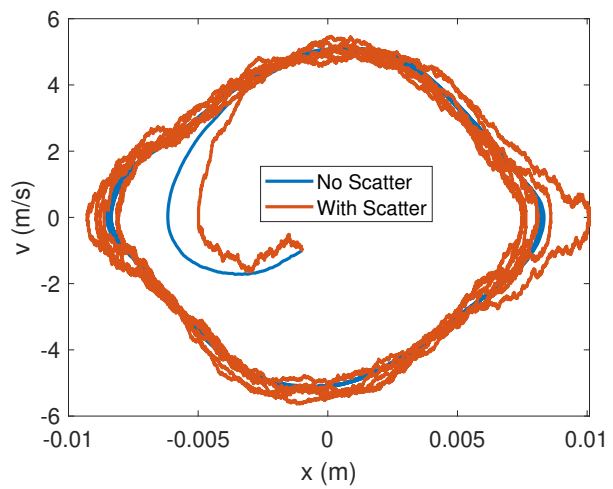


Figure 25: Phase plot with and without scatter for  $\Delta = -1.4\Gamma$ ,  $s_0 = 14$ , 5-laser dc  $|F=2\rangle$ . Here we see that the trap is robust to photon scatters.

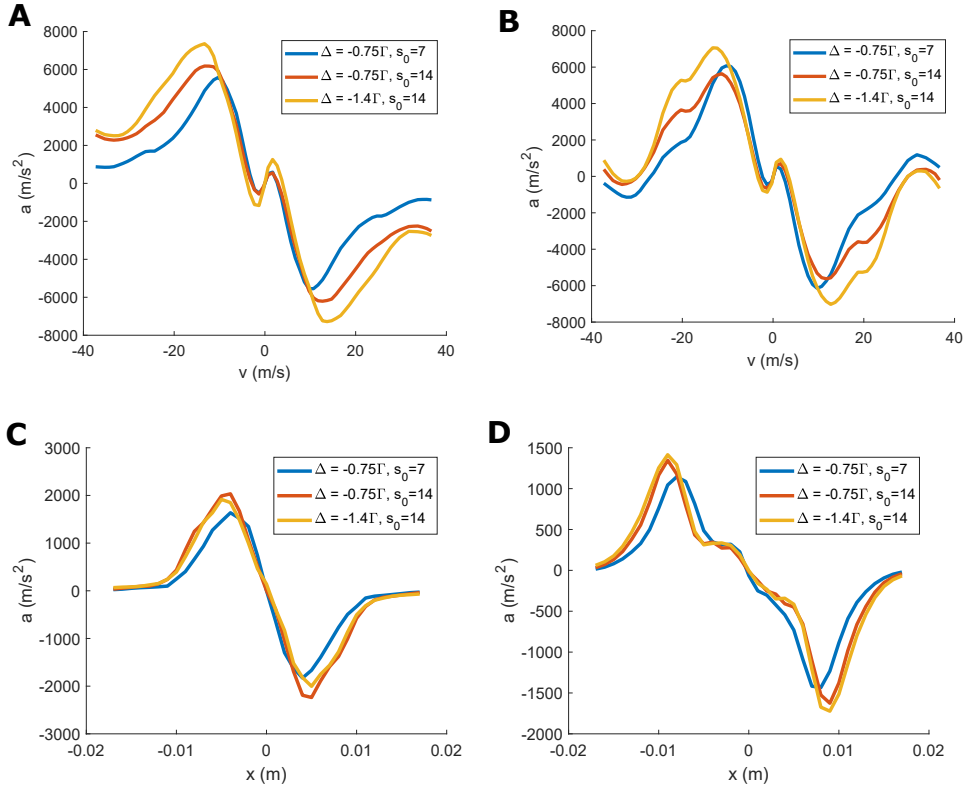


Figure 26: {A,B}:  $a$  vs  $v$  for a 5-laser dcMOT ( $|F = 2\rangle$ ) and the rfMOT, respectively, for different ‘high power’ MOTs. Notice that the sisyphus force weakens in the dc case for lower detuning, which is potentially why the Tarbutt group sees better performance for  $\Delta = -0.75\Gamma$  than for  $\Delta = -1.4\Gamma$ . {C,D}:  $a$  vs  $x$  for the same cases.

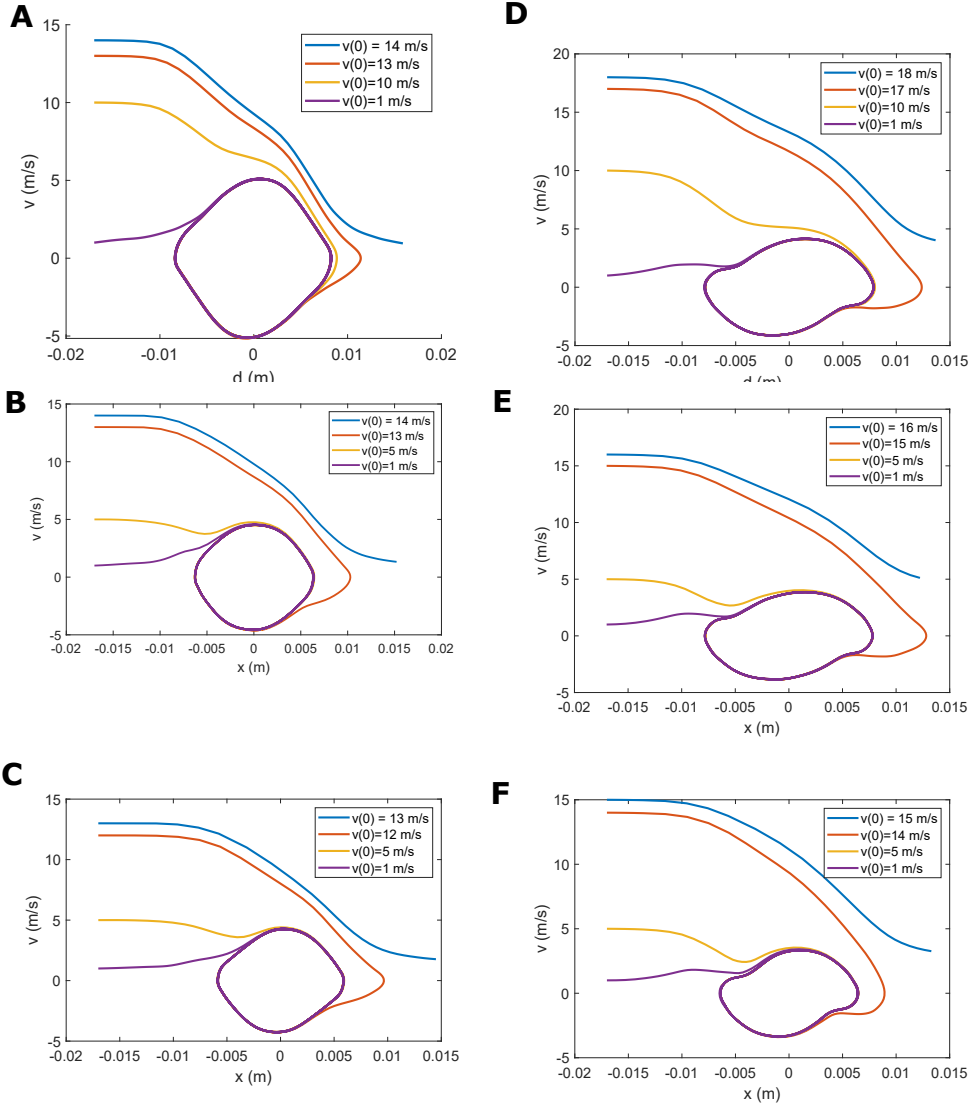


Figure 27: {A,B,C}: Capture velocity determination for a 5-laser dcMOT ( $|F = 2\rangle$ ) for  $\{(\Delta = -1.4\Gamma, s_0 = 14), (\Delta = -0.75\Gamma, s_0 = 14), (\Delta = -0.75\Gamma, s_0 = 7)\}$ . We see here that there is not much difference when  $\Delta$  is varied, contrary to what is observed by the Tarbutt group. Could be a result of some subtle differences between SrF and CaF. {D,E,F}: Same but for the rfMOT. Here we see that the performance is clearly worse for  $\Delta = -0.75$ .

### 3.2. Compressed/low power MOTs

After the initial capture of molecules, we decrease the laser power while increasing the gradient. This lowers the MOT temperature and compresses it as well. In our rfMOT, we lower the intensity from 100% to 4%, resulting in a  $s_0$  of 0.7 for each hyperfine level. I ran simulations at  $\Delta = -1.4\Gamma$  and  $\Delta = -0.75\Gamma$  for both dc and rfMOTs. Fig. 28 shows  $a(v)$  and  $a(x)$ . We also show example phase plots, with scatters included, for  $\Delta = -1.4\Gamma$  ( $R_s = 0.02\Gamma$  from simulation) (Fig. 29) and  $\Delta = -0.75\Gamma$  ( $R_s = 0.04\Gamma$  from simulation) (Fig. 30).

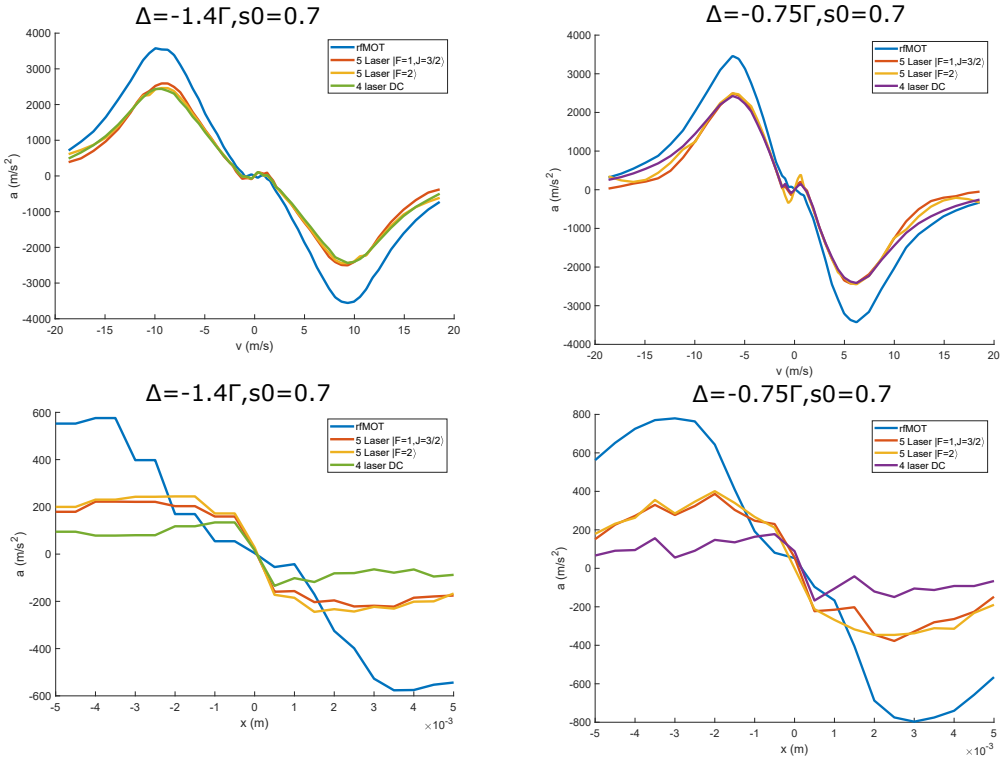


Figure 28:  $a(x)$  and  $a(v)$  for different MOT configurations for  $\Delta = -1.4\Gamma$  and  $\Delta = -0.75\Gamma$ . Clearly the rfMOT performs best.

The temperature that we observe for the dcMOT here is quite a bit higher than what is observed by the Tarbutt group for their optimum configuration (see Fig. 31) of  $10 \text{ mW/cm}^2$ ,  $\Delta = -0.75\Gamma$ . When they say their intensity is  $10 \text{ mW/cm}^2$ , they mean the total intensity at the MOT center (so, 24x the intensity of a single pass of 1 of the hyperfine addressing lasers). Thus, the intensity of a single pass of one laser addressing one hyperfine level is  $0.4 \text{ mW/cm}^2$ . The  $I_{sat}$  for CaF is  $4.9 \text{ mW/cm}^2$ , and so their saturation parameter is 0.1, not 0.7, which would correspond to  $83 \text{ mW/cm}^2$  when all beams are considered, for which they measure a temperature of roughly  $3.5 \text{ mK}$ , much closer to what we see in Fig. 30B.

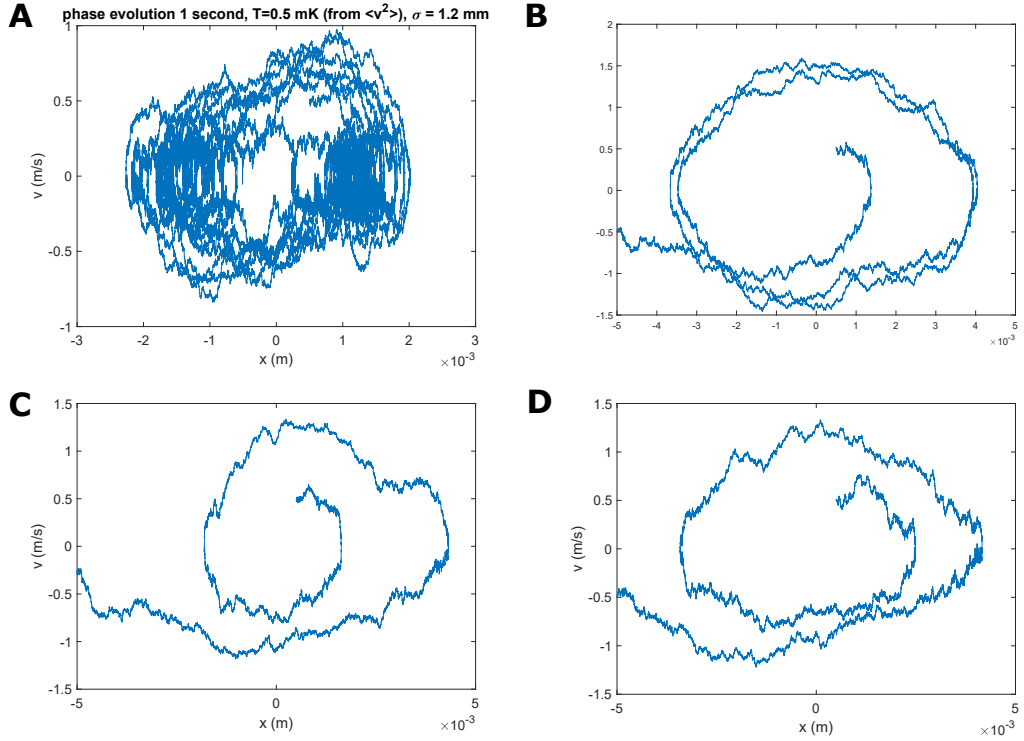


Figure 29: {A,B,C,D}: {RFMOT, 5-laser DC MOT ( $|F = 1, J = 3/2\rangle$ ), 5-laser DC MOT ( $F=2$ ), 4-laser DC MOT}. Phase plots with scatter for initial conditions  $(x,v) = (0.5 \text{ mm}, 0.5 \text{ m/s})$  for  $\Delta = -1.4\Gamma$ ,  $s_0 = 0.7$  ( $R_s = 0.02\Gamma$  from simulation). Clearly, the trapping is quite weak for all DC cases (I consider the molecule 'untrapped' if  $|x| > 5 \text{ mm}$ . It's possible the molecule could come back). For the rfMOT, the  $T$  and  $\sigma$  values are pretty much what we see in the experiment.

It's possible that a dcMOT wants to operate at a lower intensity than what we use for our rfMOT. I thus ran simulations for  $s_0 = 0.1$ ,  $\Delta = -0.75\Gamma$  ( $R_s = 0.01\Gamma$  from simulation). Fig. 32 shows  $a(v)$  and  $a(x)$ . We also show example phase plots, with scatters included, in Fig. 33. The temperature is indeed lower for the dc case at this intensity. We once again see that only the 5-laser  $|F = 1, J = 3/2\rangle$  configuration keeps the molecule within  $|x| < 5 \text{ mm}$ .

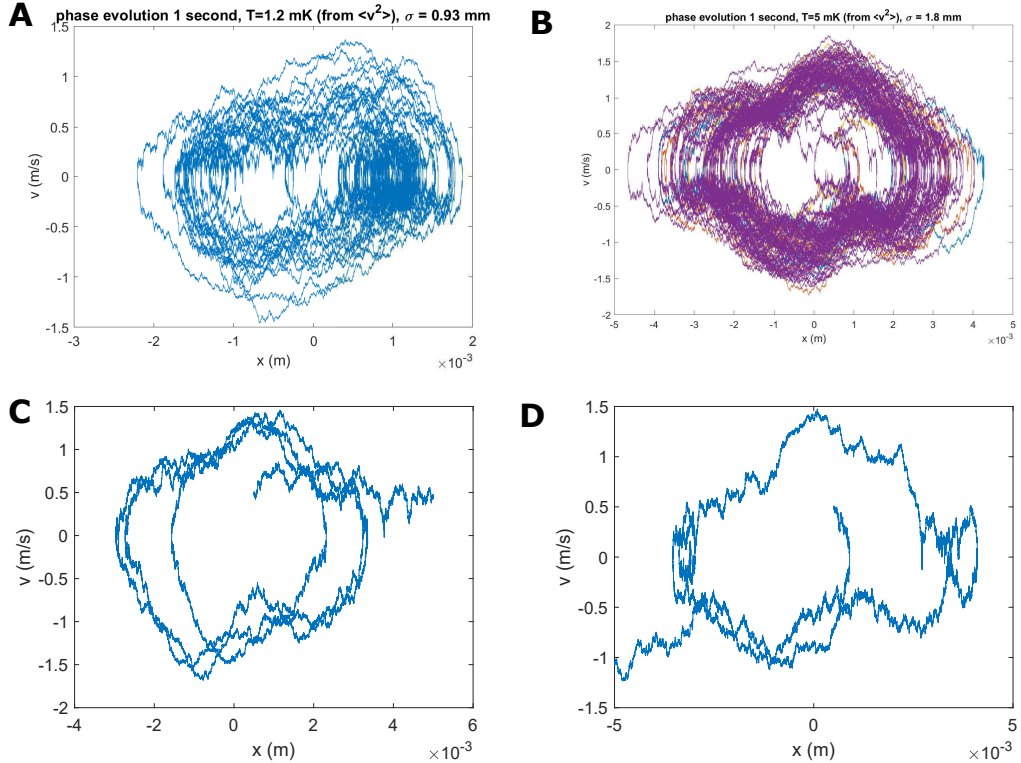


Figure 30: {A,B,C,D}: {RFMOT, 5-laser DC MOT ( $|F = 1, J = 3/2\rangle$ ), 5-laser DC MOT ( $F=2$ ), 4-laser DC MOT}. Phase plots with scatter for initial conditions  $(x,v) = (0.5 \text{ mm}, 0.5 \text{ m/s})$  for  $\Delta = -0.75\Gamma$ ,  $s_0 = 0.7$  ( $R_s = 0.04\Gamma$  from simulation). The trapping is a bit better for the DC cases at this detuning, and the molecule remains trapped for the 5-laser  $|F = 1, J = 3/2\rangle$  case (though the temperature and spread are higher than for the rfMOT). For the rfMOT, the  $T$  and  $\sigma$  values are pretty much what we see in the experiment.

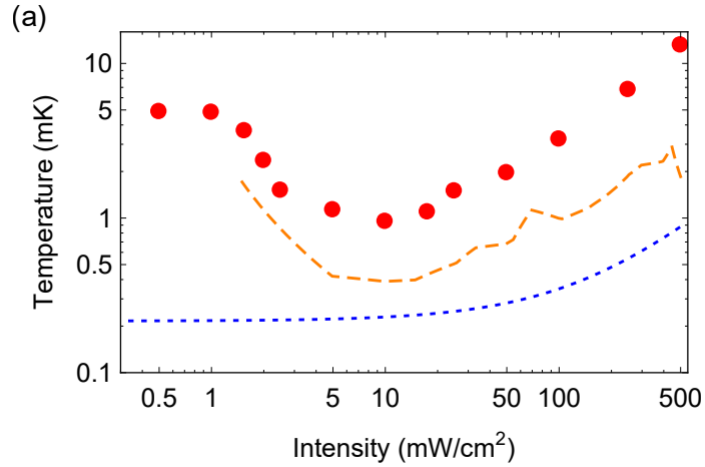


Figure 31: Taken from [here](#). The optimum intensity corresponds to  $s_0$  of 0.1.

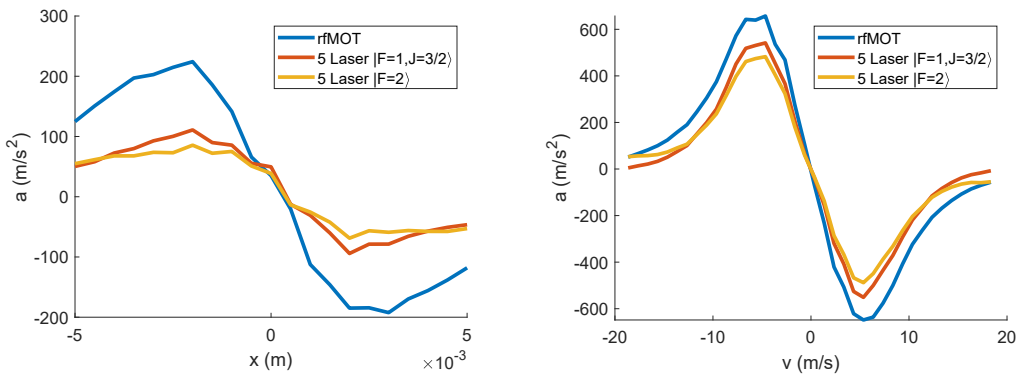


Figure 32:  $a(x)$  and  $a(v)$  for different MOT configurations for  $s_0 = 0.1$ ,  $\Delta = -0.75\Gamma$ . Clearly the rfMOT performs best.

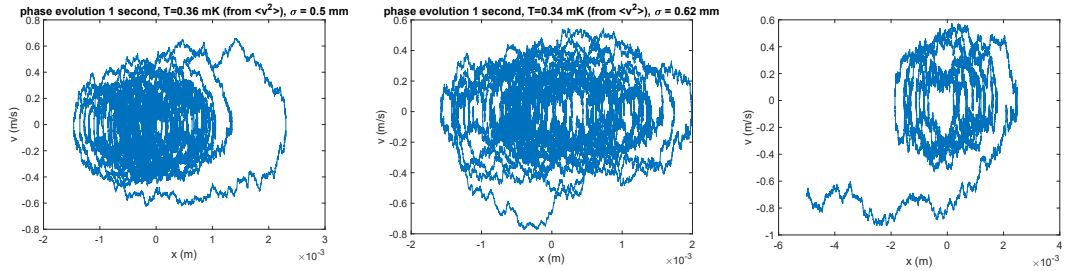


Figure 33: Left to right: rf, 5-laser  $|F = 1, J = 3/2\rangle$ , 5-laser  $|F = 2\rangle$ . Phase plots with scatter for initial conditions  $(x, v) = (0.5 \text{ mm}, 0.5 \text{ m/s})$  for  $\Delta = -0.75\Gamma$ ,  $s_0 = 0.1$  ( $R_s = 0.01\Gamma$  from simulation). The molecule remains trapped for the 5-laser  $|F = 1, J = 3/2\rangle$  case, and at a lower temperature than for  $s_0 = 0.7$  (Fig. 30), as predicted in Fig. 31.

### 3.3. Blue MOTs

For any kind of MOT, it is true that the sign of  $a(v)$  will flip with detuning (e.g. for ‘Type-I’ MOTs the force shifts from cooling to heating), while the sign of  $a(x)$  will flip with either detuning, polarization, or field orientation (just think about how a MOT works). So, if both detuning and polarization, for example, are flipped, the sign of  $a(v)$  will reverse while the sign of  $a(x)$  will not.

For Type-I MOTs, this has no utility: there’s no case where you would want a purely ‘heating’ force. For Type-II MOTs, however, one could imagine creating a blue-detuned MOT where the cooling force is provided by the Sisyphus cooling. This would be terrible for the initial trapping: the sub-Doppler force is only effective for low velocities, while you want as high of a capture velocity as possible when initially trapping. But, once you’ve trapped the molecules and cooled them sufficiently, it can make sense to ‘switch’ both polarization and detuning, retaining your confinement while switching from ‘Doppler-cooling + Sisyphus heating’ to ‘Doppler-heating + Sisyphus-cooling’. This will work as long as the sub-Doppler cooling is robust to magnetic fields, which is true up to surprisingly large fields (see Sec. 2.6)

This was implemented by the Tarbutt group in Rb. The Rb level-diagram used in this case is shown in Fig. 34. Initially, atoms were collected in a conventional MOT, operating on the  $F = 2 \rightarrow F' = 3$  transition. After molecules are collected, the MOT laser frequencies are shifted such that only the  $F = 2 \rightarrow F' = 2$  and  $F = 1 \rightarrow F' = 1$  transitions are driven, at detuning  $\Delta > 0$ . The resulting MOT had a number of interesting properties: it was pretty small ( $\sim 300\mu\text{m}$ ), it was a very low temperature ( $30\mu\text{K}$ ), and it had a density comparable to dark SPOT MOTs, and better than conventional MOTS (this is due to the reduced scattering during Sisyphus-like excitations, during which the atoms are spending lots of time in dark-states, reducing the multiple-scattering events that otherwise limit peak density).

Molecule experiments would benefit a lot from this: we’re forced to use Type-II transitions anyway, so we may as well get something out of it. Lower temperatures and smaller and denser clouds would help a lot for optical dipole trapping. Plus, if our sizes and temperatures wind up even close to what was observed in Rb, I can easily imagine that we could simply hold molecules in the blueMOT while the ODT is active, collecting molecules into the ODT the whole time (as opposed to trying to catch molecules from a falling, expanding cloud, even if that expansion and descent are slowed by  $\Lambda$ -cooling).

To that end, I ran similar simulations for a 4-laser blueMOT (see Fig. 35). For this MOT, all frequencies except for the one corresponding to  $|F = 0\rangle$  are blue-shifted and have reversed-polarization with respect to their optimum 4-laser dc-redMOT configuration. The  $|F = 0\rangle$  transition is a Type-I transition, and so is always optimized for red-detuning, hence why I left it unchanged.

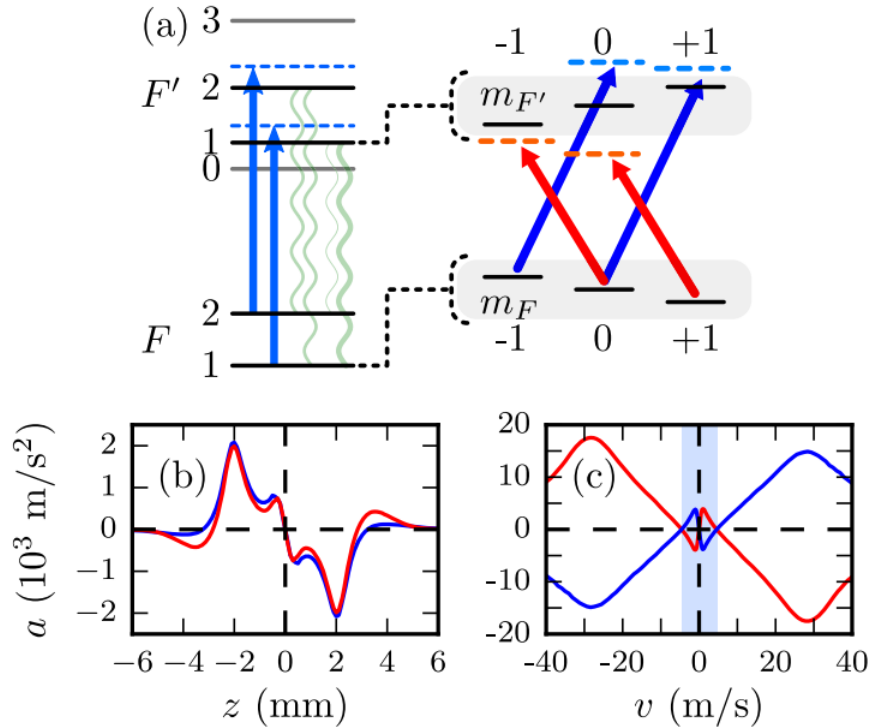


Figure 34: Figure from [PRL 120 083201 \(2018\)](#)(a): Level diagram for Type-II Rb MOT.  $F=1 \rightarrow F'=1$  and  $F=2 \rightarrow F'=2$  must be driven. As they note: the g-factor for  $F = 1$  and  $F' = 1$  have opposite sign. As indicated: the red-detuned MOT and blue-detuned MOT will work on opposite polarization. (b):  $a(z)$  for  $\{(red, \sigma^-), (blue, \sigma^+)\}$  (results from OBE simulations). As expected, the curves are similar. (c) Same but for  $a(v)$ . This curve has flipped sign, also as expected. The red-detuned case will have doppler-cooling and sub-Doppler heating while the blue-detuned case will have doppler-heating and sub-doppler cooling. If velocities are already low enough ( $< 5 \text{ m/s}$  in this case.  $v_T = 5 \text{ m/s}$  for  $T = 250 \text{ mK}$  so this isn't especially difficult), the blue-MOT will work.

What I found surprised me: according to the simulations, an SrF blue-MOT should perform very well. The resulting  $a(x, v)$  heat map and associated ‘phase-with-scatter’ plot (from which temperature,  $\sigma$  are determined as explained previously) are shown in Fig. 36 (simulation found  $R_s = 0.015\Gamma$ ). The integrated  $a(x)$  and  $a(v)$  curves are shown in Fig. 37.

Since one could argue that the  $a(x)$  curve is obtained in a somewhat biased manner by averaging over  $\int_{v_{min}}^{v_{max}} a(d, v)$  where  $v$  is coaligned with  $\hat{d}$  (random velocities corresponding to 100 \$\mu\$K distribution were chosen for the velocities along axes orthogonal to  $\hat{D}$ ), I also

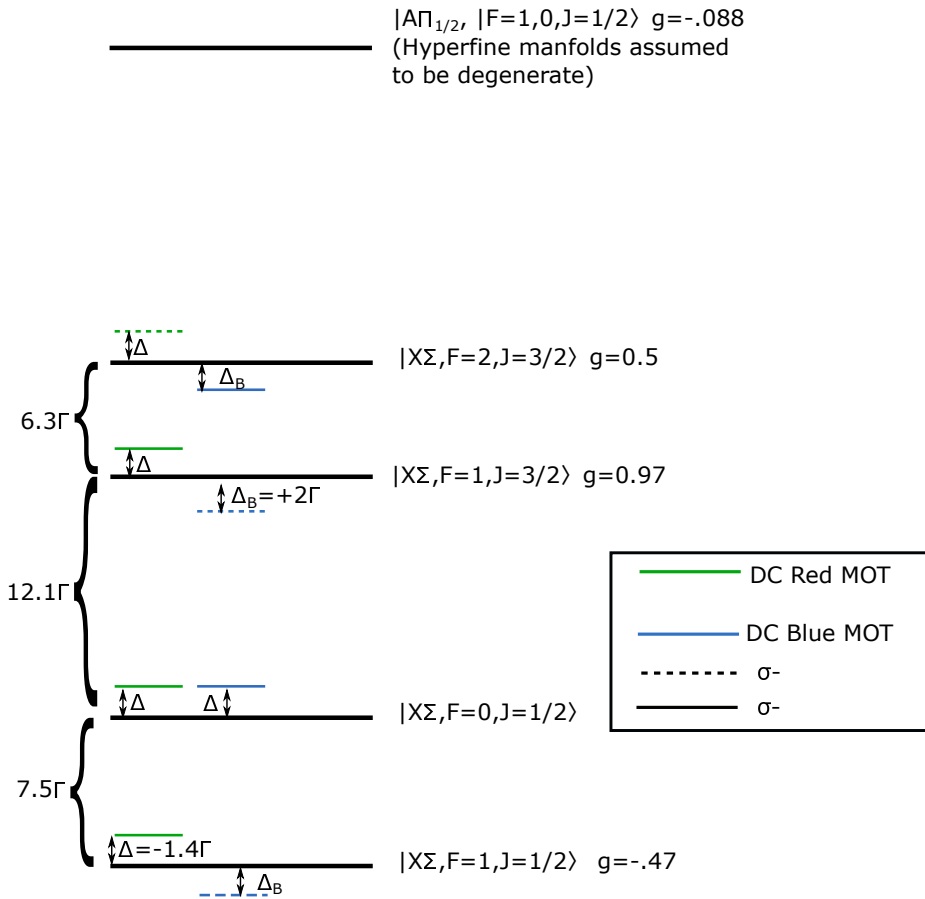


Figure 35: Level diagram for DC blue MOT. All polarizations and detunings are reversed with respect to the optimum 4-laser red-dcMOT except for  $|F = 0\rangle$ , since that state does not have a sisyphus effect, switching it to blue would only hurt us.

ran a different simulation for which the direction of  $v$  is chosen randomly for a given displacement  $d$ , after which  $F \cdot \hat{d}$  is calculated. I then run the same simulation for  $-\vec{v}$  and once again record  $F \cdot \hat{d}$ . I did this 1280 times and averaged the results (this is also what I did in Fig. 3, which worked pretty well, and I believe what M Tarbutt did in <https://arxiv.org/pdf/1608.04645.pdf>). The data is noisy (cyan dots in Fig. 37), but it is consistent with the integrated plot.

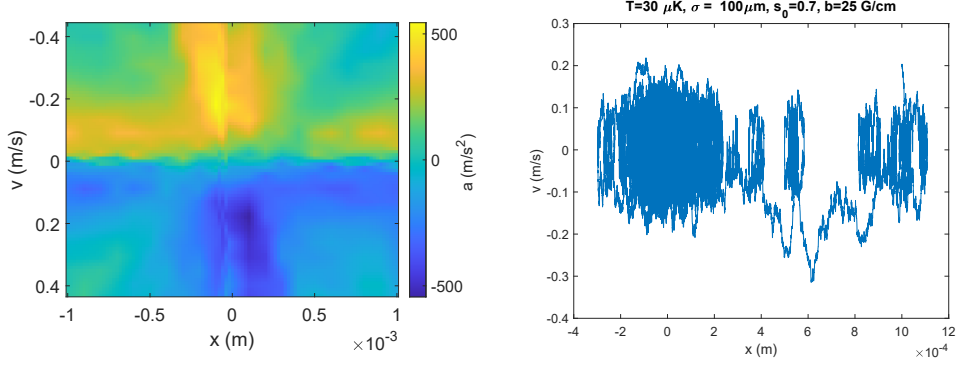


Figure 36: Left:  $a(x, v)$  for blue MOT ( $\Delta_B = 2\Gamma$ ,  $\Delta_{F=0} = -1.4\Gamma$ ,  $s_0 = 0.7$ , measured  $R_s = 0.015\Gamma$ ). Right: Resultant phase map + scatters plot, with  $T$  and  $\sigma$  from  $\langle v^2 \rangle$  and  $\langle x^2 \rangle$ . These numbers almost seem too good to be true: if we get anything close to this I'd be ecstatic

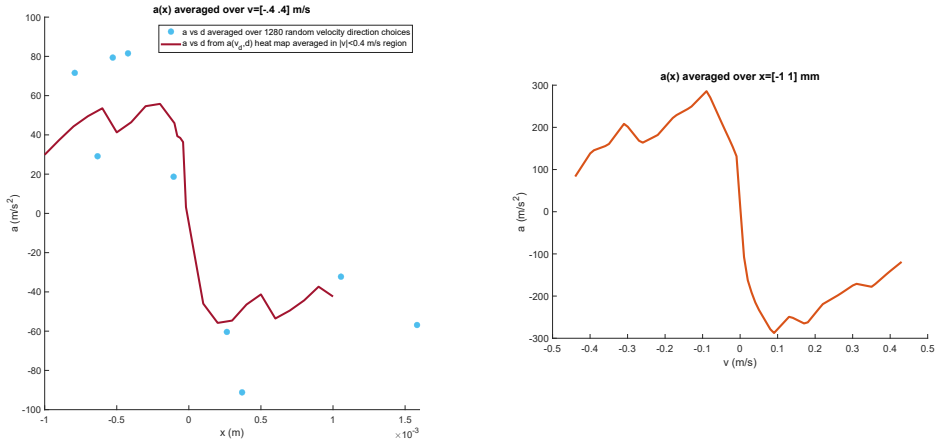


Figure 37: Left:  $a(x)$ . Line is taken by integrating the heat map on the left of Fig. 36. Dots from simulating 1280 velocity directions for a given  $d$  and averaging the resulting  $F \cdot \hat{d}$ . Inherently noisier but no-longer assumes that velocity is along  $\hat{d}$ . The results are definitely consistent. Right:  $a(v)$ . If we went much further in  $v$ , we would escape the Sisyphus region and the force sign would reverse.

### 3.4. The 'simple' approach: a way to seamlessly transition from red dcMOT to blue dcMOT without any polarization switching, without turning the coils on/off, and without switching coil direction

Consider the following laser excitation scheme (schematically illustrated on the left hand side of Fig. 38):

- $\sigma^-$  laser carrier frequency red-detuned with respect to  $|F = 1, J = 3/2\rangle$ . This passes thru an EOM driven with a frequency of 41.4 MHz (the difference between  $|F = 1, J = 3/2\rangle$  and  $|F = 2, J = 3/2\rangle$ ). The EOM is driven strongly enough that the carrier and the 1st-order sidebands have similar intensity (this gives roughly a 3:31:31:31:3 power ratio, where I've included the 2nd order sidebands).
- $\sigma^+$  laser carrier frequency red detuned with respect to  $|F = 0\rangle$  and driven with a 53.4 MHz EOM (a little bit larger than the difference between  $|F = 1, J = 1/2\rangle$  and  $|F = 0\rangle$ , and a lot less than the difference between  $|F = 0\rangle$  and  $|F = 1, J = 3/2\rangle$ ). Similarly, this EOM is driven such that the carrier and the 1st-order sidebands have similar intensity (again, giving roughly a 3:31:31:31:3 power ratio, where I've included the 2nd order sidebands).

On inspection, this configuration is pretty close to the  $|F = 1, J = 3/2\rangle$  5-laser DC-MOT configuration (See Fig. 21, the optimal configuration is replicated by the red lines in Fig. 38), so it seems likely that this should work for molecule trapping. To make it clearer, let's consider the 8 total 'lasers' illustrated by the green lines on the left hand side of Fig. 38 one-by-one, starting from the 'top' (e.g., red-detuned of  $|F = 2, J = 3/2\rangle$ ) (NOTE: I included 2nd order sidebands that I thought may be relevant. These have 1/10 the power of the carrier (indicated by 'C') and the first order sidebands, and the lines are smaller to reflect this):

- 1st order red-sideband of the  $\sigma^-$  carrier. This is detuned by -6 MHz from  $|F = 2, J = 3/2\rangle$ , with the correct polarization for spatial confinement.
- 2nd order red-sideband of the  $\sigma^+$  carrier. This is detuned by +4.1 MHz from  $|F = 2, J = 3/2\rangle$ . This may harm Doppler-cooling somewhat, although since it's 1/10 the intensity of the red-detuned light addressing this transition I'd think it wouldn't hurt too much. As for confinement: this happens to be the correct polarization for confinement with blue-detuned light addressing this state, so it may help the confinement even if it hurts Doppler-cooling.
- The  $\sigma^-$  carrier. This is detuned by -6 MHz from  $|F = 1, J = 3/2\rangle$  and, combined with the next beam, gives the correct polarization scheme for dual-Frequency dc-MOT confinement (see Sec. 3.1.1).
- 1st order red-sideband of the  $\sigma^+$  carrier. This is detuned by +16.3 MHz from  $|F = 1, J = 3/2\rangle$  and, combined with the previous beam, gives correct polarization for dcMOT confinement.

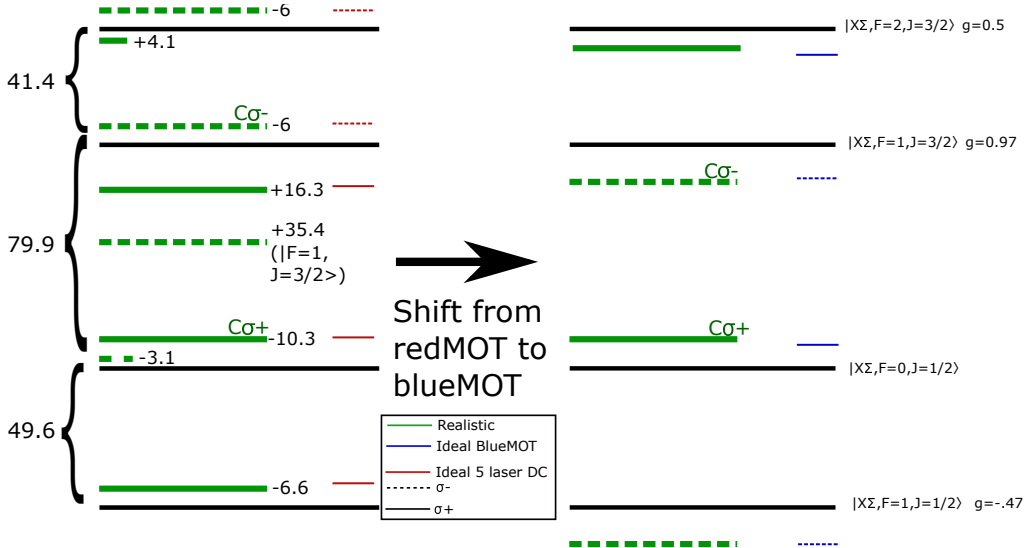


Figure 38: Experimentally accessible configurations for a DC redMOT and a blue MOT without having to switch either polarization or MOT coil current direction. The length of the green lines indicate the relative intensity of that carrier/sideband. The number next to the green line indicates the detuning (in MHz) with respect to the closest hyperfine level. The  $C\sigma^\pm$  indicate the carrier. **Left:** red dcMOT designed to replicate, as closely as possible, the conditions of the 5-laser dual-frequency ( $|F = 1, J = 3/2\rangle$ ) dcMOT. **Right:** If the  $\sigma^-$  carrier is blue-shifted (via an AOM), and the EOM frequencies are changed (either by using a wideband fiber EOM or just using a separate EOM), the optimal blueMOT configuration is replicated, without having to use either a Pockel's Cell or switch the MOT coil current direction.

- 1st order blue-sideband of the  $\sigma^-$  carrier. This is pretty far detuned from all transitions (closest is  $|F = 1, J = 3/2\rangle$ , to which it is +34.7 MHz detuned). I don't anticipate this laser being relevant, but I included it in my simulations just to be safe.
- The  $\sigma^+$  carrier. This is detuned by -10.3 MHz from the  $|F = 0, J = 1/2\rangle$  transition. The polarization of this beam does not matter too much for confinement, however, to the extent that it does matter, this is the correct polarization for confinement.
- 2nd order blue sideband of  $\sigma^-$  carrier. This is a weak beam but it's close to resonance for the  $|F = 0, J = 1/2\rangle$  state, only being detuned by -3.1 MHz. It probably doesn't matter but I include it in the simulation anyway.
- 1st order blue-sideband of the  $\sigma^+$  carrier. Red detuned by -6.6 MHz from  $|F = 1, J = 1/2\rangle$ . This has the correct polarization for confinement from this state.

Next, consider what happens if we do the following:

- The  $\sigma^-$  laser is blue-shifted by  $\sim 3\Gamma$  (using double pass AOM, as we do now), such that it is now blue-detuned with respect to  $|F = 1, J = 3/2\rangle$ . Simultaneously, switch the EOM frequency to 129.5 MHz (the frequency difference between  $|F = 1, J = 3/2\rangle$  and  $|F = 1, J = 3/2\rangle$ ), such that ‘blue’ sideband is blue detuned with respect to  $|F = 1, J = 1/2\rangle$ . The red sideband will be very far red-detuned with respect to all transitions, and so I assume it is irrelevant.
- Do not change the frequency of the  $\sigma^+$  laser. Instead, just change the EOM frequency to roughly 104 MHz. The difference between  $|F = 0\rangle$  and  $|F = 2, J = 3/2\rangle$  is 121.3 MHz, and thus if the carrier is, say, 7 MHz red-detuned with respect to  $|F = 0\rangle$ , then the red-detuned sideband will be 10 MHz **blue**-detuned with respect to  $|F = 2, J = 3/2\rangle$ . The blue sideband will be very far blue-detuned with respect to all transitions, and so I assume it is irrelevant.

As we see in Fig. 38, this configuration is identical to the optimum blueMOT configuration (see Fig. 35, which is replicated in blue in Fig. 38). As such, I don’t need to simulate this again. The ‘realistic’ redMOT though has enough differences that I figured it was worth it to simulate this particular configuration.

### 3.4.1. High Power redMOT

In order to see whether this could be made to work for our system, I first simulated the high power ‘collection’ MOT (note: I chose  $s_0 = 10$  for the ‘intense’ sidebands and  $s_0 = 1$  for the ‘weak’ sidebands in Fig. 38). In Fig. 39 I compare the resulting  $a(x)$  and  $a(v)$  curves from the ‘realistic’ 8-laser case to the ‘ideal’ 5-laser case. Curiously, the realistic simulation seems to do better in some ways, specifically, the sisyphus heating seems to have somehow been negated, either by the addition of all the other lasers, or else by the specific detunings that I had to use. The capture velocity winds up a little bit higher as well, see Fig. 40.

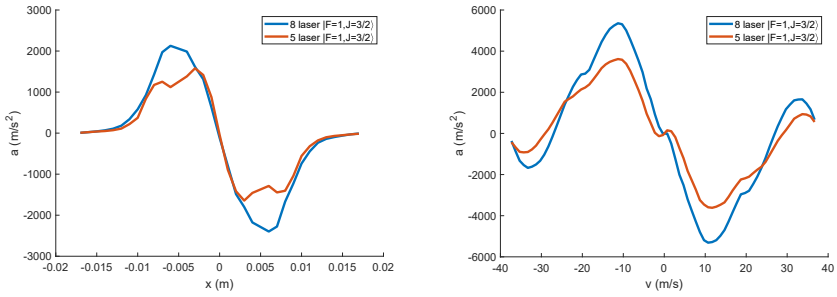


Figure 39:  $a$  vs  $x, v$  plots for the ‘realistic’ (Fig. 38, left, green) and ‘ideal’ (Fig. 38, left, red) cases ( $b = 12.5 \text{ G/cm}$ ). We observe that the ‘realistic’ case actually looks better in a number of ways: The overall forces are a bit larger and the sisyphus heating is much lower.

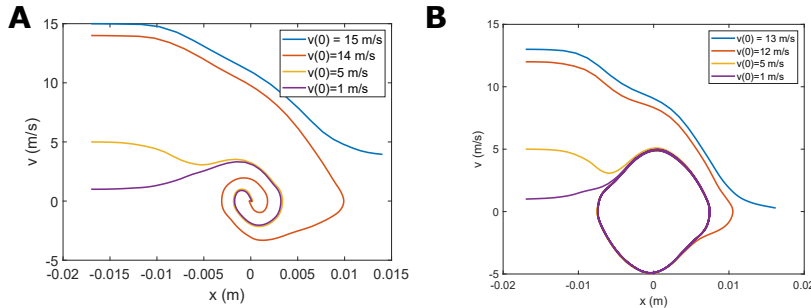


Figure 40: **A:** Phase plots for  $v_{capture}$  for the ‘realistic’ configuration (Fig. 38, left, green). **B:** Same, but for ‘ideal’ case (Fig. 38, left, red). Curiously, it looks like the ‘realistic’ scheme works a bit better, I think primarily due to whatever is destroying the Sisyphus heating.

I also took a look at the trap stability and expected properties by modeling the scattering (see Sec. 3.1.2). The simulation found a scattering rate of  $R_s = 0.15\Gamma$ . As a result of the sisyphus force being so weak for this configuration, the equilibrium

temperature and size are both quite small, see Fig. 41! I don't know how optimistic to be regarding whether I would see a similar result in the lab, but it's not *not* promising...

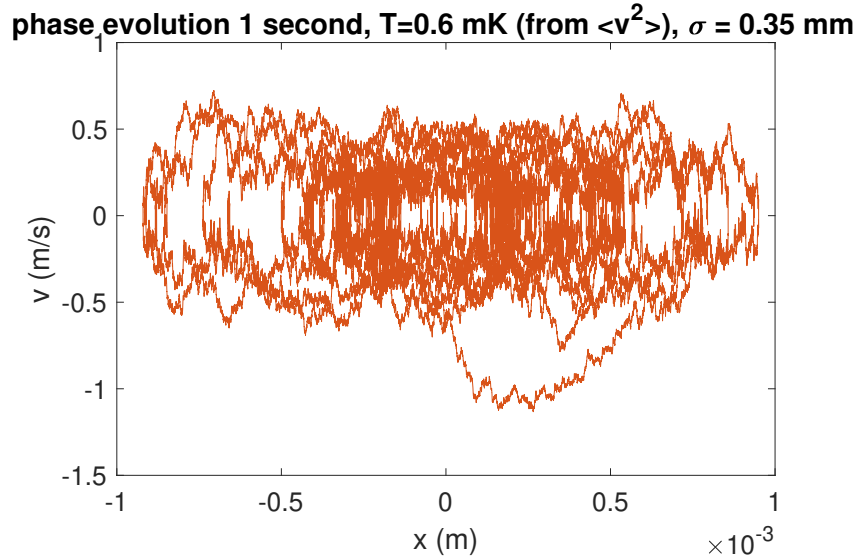


Figure 41: Phase plot with scatter for ‘realistic’ high power configuration. Here we see a pretty tight, low-ish temperature cloud, in contrast to what we see for our current high power rfMOT, which is roughly 4 mm wide and quite hot ( $T \geq 20$  mK). No clue whether we’d actually see this in the lab but it’s worth investigating I suppose.

### 3.4.2. Lower Power ‘8-laser’ MOTS

Of course, I don’t think it’s wise to assume that these interesting features (low size, low temperature due to little/no Sisyphus force) that I see in the simulation will necessarily show up in the experiment, since in all other cases we have had to lower power and increase gradients to achieve low  $T$  and  $\sigma$ . Since this is a case I wanted to study in great detail, I ran simulations during ‘middle’ stages of a mock compression ramp, specifically, one for  $\{s_0 = 5, b = 12.5 \text{ G/cm}\}$  and another for  $\{s_0 = 2.5, b = 19 \text{ G/cm}\}$ , in addition to at the ‘end’ low-power high gradient stages (discussed later). As the power is lowered, the sisyphus-heating seems to show up again (Fig. 42). Nevertheless, the molecules still remain trapped (Fig. 43), so if the anomalous high-power behavior (low  $T$  and  $\sigma$  due to no Sisyphus) doesn’t actually manifest, at the very least we should be able to go to a ‘compressed’ MOT in the normal way.

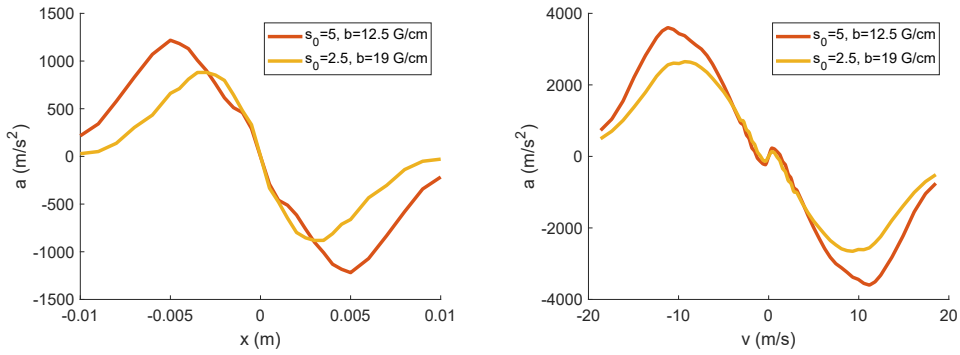


Figure 42:  $a$  vs  $x, v$  plots for the ‘realistic’ (Fig. 38, left, green) case for ‘mid-range’ powers during the mock compression ramp.

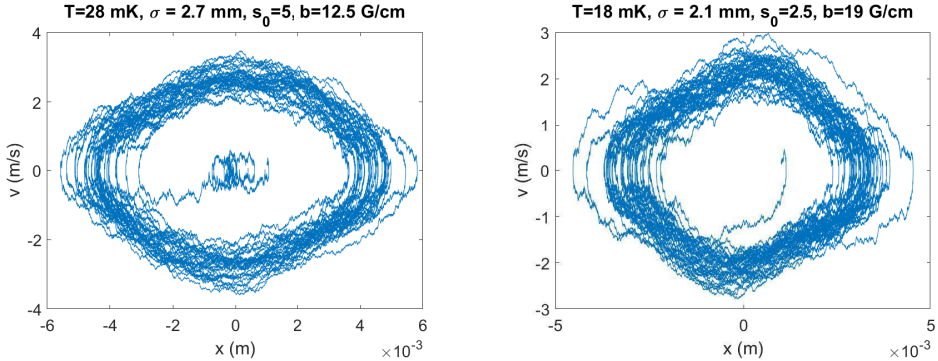


Figure 43: Phase plot with scatter for ‘realistic’ powers accessed during a mock compression ramp. The molecules do not seem to escape the trap at either power + gradient combination.

I also ran a few other simulations at the end stage of compression, specifically for

$s_0 = 1$  and  $s_0 = 0.1$  (these are intensities of the ‘intense’ lines, the 2nd order sideband intensities are thus 0.1 and 0.01 for the respective simulations), both at  $b = 25 \text{ G/cm}$ , just to make sure that the molecules still experience both damping and confinement.

Here, I would argue that we observe a greater level of similarity between the results for the ‘8-laser’ case and the ‘ideal-case’ than in the ‘high power’ MOTS. As a result, for the  $s_0 = 1$  MOT I find an expected  $T = 6.7 \text{ mK}$  and  $\sigma = 1.6 \text{ mm}$  (Fig. 45), while for  $s_0 = 0.1$  I find  $T = 0.37 \text{ mK}$  and  $\sigma = 0.65 \text{ mm}$  (Fig. 47), which is similar to what we observed in the ‘ideal’ case (Figs. 30 and 33).

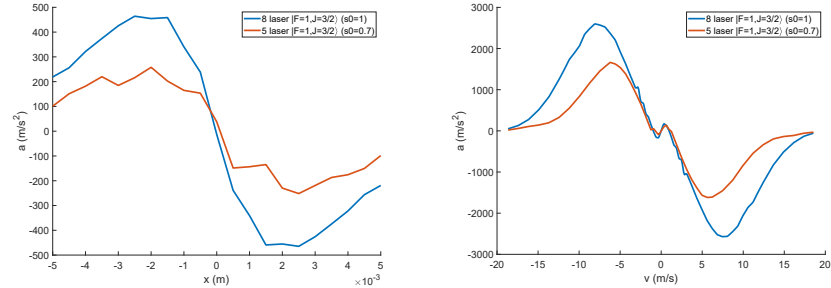


Figure 44:  $a$  vs  $x, v$  plots for the ‘realistic’ (Fig. 38, left, green) and ‘ideal’ (Fig. 38, left, red) cases for ‘moderate’  $s_0 = 1$  ( $b = 25 \text{ G/cm}$ ). Unlike the high power case (Fig. 39), we observe that the 8-laser case retains a substantial sisyphus force similar in strength to the ‘ideal’ 5-laser case.

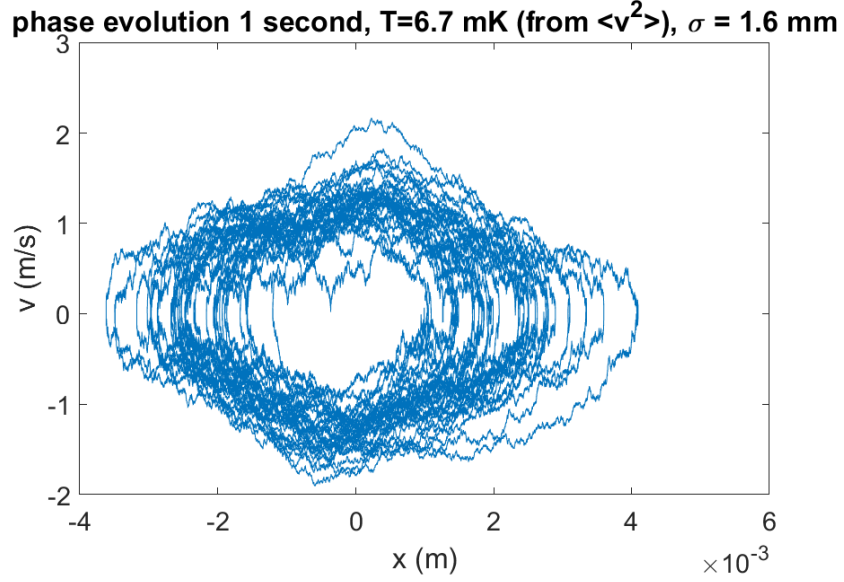


Figure 45: Phase plot with scatter for ‘realistic’ moderate power ( $s_0 = 1$ ) configuration. The size and temperature we find are similar to the ‘ideal’ case (Fig. 30)

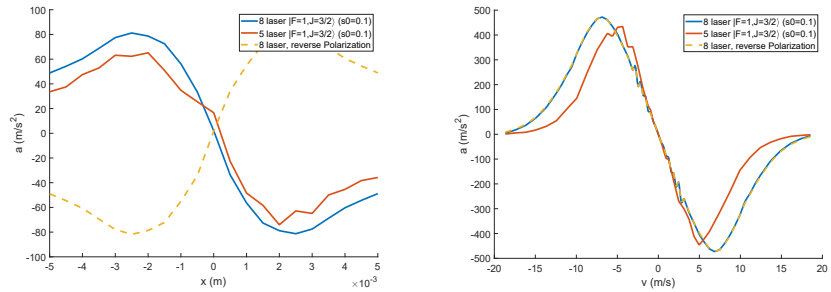


Figure 46:  $a$  vs  $x, v$  plots for the ‘realistic’ (Fig. 38, left, green) and ‘ideal’ (Fig. 38, left, red) cases for ‘low’  $s_0 = 0.1$  ( $b = 25 \text{ G/cm}$ ). The results are very similar. Also, as a sanity check I re-ran the simulation with reversed polarizations. I observed that the  $a(x)$  curve is negated while the  $a(v)$  curve remains the same: the latter should depend only on the detuning, which remained the same, while the former should flip with either the polarization or detuning. Thus, at least in this regard the simulation matches expectations.

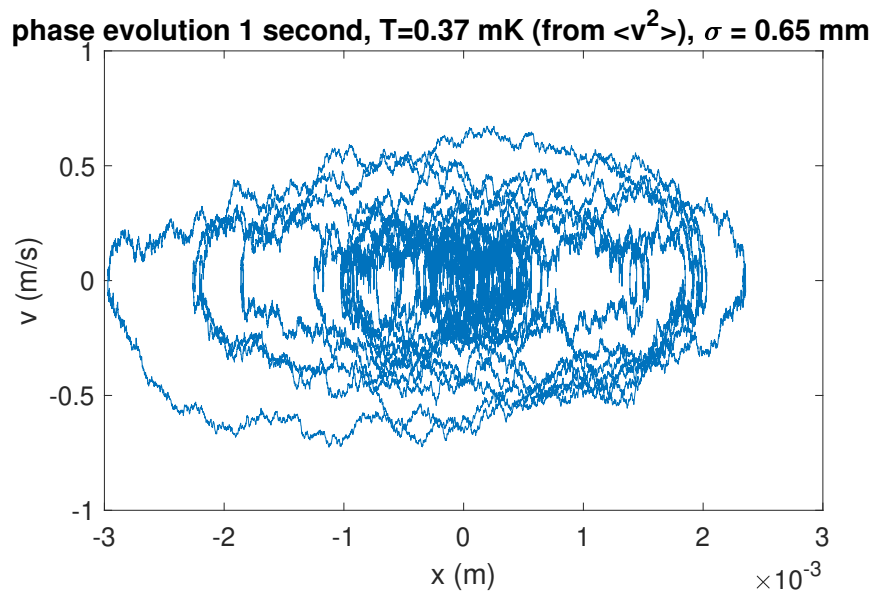


Figure 47: Phase plot with scatter for ‘realistic’ low power configuration. The size and temperature we find are similar to the ‘ideal’ case (Fig. 33)

## 4. Type II Zeeman Slower

Another application of this code could be to simulate a Type-II Zeeman Slower. This is described [here](#). A Type-II slower seems impossible for the same reason that a Type-II MOT seems impossible, namely that there cannot be a cycling transition between stretched states. However, unlike the MOT, we can't really use an 'rf-Zeeman slower', since a Zeeman slower depends on there being a static relationship between the magnitude of the Zeeman shift and the position along the molecular beam axis (perhaps if you had an 'rf-square wave' field...but that seems tough particularly since the coil inductance is going to be pretty large for Zeeman coils). Further, there are no polarization or intensity gradients, and so even the things that make dcMOTs feasible do not work for Zeeman slowers.

Nevertheless, it seems like a Type-II slower can work. To demonstrate the scheme, I will consider the simplest possible Type-II system: a  $J = 1/2 \rightarrow J' = 1/2$  system. This system is considered in Fig. 48. Here, we have one laser that acts like a conventional Zeeman slowing laser: narrow, red-detuned, and circularly polarized, such that, at a given field, only atoms with a given velocity are resonant. If the field strength increases as the atoms move (while also being slowed), then this condition occurs for progressively lower velocity (thus keeping the progressively slower atoms on resonance as they traverse the slowing region). In this way, you can continuously both reduce the atom velocity while also compressing the velocity profile (unlike for white-light slowing, where all molecules are 'equally' likely to scatter and thus no compression can occur).

However, since we are not exciting a stretched transition, atoms can decay to the opposite zeeman state, from which it must be repumped. The dependence of the velocity for which this repump is resonant has the *opposite* dependence on the B field (Fig. 48). So, if both lasers are narrow, then there is only one combination of velocity and B field for which both lasers are resonant (where the thick green and purple lines cross in the right hand side of Fig. 48), and so all other atoms are quickly pumped to the dark ground zeeman state, destroying the slowing mechanism. We can get around this by broadening the repump laser widely enough that it is always has some component on resonance given the combined doppler and zeeman shift for the transition (magenta shading in Fig. 48).

Then, if the  $\nu_{slow}$  transition, after Zeeman, doppler, and laser detuning are considered, is resonant, the atom will cycle photons no matter which ground state zeeman level it is in. If it is off resonant (e.g. if it is moving too slowly for the B-field at the atom's location), then it will be pumped to  $m_s = 1/2$  and no-longer scatter from the narrow laser that is exciting that transition until it travels to a region of higher magnetic field.

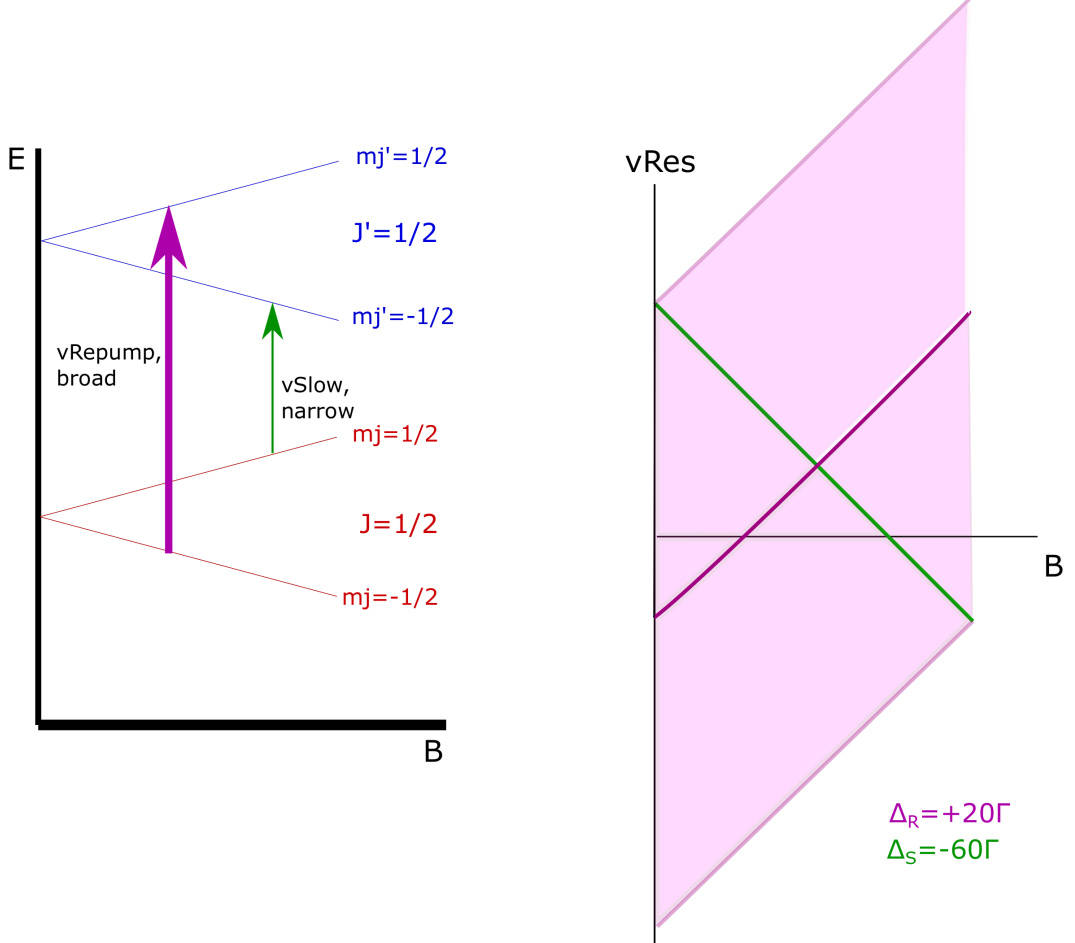


Figure 48: Left: energy levels of a  $J=1/2 \rightarrow J' = 1/2$  transition in the presence of a magnetic field. In a ‘normal’ zeeman scheme, you would drive the transition between stretched states (e.g.,  $m_j = -1/2 \rightarrow m'_{j'} = -3/2$  for a  $J=1/2 \rightarrow J' = 3/2$ ). Right: resonant velocity for each transition as a function of the field (thick green and magenta lines). The green transition illustrates the normal slowing mechanism: only fast atoms scatter photons initially, then, as the atom travels towards higher field, progressively slower atoms are brought into resonance, thus compressing the velocity distribution of some low value defined by the last ‘B’ field seen by the atoms. However, because we are not using a stretched state, we must repump from the dark  $m_j = -1/2$  state. If this repump laser is narrow, then it and the slowing laser are only simultaneously resonant for one combination of  $B$  and  $v$  (where the thick lines cross). Thus, we must broaden the repump laser wide enough such that there is always some component on resonance with the velocity class that we want the slowing laser to ‘talk to’, regardless of the field. This broadening is modeled by the shaded purple region.

## 4.1. Implementing sidebands in my OBE solver

The broadening described above is most easily accomplished with high modulation depth sidebands (kind of like what we do now for white-light slowing). This can be simulated directly in my code by just adding a time dependent phase term to the  $\exp(i\omega_L t)$  terms in the  $L_k$  matrices (see Eq. 55 for a reminder of what these look like). So, instead of the phase being  $i\omega_L t$ , it instead becomes  $i\omega_L t + i\beta \sin(\Omega t)$ , where  $\beta$  is the modulation depth and  $\Omega$  the frequency applied to the EOM.

To check if this works, I first considered just a two level system coupled by one laser. I then varied the velocity of the atom and recorded the average number in the excited state over some appropriately long time frame ( $\sim 70\Gamma^{-1}$ ) after transients had died out (roughly  $10\Gamma^{-1}$ ) for cases with and without the sidebands applied. The resulting  $N_e(v)$  profiles are in left hand side of Fig. 49 for cases of ‘low’  $\beta$  ( $\beta \leq \pi$ ), while the right hand side shows the results for ‘high’  $\beta = 60$ ,  $\Omega = 1$ , which is closer to what we’ll need in the Type-II Zeeman slower.

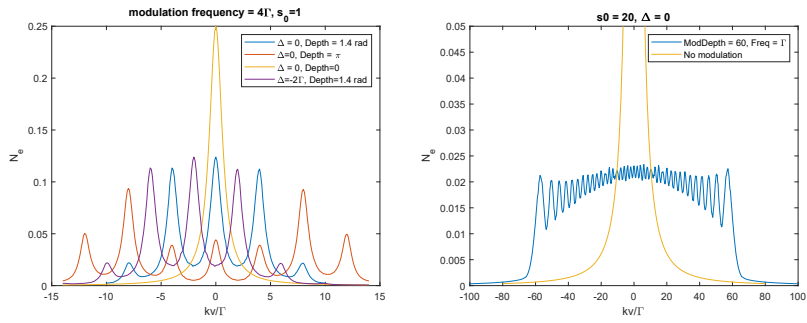


Figure 49: Left:  $N_e(v)$  with and without sidebands for  $\Omega = 4\Gamma$ , and  $\beta \leq \pi$ . The sidebands match expectations (typo: that should read  $\Delta = +2\Gamma$  on the purple curve). Right: High modulation, high intensity results compared to high intensity no-modulation. We see that the modulation results in the excitation being driven over a very large range of velocities, as is needed for repumping in the Type-II Zeeman slowing.

## 4.2. Implementing the simplest Type-II Zeeman slower ( $J = 1/2 \rightarrow J' = 1/2$ )

Let's consider a mock  $J = 1/2 \rightarrow J' = 1/2$  with 'mock'  $g_J = g_{J'} = 1$  that otherwise has similar parameters to SrF ( $k = 2\pi/663\text{nm}$ ,  $\Gamma/2\pi = 6.63\text{MHz}$ ,  $\mu_B B/\hbar\Gamma = 0.2118B$ , where  $B$  is in Gauss, etc.). Let's assume that we want the Zeeman slower to 'start out' slowing molecules with  $v \sim 240\text{ m/s}$  (this is a bit faster than the fastest SrF molecule), and 'finish' by being on resonance with  $v = 0$  (again, probably wouldn't want this in an experiment since we want the molecules to actually still be, slowly, moving towards the MOT, but this is just a proof of concept). This is illustrated in Fig. 50, with a level diagram similar to the one displayed in Fig. 48.

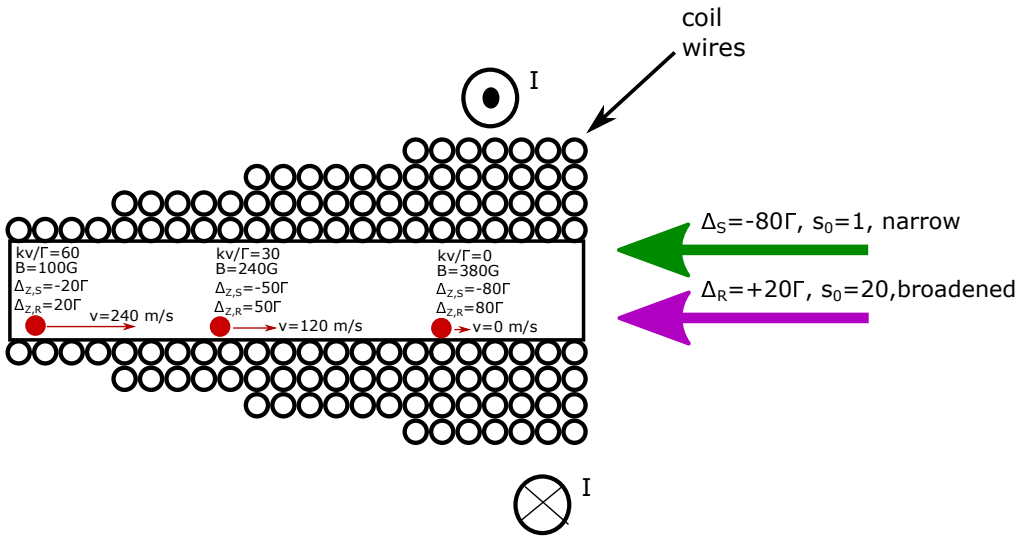


Figure 50: Schematic illustration of the type two zeeman slower. The subscripts  $R$  and  $S$  refer to the repump and slowing lasers. I have indicated the velocity at three points along the path that correspond to the resonance condition for the narrow 'slowing' laser, set to  $-80\Gamma$ . Since the repump transition is shifted overall by  $-40\Gamma$  for the fast atom at low field, and by  $+80\Gamma$  MHz for the stationary atom at high field, I give it an overall detuning of  $+20\Gamma$ . Since this laser is broad it must also be very intense.

In Figure 51, I show the  $N_e(v)$  curves obtained in my simulation for various fields in the region of the resonance condition for the slowing laser, with and without broadening of the repump beam. We see that, except for at  $kv/\Gamma = 30$ ,  $B = 240\text{G}$ , where both the repump beam carrier frequency and the slowing laser happens to be resonant,  $N_e$  is minimal when the repumper is not broadened. If the repumper is not broadened, atoms will just pile up in the  $m_s = -1/2$  ground state.

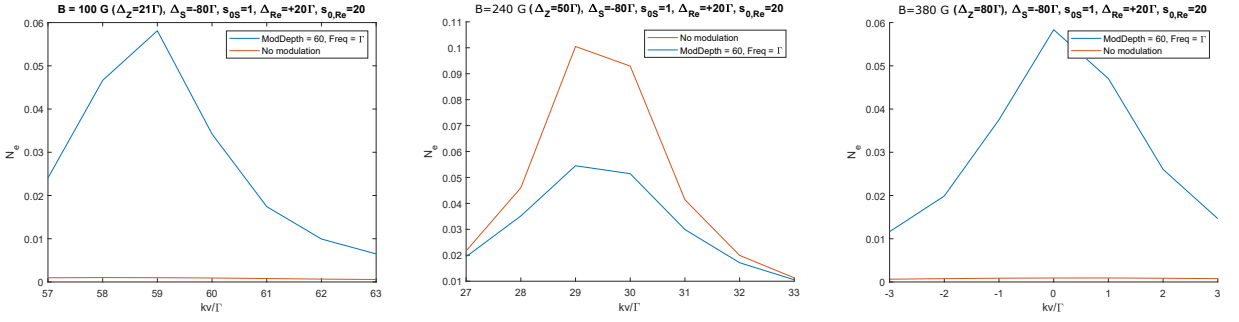


Figure 51:  $N_e(v)$  curves near the resonance condition for the slowing laser at various fields. We see that the only way to achieve decent excited state population for all cases is to have a broadened repump laser. The velocity selectivity is also clearly illustrated here, and comes from the narrowness of the slowing laser.

### 4.3. Application to K

In this document, I describe a code that handles the full optical bloch equations for an arbitrary number of lasers, B field, etc. in the  $|F, m_F\rangle$  basis. I'd like to keep that machinery as much as possible. However, we are dealing with Zeeman fields strong enough to couple states of different  $F$  but the same  $m_F$ , which is not the case in the MOT. The best basis to use for describing the Zeeman Hamiltonian  $V_z$  is the  $|m_{J/S}\rangle|m_I\rangle$  basis. So, what I will do is write the Zeeman hamiltonian in that basis, and then convert it to the  $|F, m_F\rangle$  basis using unitary transformations. This looks something like this:

$$\langle F', m'_F | V_z | F, m_F \rangle = \sum_{m'_J, m'_I, m_J, m_I} \langle F', m'_F | m'_J, m'_I \rangle \langle m'_J, m'_I | V_z | m_J, m_I \rangle \langle m_J, m_I | F, m_F \rangle \quad (64)$$

Next, consider the unitary transform that converts the  $|m_J, m_I\rangle$  basis to the  $|F, m_F\rangle$  basis  $|F, m_F\rangle = U|m_J, m_I\rangle$ . Expressing  $U$  in the  $|m_J, m_I\rangle$  basis, it is clear that  $\langle m'_J, m'_I | U | m_J, m_I \rangle = \langle m'_J, m'_I | F, m_F \rangle$ . From this then, it is also clear that  $V_Z^{F, m_F} = U^{\dagger, m_J, m_I} V_Z^{m_J, m_I} U^{m_J, m_I}$ , where the superscripts indicate which basis the matrix is expressed in.

All that remains is to determine what  $U$  is. First, we determine what  $|F, m_F\rangle$  is expressed in the  $|m_J, m_I\rangle$  basis (very easy, just use a Clebsch-Gordan table). For our model atom of potassium, we are considering the  ${}^2\text{S}_{1/2} \rightarrow {}^2\text{P}_{1/2}$  transition, where  $I = 3/2$  and thus  $F = \{2, 1\}$  for both states. In the list below, the left hand side is the  $|F, m_F\rangle$  state and the right hand side is  $|m_J, m_I\rangle$ :

- $|1, -1\rangle = \frac{\sqrt{3}}{2} |\frac{1}{2}, -\frac{3}{2}\rangle - \frac{1}{2} |\frac{-1}{2}, -\frac{1}{2}\rangle$
- $|1, 0\rangle = \frac{1}{\sqrt{2}} |\frac{1}{2}, -\frac{1}{2}\rangle - \frac{1}{\sqrt{2}} |\frac{-1}{2}, \frac{1}{2}\rangle$
- $|1, 1\rangle = \frac{1}{2} |\frac{1}{2}, \frac{1}{2}\rangle - \frac{\sqrt{3}}{2} |\frac{-1}{2}, \frac{3}{2}\rangle$
- $|2, -2\rangle = |\frac{-1}{2}, -\frac{3}{2}\rangle$
- $|2, -1\rangle = \frac{1}{2} |\frac{1}{2}, -\frac{3}{2}\rangle + \frac{\sqrt{3}}{2} |\frac{-1}{2}, -\frac{1}{2}\rangle$
- $|2, 0\rangle = \frac{1}{\sqrt{2}} |\frac{1}{2}, -\frac{1}{2}\rangle + \frac{1}{\sqrt{2}} |\frac{-1}{2}, \frac{1}{2}\rangle$
- $|2, 1\rangle = \frac{\sqrt{3}}{2} |\frac{1}{2}, \frac{1}{2}\rangle + \frac{1}{2} |\frac{-1}{2}, \frac{3}{2}\rangle$
- $|2, 2\rangle = |\frac{1}{2}, \frac{3}{2}\rangle$

Next, I need to define the 'order' of the states within each basis. For the  $|F, m_F\rangle$  basis, column 1 is  $|1, -1\rangle$  and column 8 is  $|2, 2\rangle$  (the rest are intiuitive from here). For the  $|m_J, m_I\rangle$  basis, column 1 is  $|\frac{-1}{2}, -\frac{3}{2}\rangle$ , 2 is  $|\frac{-1}{2}, -\frac{1}{2}\rangle$ , etc. up to 8 being  $|\frac{1}{2}, \frac{3}{2}\rangle$ . From inspection, we obtain:

$$U = \begin{pmatrix} 0 & 0 & 0 & 1 & 0 & 0 & 0 & 0 \\ -\frac{1}{2} & 0 & 0 & 0 & \frac{\sqrt{3}}{2} & 0 & 0 & 0 \\ 0 & -\frac{1}{\sqrt{2}} & 0 & 0 & 0 & \frac{1}{\sqrt{2}} & 0 & 0 \\ 0 & 0 & -\frac{\sqrt{3}}{2} & 0 & 0 & 0 & \frac{1}{2} & 0 \\ \frac{\sqrt{3}}{2} & 0 & 0 & 0 & \frac{1}{2} & 0 & 0 & 0 \\ 0 & \frac{1}{\sqrt{2}} & 0 & 0 & 0 & \frac{1}{\sqrt{2}} & 0 & 0 \\ 0 & 0 & \frac{1}{2} & 0 & 0 & 0 & \frac{\sqrt{3}}{2} & 0 \\ 0 & 0 & 0 & 0 & 0 & 0 & 0 & 1 \end{pmatrix} \quad (65)$$

Since this is a concrete example, I will walk through it step by step. In the  $|m_J, m_I\rangle$  basis, we find:

$$V_Z^{m_J, m_I} = \mu_B B g_J \begin{pmatrix} -\frac{1}{2} & 0 & 0 & 0 & 0 & 0 & 0 & 0 \\ 0 & -\frac{1}{2} & 0 & 0 & 0 & 0 & 0 & 0 \\ 0 & 0 & -\frac{1}{2} & 0 & 0 & 0 & 0 & 0 \\ 0 & 0 & 0 & -\frac{1}{2} & 0 & 0 & 0 & 0 \\ 0 & 0 & 0 & 0 & \frac{1}{2} & 0 & 0 & 0 \\ 0 & 0 & 0 & 0 & 0 & \frac{1}{2} & 0 & 0 \\ 0 & 0 & 0 & 0 & 0 & 0 & \frac{1}{2} & 0 \\ 0 & 0 & 0 & 0 & 0 & 0 & 0 & \frac{1}{2} \end{pmatrix} \quad (66)$$

Then, using  $V_Z^{F, m_F} = U^\dagger V_Z^{m_J, m_I} U$ , we obtain:

$$V_Z^{F, m_F} + V_{HF} = \mu_B B g_J \begin{pmatrix} \frac{1}{4} & 0 & 0 & 0 & \frac{\sqrt{3}}{4} & 0 & 0 & 0 \\ 0 & 0 & 0 & 0 & 0 & \frac{1}{2} & 0 & 0 \\ 0 & 0 & -\frac{1}{4} & 0 & 0 & 0 & \frac{\sqrt{3}}{4} & 0 \\ 0 & 0 & 0 & -\frac{1}{2} & 0 & 0 & 0 & 0 \\ \frac{\sqrt{3}}{4} & 0 & 0 & 0 & -\frac{1}{4} & 0 & 0 & 0 \\ 0 & \frac{1}{2} & 0 & 0 & 0 & 0 & 0 & 0 \\ 0 & 0 & \frac{\sqrt{3}}{4} & 0 & 0 & 0 & \frac{1}{4} & 0 \\ 0 & 0 & 0 & 0 & 0 & 0 & 0 & \frac{1}{2} \end{pmatrix} + A \begin{pmatrix} -\frac{5}{8} & 0 & 0 & 0 & 0 & 0 & 0 & 0 \\ 0 & -\frac{5}{8} & 0 & 0 & 0 & 0 & 0 & 0 \\ 0 & 0 & -\frac{5}{8} & 0 & 0 & 0 & 0 & 0 \\ 0 & 0 & 0 & \frac{3}{8} & 0 & 0 & 0 & 0 \\ 0 & 0 & 0 & 0 & \frac{3}{8} & 0 & 0 & 0 \\ 0 & 0 & 0 & 0 & 0 & \frac{3}{8} & 0 & 0 \\ 0 & 0 & 0 & 0 & 0 & 0 & \frac{3}{8} & 0 \\ 0 & 0 & 0 & 0 & 0 & 0 & 0 & \frac{3}{8} \end{pmatrix} \quad (67)$$

where  $V_{HF}$  is the hyperfine hamiltonian and  $A$  is the hyperfine splitting (461.7 MHz, or  $77.5\Gamma$  for potassium S state). For potassium,  $\mu_B/(\hbar\Gamma) = 0.235 \times B$  (Gauss). Solving for the eigenvalues of this matrix as a function of  $B$ , I obtain the energy level diagram in figure Fig. 52 (for  $g_J = 2$ , corresponding to the  $^2S_{1/2}$  state...for the  $^2P_{1/2}$  state,  $g_J = 2/3$  and  $A = 55.5$  MHz, or  $9.3\Gamma$ ), which matches figure 4 of the type II Zeeman slower paper.

#### 4.3.1. Explicit Matrices for K OBE solver

In this subsection I will write down the explicit matrices used in the OBE solver. Here, unlike for the SrF simulations described in previous chapters, I will explicitly include the

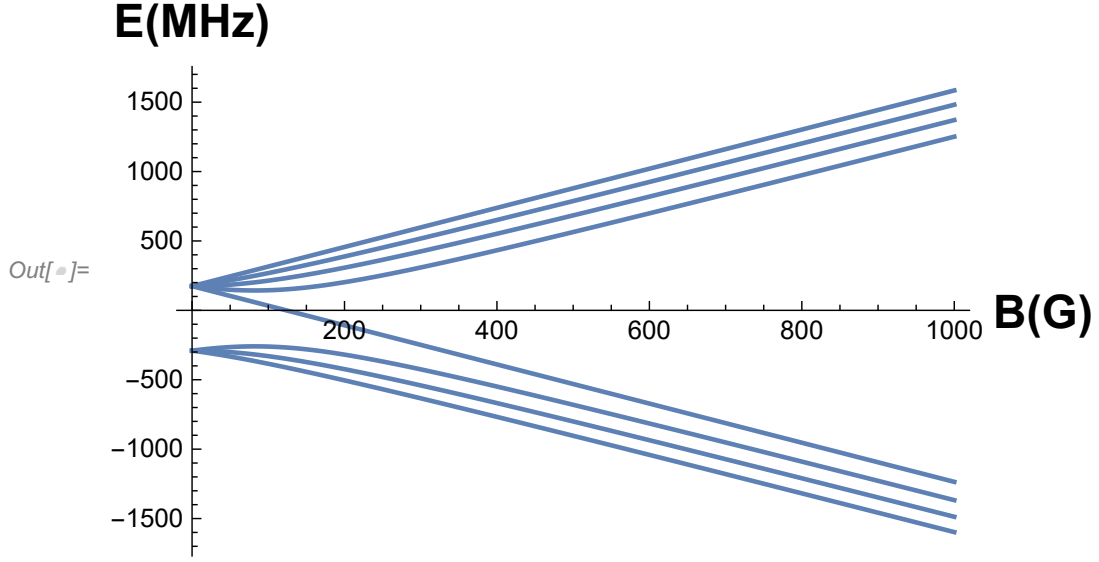


Figure 52: Eigenvalues of  $V_z + V_{HF}$  for the  $^2S_{1/2}$  state. Results match those found [here](#)

hyperfine hamiltonian (before, this was done by adding a fixed energy shift to each of the hyperfine energies whenever we calculated things like the energy difference between one of the excitation lasers and a given lower level hyperfine state, hence all the talk of indexing the laser frequencies to the transition between  $|F = 1, J = 1/2\rangle$  and the  $A\Pi$  state). The laser frequency will now be indexed to the bare energy difference between  $^2S_{1/2}$  and  $^2P_{1/2}$ . So, the total hamiltonian  $H_{AL}$  used in the master equation (Eq. 1) becomes:

$$H_{AL} = -\vec{D} \cdot \vec{E} + V_Z^{F,m_F} + V_{HF} \quad (68)$$

As before, we have (this is just Eq. 23)

$$\tilde{H}_{-\vec{D} \cdot \vec{E}} = -\langle \vec{D} \cdot \vec{E} \rangle = \sum_{kp} \frac{1}{2} \sqrt{\frac{s_{0,k}}{2}} \tilde{L}_{k,p} \cdot * \tilde{E}_p(a_k) \cdot * (-C_p) \quad (69)$$

Now, we find the following for the  $C_p$  matrices:



$$C_1 = \begin{pmatrix} 0 & 0 & 0 & 0 & 0 & 0 & 0 & 0 & 0 & 0 & 0 & 0 & 0 & 0 & 0 & 0 \\ 0 & 0 & 0 & 0 & 0 & 0 & 0 & 0 & -\frac{1}{2\sqrt{3}} & 0 & 0 & 0 & \frac{1}{2} & 0 & 0 & 0 \\ 0 & 0 & 0 & 0 & 0 & 0 & 0 & 0 & 0 & -\frac{1}{2\sqrt{3}} & 0 & 0 & 0 & \frac{1}{2\sqrt{3}} & 0 & 0 \\ 0 & 0 & 0 & 0 & 0 & 0 & 0 & 0 & 0 & 0 & 0 & 0 & 0 & 0 & 0 & 0 \\ 0 & 0 & 0 & 0 & 0 & 0 & 0 & 0 & 0 & 0 & 0 & \frac{1}{\sqrt{6}} & 0 & 0 & 0 & 0 \\ 0 & 0 & 0 & 0 & 0 & 0 & 0 & 0 & -\frac{1}{2\sqrt{3}} & 0 & 0 & 0 & \frac{1}{2} & 0 & 0 & 0 \\ 0 & 0 & 0 & 0 & 0 & 0 & 0 & 0 & 0 & -\frac{1}{2} & 0 & 0 & 0 & -\frac{1}{2} & 0 & 0 \\ 0 & 0 & 0 & 0 & 0 & 0 & 0 & 0 & 0 & 0 & -\frac{1}{\sqrt{2}} & 0 & 0 & 0 & \frac{1}{\sqrt{6}} & 0 \\ 0 & 0 & 0 & 0 & 0 & 0 & 0 & 0 & 0 & 0 & 0 & 0 & 0 & 0 & 0 & 0 \\ 0 & 0 & 0 & 0 & 0 & 0 & 0 & 0 & 0 & 0 & 0 & 0 & 0 & 0 & 0 & 0 \\ 0 & 0 & 0 & 0 & 0 & 0 & 0 & 0 & 0 & 0 & 0 & 0 & 0 & 0 & 0 & 0 \\ 0 & 0 & 0 & 0 & 0 & 0 & 0 & 0 & 0 & 0 & 0 & 0 & 0 & 0 & 0 & 0 \\ 0 & 0 & 0 & 0 & 0 & 0 & 0 & 0 & 0 & 0 & 0 & 0 & 0 & 0 & 0 & 0 \\ 0 & 0 & 0 & 0 & 0 & 0 & 0 & 0 & 0 & 0 & 0 & 0 & 0 & 0 & 0 & 0 \\ 0 & 0 & 0 & 0 & 0 & 0 & 0 & 0 & 0 & 0 & 0 & 0 & 0 & 0 & 0 & 0 \\ 0 & 0 & 0 & 0 & 0 & 0 & 0 & 0 & 0 & 0 & 0 & 0 & 0 & 0 & 0 & 0 \end{pmatrix} \quad (72)$$

There will be 2  $L_{k,p}$  matrices (e.g.,  $k_{max} = 2$ ). One corresponding to the slowing laser and one to the broadened repump laser. The slowing laser must have at least 4 bands spaced by 118.6 MHz ( $19.9\Gamma$ ) and is centered at 1680 MHz red ( $281.8\Gamma$ ) of the D1 line. I'll drive this at  $\beta_{sl} = 1.8$  radians or so, such that there is non trivial amplitude in the carrier and the first and second order sidebands. They say they have 20 mW per side band, giving 80 mW total, in a 1 cm beam waist giving  $s_{0,sl} = 30$  (I'll try a few different values). They don't state the repump laser detuning, they just say they drive it at 12 MHz ( $2\Gamma$ ) and it's spread to 1.5 GHz (so, I assume they need a non-trivial amplitude of the  $1500/2/12=62$ nd sideband.) This requires driving at around  $\beta_{repump} = 60$  radians. They use  $s_{0,re} = 150$ . They don't say how far detuned it is. These lasers are oppositely circularly polarized and propagate in the same direction. In Fig. 53 I show the spectral profile of each laser.

The  $\tilde{L}_1$  matrix will correspond to the slowing laser. The terms on the upper right triangular component will all be  $\exp(-281.8it + 1.8i \sin(19.9t))$ . The  $\tilde{L}_2$  matrix will correspond to the repumping matrix. The terms on the upper right triangular component will all be  $\exp -i\delta_{Re}t + 60i \sin(2t)$ , where  $\delta_{Re}$  is the overall detuning of the repumper (I choose this to be  $+140\Gamma$  since this puts the repumper near resonance in the middle of the slowing region). The  $A_p$  terms in the  $E_p(a_1)$  matrix (see Eq. 16 and 56) are  $\{0, 0, \cos(z) - i\sin(z)\}$  while for the  $E_p(a_2)$  matrix they are  $\{\cos(z) - i\sin(z), 0, 0\}$  (opposite circular polarization).

That's all we need for the  $\vec{D} \cdot \vec{E}$  term. Next, I'll write the  $V_z^{F,m_F} + V_{HF}$  terms explicitly:

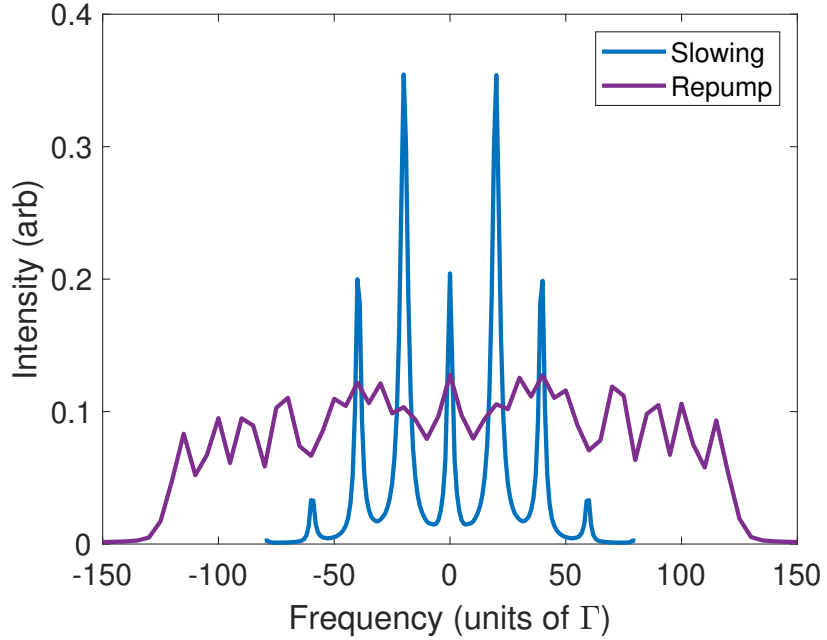


Figure 53: Slowing and Repump spectral profiles. Ideally we would just have 4 slowing frequencies but this is not possible with a sinusoidal EOM drive.

$$V_z^{F,m_F} = 0.235B(\tilde{z}) \left( \begin{array}{cccccccccccccccc} \frac{1}{2} & 0 & 0 & 0 & \frac{\sqrt{3}}{2} & 0 & 0 & 0 & 0 & 0 & 0 & 0 & 0 & 0 & 0 & 0 & 0 \\ 0 & 0 & 0 & 0 & 0 & 1 & 0 & 0 & 0 & 0 & 0 & 0 & 0 & 0 & 0 & 0 & 0 \\ 0 & 0 & -\frac{1}{2} & 0 & 0 & 0 & \frac{\sqrt{3}}{2} & 0 & 0 & 0 & 0 & 0 & 0 & 0 & 0 & 0 & 0 \\ 0 & 0 & 0 & -1 & 0 & 0 & 0 & 0 & 0 & 0 & 0 & 0 & 0 & 0 & 0 & 0 & 0 \\ \frac{\sqrt{3}}{2} & 0 & 0 & 0 & -\frac{1}{2} & 0 & 0 & 0 & 0 & 0 & 0 & 0 & 0 & 0 & 0 & 0 & 0 \\ 0 & 1 & 0 & 0 & 0 & 0 & 0 & 0 & 0 & 0 & 0 & 0 & 0 & 0 & 0 & 0 & 0 \\ 0 & 0 & \frac{\sqrt{3}}{2} & 0 & 0 & 0 & \frac{1}{2} & 0 & 0 & 0 & 0 & 0 & 0 & 0 & 0 & 0 & 0 \\ 0 & 0 & 0 & 0 & 0 & 0 & 0 & 1 & 0 & 0 & 0 & 0 & 0 & 0 & 0 & 0 & 0 \\ 0 & 0 & 0 & 0 & 0 & 0 & 0 & 0 & \frac{1}{6} & 0 & 0 & 0 & 0 & \frac{\sqrt{3}}{6} & 0 & 0 & 0 \\ 0 & 0 & 0 & 0 & 0 & 0 & 0 & 0 & 0 & 0 & 0 & 0 & 0 & 0 & \frac{1}{3} & 0 & 0 \\ 0 & 0 & 0 & 0 & 0 & 0 & 0 & 0 & 0 & 0 & 0 & 0 & 0 & 0 & 0 & \frac{\sqrt{3}}{6} & 0 \\ 0 & 0 & 0 & 0 & 0 & 0 & 0 & 0 & 0 & 0 & 0 & 0 & 0 & -\frac{1}{6} & 0 & 0 & 0 \\ 0 & 0 & 0 & 0 & 0 & 0 & 0 & 0 & 0 & 0 & 0 & 0 & 0 & -\frac{1}{3} & 0 & 0 & 0 \\ 0 & 0 & 0 & 0 & 0 & 0 & 0 & 0 & \frac{\sqrt{3}}{6} & 0 & 0 & 0 & 0 & -\frac{1}{6} & 0 & 0 & 0 \\ 0 & 0 & 0 & 0 & 0 & 0 & 0 & 0 & 0 & \frac{1}{3} & 0 & 0 & 0 & 0 & 0 & 0 & 0 \\ 0 & 0 & 0 & 0 & 0 & 0 & 0 & 0 & 0 & 0 & \frac{\sqrt{3}}{6} & 0 & 0 & 0 & 0 & \frac{1}{6} & 0 \\ 0 & 0 & 0 & 0 & 0 & 0 & 0 & 0 & 0 & 0 & 0 & 0 & 0 & 0 & 0 & 0 & \frac{1}{3} \end{array} \right) \quad (73)$$

where  $B(\tilde{z}) = 510G + 260G \times 10^{-7} \times \tilde{z}$  (note:  $\tilde{z}$  is in normalized units, e.g.  $\tilde{z} = kz$ )

$$V_{HF} = \begin{pmatrix} -\frac{5A_S}{8} & 0 & 0 & 0 & 0 & 0 & 0 & 0 & 0 & 0 & 0 & 0 & 0 & 0 \\ 0 & -\frac{5A_S}{8} & 0 & 0 & 0 & 0 & 0 & 0 & 0 & 0 & 0 & 0 & 0 & 0 \\ 0 & 0 & -\frac{5A_S}{8} & 0 & 0 & 0 & 0 & 0 & 0 & 0 & 0 & 0 & 0 & 0 \\ 0 & 0 & 0 & \frac{3A_S}{8} & 0 & 0 & 0 & 0 & 0 & 0 & 0 & 0 & 0 & 0 \\ 0 & 0 & 0 & 0 & \frac{3A_S}{8} & 0 & 0 & 0 & 0 & 0 & 0 & 0 & 0 & 0 \\ 0 & 0 & 0 & 0 & 0 & \frac{3A_S}{8} & 0 & 0 & 0 & 0 & 0 & 0 & 0 & 0 \\ 0 & 0 & 0 & 0 & 0 & 0 & \frac{3A_S}{8} & 0 & 0 & 0 & 0 & 0 & 0 & 0 \\ 0 & 0 & 0 & 0 & 0 & 0 & 0 & \frac{3A_S}{8} & 0 & 0 & 0 & 0 & 0 & 0 \\ 0 & 0 & 0 & 0 & 0 & 0 & 0 & 0 & -\frac{5A_P}{8} & 0 & 0 & 0 & 0 & 0 \\ 0 & 0 & 0 & 0 & 0 & 0 & 0 & 0 & 0 & -\frac{5A_P}{8} & 0 & 0 & 0 & 0 \\ 0 & 0 & 0 & 0 & 0 & 0 & 0 & 0 & 0 & 0 & -\frac{5A_P}{8} & 0 & 0 & 0 \\ 0 & 0 & 0 & 0 & 0 & 0 & 0 & 0 & 0 & 0 & 0 & \frac{3A_P}{8} & 0 & 0 \\ 0 & 0 & 0 & 0 & 0 & 0 & 0 & 0 & 0 & 0 & 0 & 0 & \frac{3A_P}{8} & 0 \\ 0 & 0 & 0 & 0 & 0 & 0 & 0 & 0 & 0 & 0 & 0 & 0 & 0 & \frac{3A_P}{8} \\ 0 & 0 & 0 & 0 & 0 & 0 & 0 & 0 & 0 & 0 & 0 & 0 & 0 & 0 \end{pmatrix} \quad (74)$$

Once this is all set-up in matlab, we run the simulation. First though, I will make a quick digression here to discuss what levels we are actually driving with the slowing laser (this will be more important when understanding the configuration where the beam propagates perpendicularly to the applied B-Field, discussed in the next section). If we diagonalize  $V_z + V_{HF}$  for a reasonably large  $B$ -field (510 G, which is the initial ‘offset’ field observed by the atoms), we find the following level diagram (Fig. 54).

Now for the results. First, I examined what the  $N_e(v)$  curve for 510 G looks like (this is their ‘offset’ field). I ran the simulation for  $150\Gamma^{-1}$ , and averaged  $N_e$  over the time period from 100 to 150 (Fig. 55 left).

The structure of the sidebands is evident here. Since there are five laser frequencies (carrier, 2 1st order, 2 2nd order) for 4 approximately equally spaced levels, we’d expect to see 2 velocities for which all four transitions are addressed (after diagonalizing the  $V_z + V_{HF}$  matrix, I find that this happens for  $v = 490$  m/s and  $v = 410$  m/s), 2 for which 3 are addressed, etc. One would imagine that if **any** of the 4 were not addressed, the atoms would pile up in that state. However, this may not happen for a few reasons. First, there may be some probability to off-resonantly scatter out of that state (indeed, we see that the population never really drops to zero in between resonant velocities). Second, the 3rd order sideband values are very low, but not zero (for  $\beta = 1.8$ , the ratio of carrier:1stOrder:2ndOrder:3rdOrder is roughly 10:34:10:1). If the 3rd order sidebands are indeed a significant contribution, then we may expect to have 7 equally spaced frequencies driving 4 roughly equally spaced transitions, and thus 4 velocities where all transitions are driven.

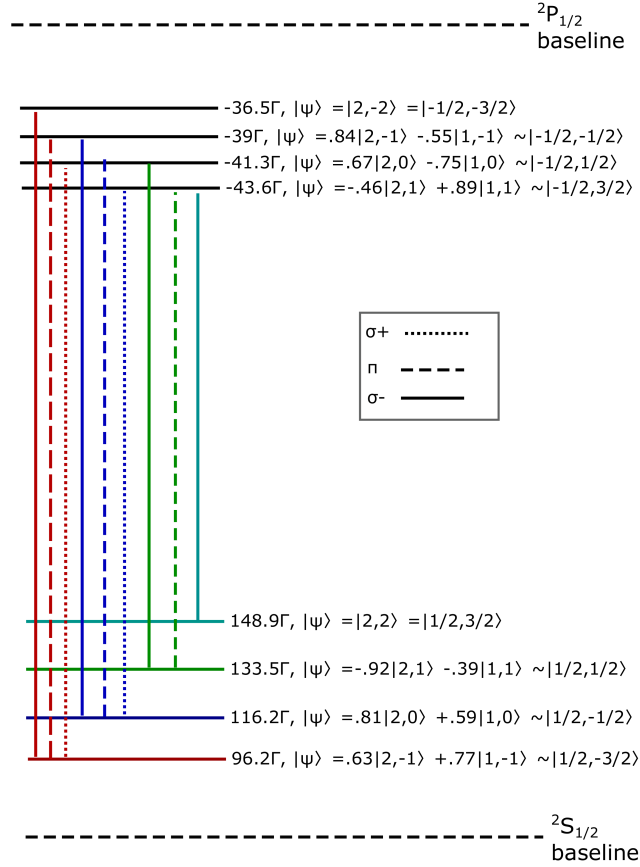


Figure 54: Level diagram for the 'slowing' transitions. From the picture, it is clear that, if there is any  $\sigma^-$  light at all, where what  $\sigma^-$  means is determined by the quantization axis, which I will always choose to be the magnetic field axis, there are no stationary dark states. If the laser propagation direction is parallel (or, as we would use, anti-parallel) to the magnetic field, then it is possible to address these states with  $\sigma^-$  **and only**  $\sigma^-$  light, if you want, which also eliminates the possibility of any 'dark' states from  $\Lambda$  configurations which can result from the (somewhat) unresolved P state hyperfine structure (in practice I think that the  $2\Gamma$  separation in K should be fine...for SrF, though, the  $\Pi$  state hyperfine structure is unresolved). Similarly, the broad repump will require  $\sigma^+$  light, and ideally only  $\sigma^+$  light. If the beam is perpendicular to the field, then by necessity you cannot have pure  $\sigma^-$  light. The resulting dark states may have a deleterious effect when slowing in this configuration. We should keep an eye on this.

To investigate the sideband issue in more detail, I simulated the time evolution at

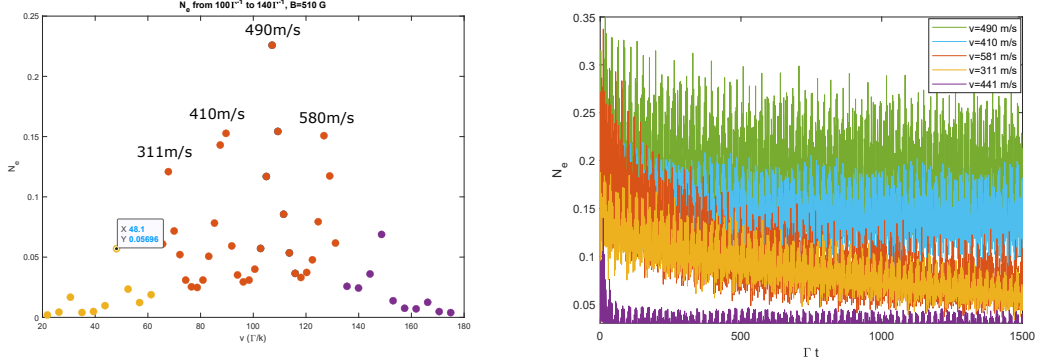


Figure 55: Left:  $N_e(v)$  for  $B = 510$  G for the K Type II Zeeman slower with detunings, sidebands, etc. discussed in the writeup (the colors don't mean anything). The velocity dependence of the slowing force is clear, as are the sidebands resulting from there being more laser frequencies than there are transitions, allowing for the resonance condition for all 4 transitions to be met for a few different velocities. This data is taken over a timeframe between  $100\Gamma^{-1}$  and  $150\Gamma^{-1}$ . Right:  $N_e(t)$  for a few selected  $v$ . Here we see that the excited state population stabilizes to non-zero values for the cases where there is significant sideband power driving each transition (410 m/s and 490 m/s). We also see that for off resonant light (440 m/s) there is very little excited state population.

each density peak for a longer period of time ( $1500\Gamma^{-1}$ ). We see that only the two peaks corresponding to the case where all 4 transitions are addressed by sidebands with substantial power clearly stabilize to a non-zero offset value (Fig. 55, right).

Next, I ran the program again for  $B = 650$  G (roughly the middle of their slowing region) and  $B = 770$  G (the end of their slowing region). The  $N_e(v)$  curves are in Fig. 56A and D respectively. Similar sidebands occur, except at lower and lower velocities as the B-field increases. I also took a closer look at how the decision I made to use sidebands from an EOM effects the behavior of the system. In the paper, the authors imply that they somehow have only 4 sidebands (perhaps they drive their EOM with some fancy non-sinusoidal field). The  $N_e(t)$  curves for the EOM case (B) and 'perfect' 4 sideband case (C) are plotted in Fig. 56 (NOTE: I added smoothing so they look less noisy than the equivalent curve in Fig. 55). We clearly see that, for the 4 side band case (C), only the center velocity (300 m/s, or  $65\Gamma/k$ ), for which all 4 transitions are driven, clearly stabilizes to a non-zero value. For the EOM driven case (B), we see that 300 and 380 m/s (and, curiously, 480 m/s...not sure what's happening there), the two cases for which 4 out of the 5 major sidebands are resonant, decay towards a stable, non-zero  $N_e$  value.

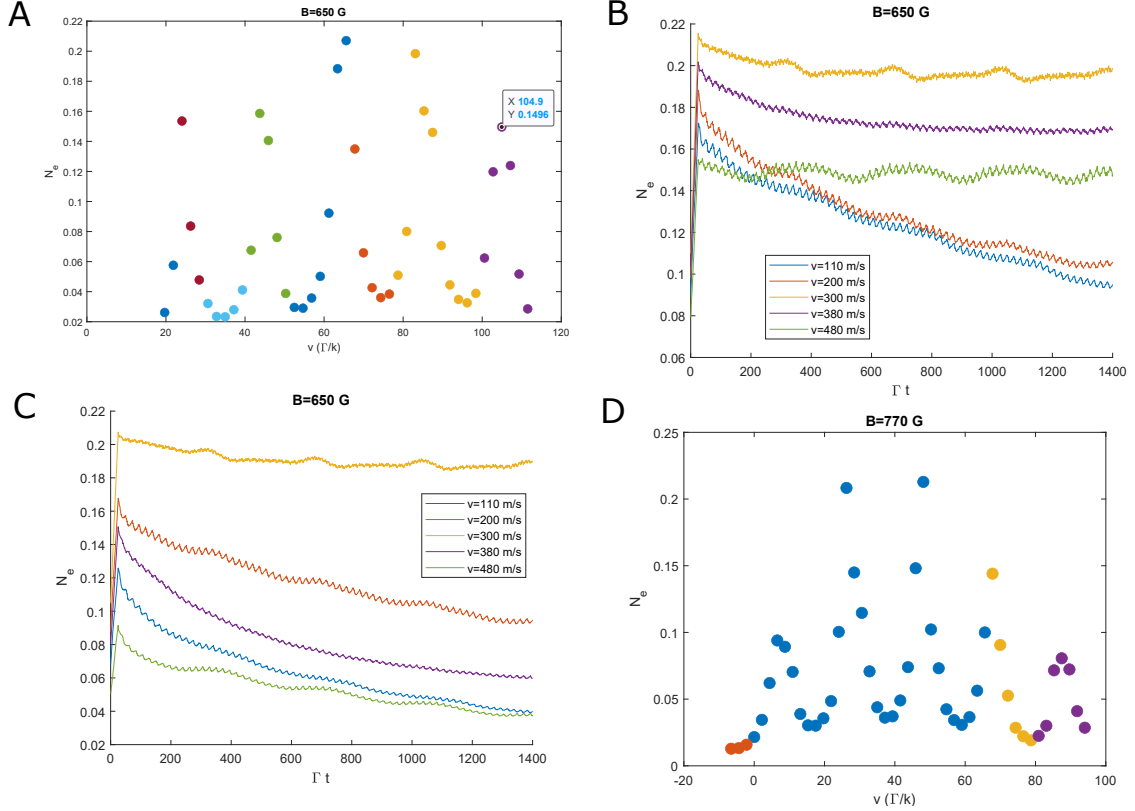


Figure 56: A:  $N_e(v)$  for  $B = 650$  G for the K Type II Zeeman slower with detunings, sidebands, etc. discussed in the writeup (the colors don't mean anything). The velocity dependence of the slowing force is clear, as are the sidebands resulting from there being more laser frequencies than there are transitions, allowing for the resonance condition for all 4 transitions to be met for a few different velocities. D: Same for 770 G. B:  $N_e(t)$  for a few selected  $v$  for the 'EOM' case. Here we see that the excited state population stabilizes to non-zero values for the cases where there is significant sideband power driving each transition (300 m/s and 380 m/s). It also seems to stabilize for 480 m/s, which I don't have a good explanation for. C:  $N_e(t)$  for the same  $v$  for the '4 sideband' case. Here we see that only  $v = 300$  m/s stabilizes to non-zero, corresponding to the case where each transition is resonant with one of the sidebands.

### 4.3.2. Zeeman slower with light axis perpendicular to B-Field

Dave suggested that it might wind up being easier to have permanent magnets aligned along an axis perpendicular to the beam propagation direction, creating a field of the form  $B(x) = B_0 + bx\hat{z}$  where  $x$  is the beam propagation direction. This is easy to implement in my code: I keep the field axis along the  $z$  axis, and thus  $V_z$  is unchanged. The only thing that changes is the form of  $A_p$  (see discussion below Eq.16):

For  $\sigma^-$  laser:

- $A_{-1,par} = \cos(z) - i \sin(z) \rightarrow A_{-1,perp} = \frac{i}{2} (\cos(x) - i \sin(x))$
- $A_{0,par} = 0 \rightarrow A_{0,perp} = -\frac{i}{\sqrt{2}} (\cos(x) - i \sin(x))$
- $A_{1,par} = 0 \rightarrow A_{1,perp} = \frac{i}{2} (\cos(x) - i \sin(x))$

For  $\sigma^+$  laser:

- $A_{-1,par} = 0 \rightarrow A_{-1,perp} = -\frac{i}{2} (\cos(x) - i \sin(x))$
- $A_{0,par} = 0 \rightarrow A_{0,perp} = -\frac{i}{\sqrt{2}} (\cos(x) - i \sin(x))$
- $A_{1,par} = \cos(z) - i \sin(z) \rightarrow A_{1,perp} = -\frac{i}{2} (\cos(x) - i \sin(x))$

The idea here is that, since there are non-zero components of the field polarizations needed to drive the desired transitions, things should still work. However, there could be some issues that stop this from working. For example, now that each laser can drive transitions between ground and excited states with  $\Delta m_J = \pm 1, 0$  (before they could only drive either  $+1$  or  $-1$ , for the repumper and 'slowing' laser, respectively), an atom moving at velocity  $v$  could be on resonant with multiple slowing transitions, potentially leading to coherent dark states forming.

However, it seems that this is not the case (Fig. 57). Unfortunately though, it does seem like, due to the fact that a lower fraction of each laser power works towards exciting the desired transition, a higher power is required to achieve the same scattering (4x power, which makes sense because  $|\epsilon_{perp} \cdot \sigma^-|^2 / (|\epsilon_{par} \cdot \sigma^-|^2) = 1/4$ ).

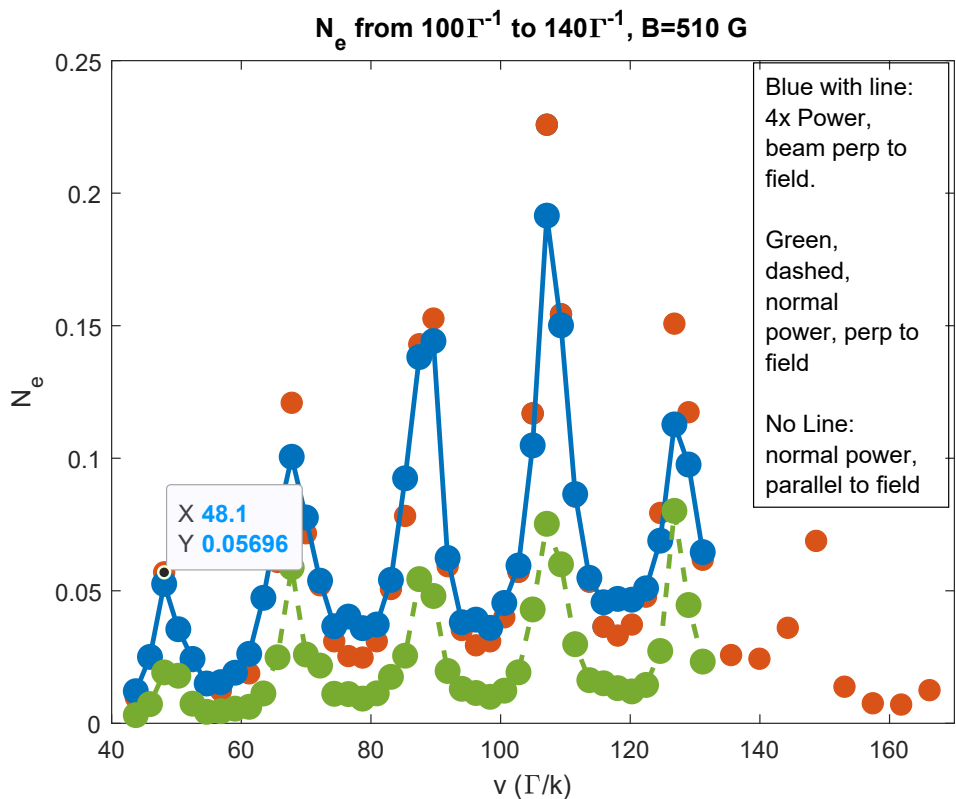


Figure 57: Comparison of Zeeman slowing using anti-parallel laser propagation and field directions vs perpendicular field and laser propagation. We see that the pattern is unchanged, however, the perpendicular configuration requires 4x the power (for both repumper and slowing laser) to achieve the same excited state population.

#### 4.4. Application to SrF

$X\Sigma$  states,  $|F = 2\rangle$ :

- $|F = 2, J = 3/2, m_F = 2\rangle = |m_s = \frac{1}{2}\rangle|m_N = 1\rangle|m_I = \frac{1}{2}\rangle$
- $|2, 3/2, 1\rangle = \frac{\sqrt{2}}{2}|\frac{1}{2}\rangle|0\rangle|\frac{1}{2}\rangle + \frac{1}{2}|\frac{1}{2}\rangle|1\rangle|-\frac{1}{2}\rangle + \frac{1}{2}|-\frac{1}{2}\rangle|1\rangle|\frac{1}{2}\rangle$
- $|2, 3/2, 0\rangle = \frac{1}{\sqrt{3}}|\frac{1}{2}\rangle|0\rangle|-\frac{1}{2}\rangle + \frac{1}{\sqrt{6}}|\frac{1}{2}\rangle|-1\rangle|\frac{1}{2}\rangle + \frac{1}{\sqrt{6}}|-\frac{1}{2}\rangle|1\rangle|-\frac{1}{2}\rangle + \frac{1}{\sqrt{3}}|-\frac{1}{2}\rangle|0\rangle|\frac{1}{2}\rangle$
- $|2, 3/2, -1\rangle = \frac{1}{2}|\frac{1}{2}\rangle|-1\rangle|-\frac{1}{2}\rangle + \frac{\sqrt{2}}{2}|-\frac{1}{2}\rangle|0\rangle|-\frac{1}{2}\rangle + \frac{1}{2}|-\frac{1}{2}\rangle|-1\rangle|\frac{1}{2}\rangle$
- $|2, 3/2, -2\rangle = |-\frac{1}{2}\rangle|-1\rangle|-\frac{1}{2}\rangle$

$|F = 1, J = 3/2\rangle$ :

- $|1, 3/2, 1\rangle = -\frac{1}{\sqrt{6}}|\frac{1}{2}\rangle|0\rangle|\frac{1}{2}\rangle + \frac{\sqrt{3}}{2}|\frac{1}{2}\rangle|1\rangle|-\frac{1}{2}\rangle - \frac{1}{\sqrt{12}}|-\frac{1}{2}\rangle|1\rangle|\frac{1}{2}\rangle$
- $|1, 3/2, 0\rangle = \frac{1}{\sqrt{3}}|\frac{1}{2}\rangle|0\rangle|-\frac{1}{2}\rangle - \frac{1}{\sqrt{6}}|\frac{1}{2}\rangle|-1\rangle|\frac{1}{2}\rangle + \frac{1}{\sqrt{6}}|-\frac{1}{2}\rangle|1\rangle|-\frac{1}{2}\rangle - \frac{1}{\sqrt{3}}|-\frac{1}{2}\rangle|0\rangle|\frac{1}{2}\rangle$
- $|1, 3/2, -1\rangle = \frac{1}{\sqrt{12}}|\frac{1}{2}\rangle|-1\rangle|-\frac{1}{2}\rangle + \frac{1}{\sqrt{6}}|-\frac{1}{2}\rangle|0\rangle|-\frac{1}{2}\rangle - \frac{\sqrt{3}}{2}|-\frac{1}{2}\rangle|-1\rangle|\frac{1}{2}\rangle$

$|F = 1, J = 1/2\rangle$ :

- $|1, 1/2, 1\rangle = \frac{1}{\sqrt{3}}|\frac{1}{2}\rangle|0\rangle|\frac{1}{2}\rangle - \frac{\sqrt{2}}{\sqrt{3}}|-\frac{1}{2}\rangle|1\rangle|\frac{1}{2}\rangle$
- $|1, 1/2, 0\rangle = \frac{1}{\sqrt{6}}|\frac{1}{2}\rangle|0\rangle|-\frac{1}{2}\rangle + \frac{1}{\sqrt{3}}|\frac{1}{2}\rangle|-1\rangle|\frac{1}{2}\rangle - \frac{1}{\sqrt{3}}|-\frac{1}{2}\rangle|1\rangle|-\frac{1}{2}\rangle - \frac{1}{\sqrt{6}}|-\frac{1}{2}\rangle|0\rangle|\frac{1}{2}\rangle$
- $|1, 1/2, -1\rangle = \frac{\sqrt{2}}{\sqrt{3}}|\frac{1}{2}\rangle|-1\rangle|-\frac{1}{2}\rangle - \frac{1}{\sqrt{3}}|-\frac{1}{2}\rangle|0\rangle|-\frac{1}{2}\rangle$

$|F = 0, J = 1/2\rangle$ :

- $|0, 1/2, 0\rangle = \frac{1}{\sqrt{6}}|\frac{1}{2}\rangle|0\rangle|-\frac{1}{2}\rangle - \frac{1}{\sqrt{3}}|\frac{1}{2}\rangle|-1\rangle|\frac{1}{2}\rangle - \frac{1}{\sqrt{3}}|-\frac{1}{2}\rangle|1\rangle|-\frac{1}{2}\rangle + \frac{1}{\sqrt{6}}|-\frac{1}{2}\rangle|0\rangle|\frac{1}{2}\rangle$

The corresponding  $U$  matrix for the 12 Zeeman states of  $X\Sigma$  is (NOTE: here I've included the  $J$  mixing terms) (note: Ordering of  $|F, m_F\rangle$  is the same as in previous chapters, the 'zeeman states' are ordered  $|m_s = -1/2\rangle|m_N = -1\rangle|m_I = -1/2\rangle$ ,  $|m_S = -1/2\rangle|m_N = -1\rangle|m_I = 1/2\rangle$ ,  $|m_S = -1/2\rangle|m_N = 0\rangle|m_I = -1/2\rangle$ ...etc ,  $|m_S = 1/2\rangle|m_N = 1\rangle|m_I = 1/2\rangle$ ):

$$U = \begin{pmatrix} 0 & 0 & 0 & 0 & 0 & 0 & 0 & 1 & 0 & 0 & 0 \\ \frac{\sqrt{3}b}{2} & 0 & 0 & 0 & -\frac{a\sqrt{3}}{2} & 0 & 0 & 0 & 0 & \frac{1}{2} & 0 \\ -\frac{a}{\sqrt{3}} - \frac{b}{\sqrt{6}} & 0 & 0 & 0 & -\frac{b}{\sqrt{3}} + \frac{a}{\sqrt{6}} & 0 & 0 & 0 & 0 & \frac{\sqrt{2}}{2} & 0 \\ 0 & -\frac{a}{\sqrt{6}} + \frac{b}{\sqrt{3}} & 0 & \frac{1}{\sqrt{6}} & 0 & -\frac{b}{\sqrt{6}} - \frac{a}{\sqrt{3}} & 0 & 0 & 0 & 0 & \frac{1}{\sqrt{3}} \\ 0 & -\frac{a}{\sqrt{3}} - \frac{b}{\sqrt{6}} & 0 & -\frac{1}{\sqrt{3}} & 0 & -\frac{b}{\sqrt{3}} + \frac{a}{\sqrt{6}} & 0 & 0 & 0 & 0 & \frac{1}{\sqrt{6}} \\ 0 & 0 & -\frac{a\sqrt{2}}{\sqrt{3}} + \frac{b}{\sqrt{12}} & 0 & 0 & 0 & -\frac{b\sqrt{2}}{\sqrt{3}} - \frac{a}{\sqrt{12}} & 0 & 0 & 0 & \frac{1}{2} \\ \frac{a\sqrt{2}}{\sqrt{3}} - \frac{b}{\sqrt{12}} & 0 & 0 & 0 & \frac{b\sqrt{2}}{\sqrt{3}} + \frac{a}{\sqrt{12}} & 0 & 0 & 0 & 0 & \frac{1}{2} & 0 \\ 0 & \frac{a}{\sqrt{3}} + \frac{b}{\sqrt{6}} & 0 & \frac{-1}{\sqrt{3}} & 0 & \frac{b}{\sqrt{3}} - \frac{a}{\sqrt{6}} & 0 & 0 & 0 & 0 & \frac{1}{\sqrt{6}} \\ 0 & \frac{a}{\sqrt{6}} - \frac{b}{\sqrt{3}} & 0 & \frac{1}{\sqrt{6}} & 0 & \frac{b}{\sqrt{6}} + \frac{a}{\sqrt{3}} & 0 & 0 & 0 & 0 & \frac{1}{\sqrt{3}} \\ 0 & 0 & \frac{a}{\sqrt{3}} + \frac{b}{\sqrt{6}} & 0 & 0 & 0 & \frac{b}{\sqrt{3}} - \frac{a}{\sqrt{6}} & 0 & 0 & 0 & 0 \\ 0 & 0 & -\frac{b\sqrt{3}}{2} & 0 & 0 & 0 & \frac{a\sqrt{3}}{2} & 0 & 0 & 0 & 0 \\ 0 & 0 & 0 & 0 & 0 & 0 & 0 & 0 & 0 & 0 & 0 \end{pmatrix} \quad (75)$$

The  $V_z^{m_S, m_I, m_N}$  matrix is, ignoring the  $g_N$  and  $g_I$  as too small to matter, simply:

$$V_z^{m_S, m_I, m_N} = \mu_B B g_S \begin{pmatrix} -\frac{1}{2} & 0 & 0 & 0 & 0 & 0 & 0 & 0 & 0 & 0 & 0 \\ 0 & -\frac{1}{2} & 0 & 0 & 0 & 0 & 0 & 0 & 0 & 0 & 0 \\ 0 & 0 & -\frac{1}{2} & 0 & 0 & 0 & 0 & 0 & 0 & 0 & 0 \\ 0 & 0 & 0 & -\frac{1}{2} & 0 & 0 & 0 & 0 & 0 & 0 & 0 \\ 0 & 0 & 0 & 0 & -\frac{1}{2} & 0 & 0 & 0 & 0 & 0 & 0 \\ 0 & 0 & 0 & 0 & 0 & -\frac{1}{2} & 0 & 0 & 0 & 0 & 0 \\ 0 & 0 & 0 & 0 & 0 & 0 & \frac{1}{2} & 0 & 0 & 0 & 0 \\ 0 & 0 & 0 & 0 & 0 & 0 & 0 & \frac{1}{2} & 0 & 0 & 0 \\ 0 & 0 & 0 & 0 & 0 & 0 & 0 & 0 & \frac{1}{2} & 0 & 0 \\ 0 & 0 & 0 & 0 & 0 & 0 & 0 & 0 & 0 & \frac{1}{2} & 0 \\ 0 & 0 & 0 & 0 & 0 & 0 & 0 & 0 & 0 & 0 & \frac{1}{2} \end{pmatrix} \quad (76)$$

$V_Z^{F, m_F}$  can then be calculated using  $U^\dagger V_z^{m_S, m_I, m_N} U$  (I won't show it here).  $V_{HF}$  for the SrF XΣ states is

$$V_{HF}^{F,m_F} = \Gamma \begin{pmatrix} -16.2 & 0 & 0 & 0 & 0 & 0 & 0 & 0 & 0 & 0 & 0 & 0 \\ 0 & -16.2 & 0 & 0 & 0 & 0 & 0 & 0 & 0 & 0 & 0 & 0 \\ 0 & 0 & -16.2 & 0 & 0 & 0 & 0 & 0 & 0 & 0 & 0 & 0 \\ 0 & 0 & 0 & -8.8 & 0 & 0 & 0 & 0 & 0 & 0 & 0 & 0 \\ 0 & 0 & 0 & 0 & 3.3 & 0 & 0 & 0 & 0 & 0 & 0 & 0 \\ 0 & 0 & 0 & 0 & 0 & 3.3 & 0 & 0 & 0 & 0 & 0 & 0 \\ 0 & 0 & 0 & 0 & 0 & 0 & 3.3 & 0 & 0 & 0 & 0 & 0 \\ 0 & 0 & 0 & 0 & 0 & 0 & 0 & 9.5 & 0 & 0 & 0 & 0 \\ 0 & 0 & 0 & 0 & 0 & 0 & 0 & 0 & 9.5 & 0 & 0 & 0 \\ 0 & 0 & 0 & 0 & 0 & 0 & 0 & 0 & 0 & 9.5 & 0 & 0 \\ 0 & 0 & 0 & 0 & 0 & 0 & 0 & 0 & 0 & 0 & 9.5 & 0 \\ 0 & 0 & 0 & 0 & 0 & 0 & 0 & 0 & 0 & 0 & 0 & 9.5 \end{pmatrix} \quad (77)$$

Solving for the eigenvalues of  $V_{HF}^{F,m_F} + V_z^{F,M_F}$  in mathematica yields Fig. 58, which is identical to what John Barry found (see Fig. 2.5 of his thesis)

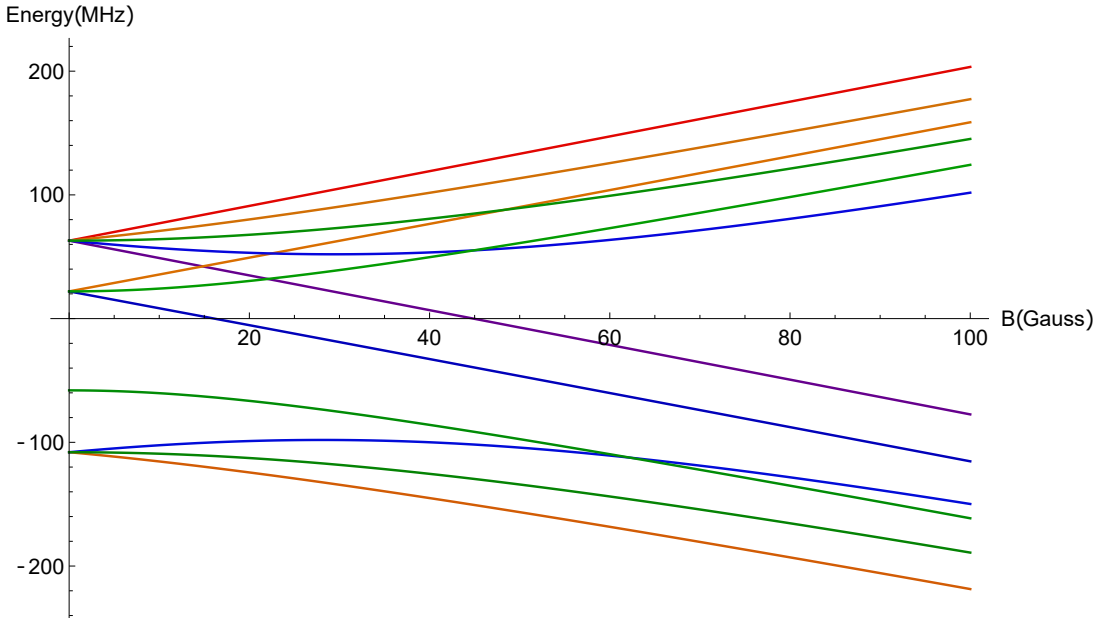


Figure 58: Energy levels of  $X\Sigma$  vs magnetic field. Colors correspond to zero-field  $m_F$  (red = 2, orange = 1, green = 0, blue = -1, purple = -2) Compare to Fig. 2.5 of John's thesis.

The AII state is easier to deal with, this is just a basic  $J = 1/2, I = 1/2$  system. The equivalent  $U, V_z^{m_J, m_I}$  are below (recall:, the ordering of the hyperfine levels here is  $|1, -1\rangle, |1, 0\rangle, |1, 1\rangle, |0, 0\rangle$ . The Zeeman levels are in order  $|m_J = -1/2, m_I = -1/2\rangle, | -1/2, 1/2\rangle, |1/2, -1/2\rangle, |1/2, 1/2\rangle$ ). The value of  $g_J = -.176$  (this is 2x the value of  $g_F = -0.088$  for the A state)

$$U = \begin{pmatrix} 1 & 0 & 0 & 0 \\ 0 & \frac{1}{\sqrt{2}} & 0 & -\frac{1}{\sqrt{2}} \\ 0 & \frac{1}{\sqrt{2}} & 0 & \frac{1}{\sqrt{2}} \\ 0 & 0 & 1 & 0 \end{pmatrix} \quad (78)$$

$$V_z^{m_J, m_I} = \mu_B B g_J \begin{pmatrix} -1/2 & 0 & 0 & 0 \\ 0 & -1/2 & 0 & 0 \\ 0 & 0 & 1/2 & 0 \\ 0 & 0 & 0 & 1/2 \end{pmatrix} \quad (79)$$

Similarly to what we did for K, we will add  $V_z^{F, m_F} + V_{HF}$  to  $-\vec{D} \cdot \vec{E}$  (NOTE: this is calculated in almost the same way as in chapter 1, with the only exception being that now the laser frequency is indexed to the energy difference between X $\Sigma$  and AII before hyperfine splitting, whereas before it was indexed to the energy between the  $|X\Sigma, F = 1, J = 1/2\rangle$  state and the AII manifold). The decay term is also the same, and so no further changes need to be made.

#### 4.4.1. SrF Zeeman spectrum

One image from the Type II Zeeman slowing paper has always confused me (Fig. 1B from their paper, reproduced below as Fig. 59). In it, they show that they couple states in the  $m_S = 1/2$  X manifold to either the upper or lower state A manifold, as opposed to all of them going to the lower manifold. I assume this is because they wanted to not couple states of the same  $m_F$  to the same excited state, figuring that it would reduce the likelihood of populating dark states.

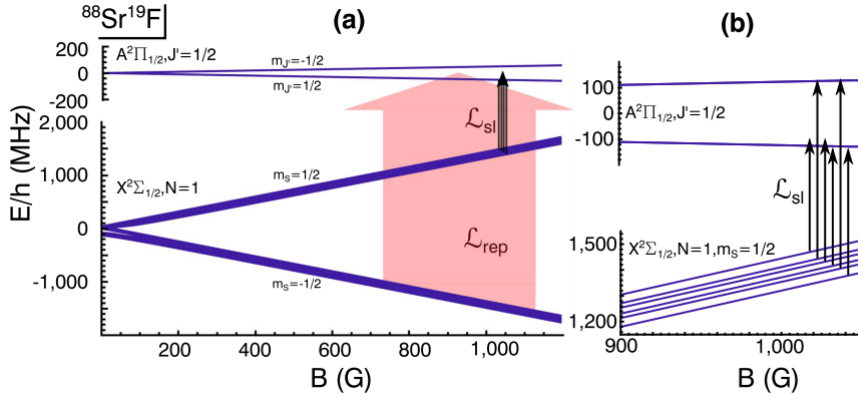


Figure 59: Fig. 1 from [type II zeeman slower paper](#). 1b is a bit confusing to me, since I've never been sure why one each of the  $m_I + m_J + m_N = 1$  and  $m_I + m_J + m_N = 0$  states (see Fig. 58) should have to connect to the upper AII manifold. My guess is that they wanted to not couple states of the same  $m_F$  to the same excited state, figuring that it would reduce the likelihood of populating dark states.

What I find though, if I diagonalize the  $V_z^{F,m_F} + V_{HF}$  matrix for a large  $B$  field and then use  $\langle \psi_{eigen,i} | C_p | \psi_{eigen,j} \rangle$  to look at the transition element for the polarization  $p$  that couples  $i$  to  $j$ , is that the  $m_s = 1/2$  states all preferentially connect to one of the lower AII levels (see Fig. 60). Moreover, the X states with the same  $m_F$  value couple to different AII states, so I don't think we should worry too much about the dark state issue.

Also, it looks like you will need components that 'talk to' all possible polarizations ( $\sigma^-$ ,  $\sigma^+$  and  $\pi$  are all needed in order for each X state to connect to the desired A state). Thus, the configuration with the laser direction *perpendicular* to the field will actually be preferable to the one where they are anti-parallel (see discussion in Sec. 4.3.2).

Unfortunately, though, the splittings within the ground state do not divide in a convenient way to address each one exactly using a EOM (the  $3.5\Gamma$  splitting between '1b' and '0a' is the problem here). Nevertheless, with enough power, being off by a few tenths of  $\Gamma$  when driving some of the transitions shouldn't be such a big deal...let's find out.

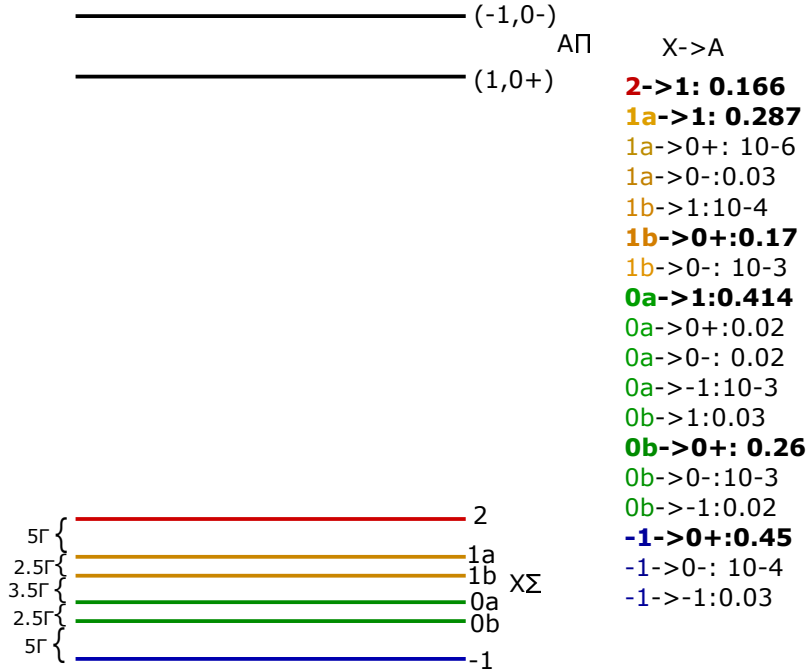


Figure 60: Upper state ( $m_S = 1/2$ ) X manifold coupling to the two A $\Pi$  manifolds (listed splitting values in X manifold result from hyperfine splitting, so as long as the B-Field is large enough these values will remain approximately the same at all B-Fields. The splitting between the A states is unlisted because that does depend on B Field). States are labeled by their effective  $m_F$  number (A has unresolved hyperfine structure). The transition elements calculated by taking  $\langle \psi_{eigen,i} | C_p | \psi_{eigen,j} \rangle$  are listed on the right. The non-trivial ones are bolded: going through the list, it is clear that each state in the X manifold primarily ‘connects’ to a A state in the lower manifold.

#### 4.4.2. SrF Results

**Realistic case (achievable with just Tapered-Amplifiers), no repump** (NOTE: For all results here I simulated out to  $1500\Gamma^{-1}$  and averaged  $N_e$  from  $750\Gamma^{-1}$  to  $1500\Gamma^{-1}$ . The results don't change if I instead average from  $1250\Gamma^{-1}$  to  $1500\Gamma^{-1}$  so I believe that this is a sufficient time frame for transient behavior to die out)

In the Ospelkaus paper, they simulate Type-II slowing assuming  $860 \text{ mW/cm}^2$  in their broad repump beam. This would obviously be nice to have, but would require  $> 1 \text{ W}$  of power to have over a 7.5 mm radius (roughly what our slowing beam width is right now). Instead, I decided to simulate it with a more realistic value of  $113 \text{ mW/cm}^2$  (what you get if you assume 200 mW, roughly a typical TA output after fiber coupling, over a 7.5 mm radius...I figured average power would be more relevant than peak power for this application). I also set the slowing power to the same value, but the opposite circular polarization (here I'm imagining you combine the two beams on a PBS and then circularize them with a 1/4 wave plate).

I chose to target **520 G** as the 'final' B-Field (where we want to be basically resonant with  $v = 0$ ). The Zeeman shift (excluding hyperfine splitting) between the 'slowing states' in the X and A manifold is  $-120\Gamma$ , and so I choose  $\Delta_s = -120\Gamma$ . Our peak velocity is roughly 150 m/s. I figured we may as well at least try to slow all of the molecules, so I needed to determine the change in B-Field required to cancel out a doppler shift from a 150 m/s molecule...this will be the B-Field at the 'start' of the slowing region. This winds up being **380 G**.

Thus, the B-Field in the 'middle' of the slowing region would be roughly **450 G** (it will likely be the case that a linearly increasing field is not optimal but it's a decent starting point). This is what I used to determine what the repump detuning should be (it should be on resonance in the middle of the slower for a molecule with 75 m/s velocity). After diagonalizing the zeeman hamiltonian, I found that this happens when  $\Delta_{re} = +86\Gamma$ . In order for the repump spectrum to incorporate molecules with  $v = 150 \text{ m/s}$  at  $B = 380 \text{ G}$  and with  $v = 0 \text{ m/s}$  at  $B = 520 \text{ G}$ , I found that we need to broaden the laser by roughly  $45\Gamma$  in each direction, which I did by driving it at  $\Omega_{Re} = \Gamma$  and  $\beta_{Re} = 45 \text{ rad}$ . This is a width of roughly 600 MHz. The Ospelkaus paper used 1.1 GHz but since I am trying to use a lot less power I decided I should remove that head-room (it turns out to work out okay per my results).

It wasn't obvious what I should pick for  $\beta_s$  or  $\Omega_s$ . So, I tried a bunch of different values and looked at the  $N_e(v)$  curves at the end, middle, and beginning of the slowing region. Fig. 61 is an example of the sort of data I was looking at. We see that, as we increase the sideband amplitude  $\beta$ , the peak in  $N_e$  increases up until roughly  $\beta = 6$ , after which the peak start shrinking and broadening (indicative of enhanced slowing light 'talking' to velocity classes other than the ones I intended to excite). Similar behavior was observed

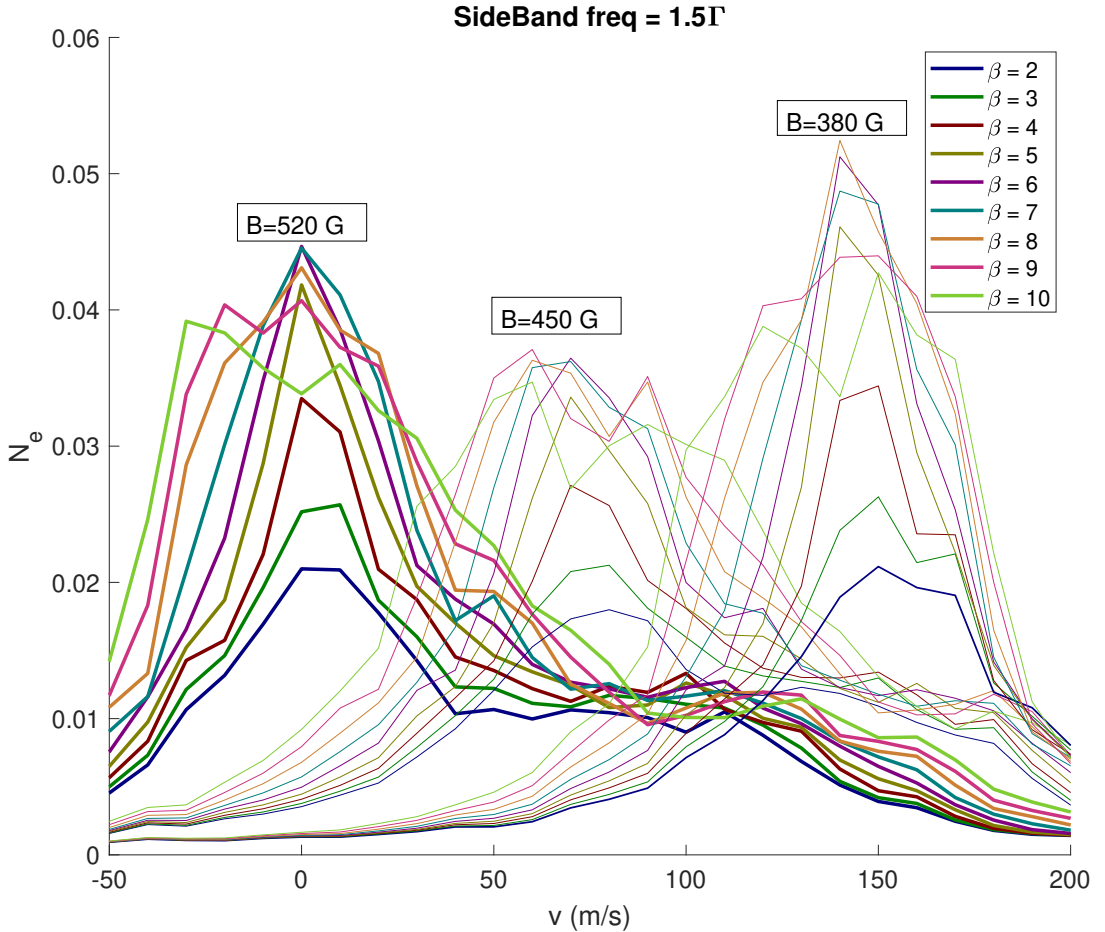


Figure 61: Plots of  $N_e(v)$  for each of the example magnetic fields for  $\Omega_s = 1.5\Gamma$ ,  $\Omega_{Re} = \Gamma$ ,  $\beta_{Re} = 45$  for various  $\beta_s$ . As  $\beta$  increases from 2 to 6, the peak of  $n_e(v)$  increases. Beyond 6, the peak diminishes and the width increases. This is because, for  $\beta > 6$ , the spectral width of the slowing laser becomes broader than the hyperfine induced spread in the  $m_s = 1/2$  portion of the X state manifold (roughly  $18\Gamma$ ).

for each sideband frequency  $\Omega$  that I attempted. In Fig. 62 I plot the  $N_e(v)$  curves for the optimum  $\beta$  for each  $\Omega$  that I attempted. Curiously, the curves look very similar, suggesting that the exact values of  $\Omega$  and  $\beta$  don't matter much. Instead, what seems to matter is how far the slowing spectrum is broadened.

I think that this is due to the small-ish splitting in the X manifold. Since the splittings are only a few  $\Gamma$  and ideally we are in the power broadened regime, such that the power broadened linewidth will also be a few  $\Gamma$ , the sideband ‘spectrum’ will blend together,

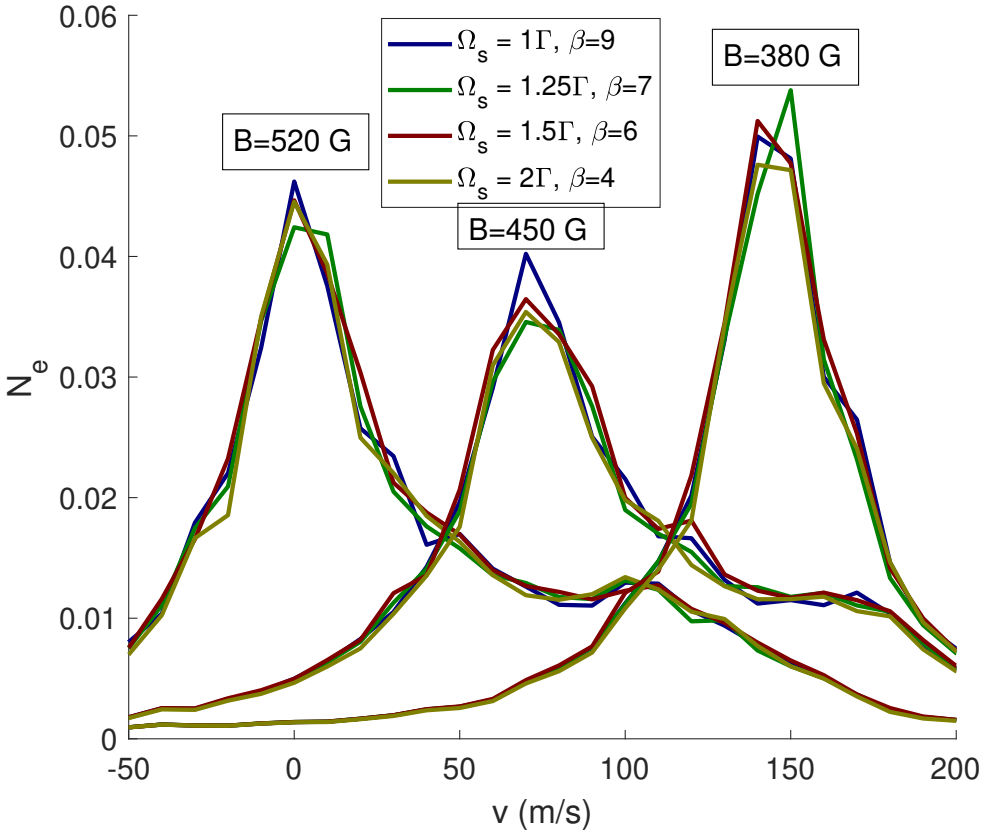


Figure 62:  $N_e(v)$  curves for the optimum  $\beta_s$  for a given  $\Omega_s$ . These curves all look very similar. This is because the excitation spectra for a power broadened systems with relatively low sideband frequencies do not have any resolved sideband structure (see Fig. 63), so all that matters is picking whatever  $\beta$  is needed to broaden the spectrum to cover the X manifold hyperfine structure.

making it less critical whether each sideband is on resonance with a given transition. As an example, I ran a OBE simulation for a 2 level system in the power broadening regime for  $\Omega = \{1, 2\}$  and a few different values of  $\beta$ . Sure enough, we don't really see much in the way of sideband peaks. Furthermore, it seems like for the parameters that optimize SrF slowing (either  $(\Omega = 2, \beta = 4)$  or  $(\Omega = 1, \beta = 9)$ ), the width of the spectrum is roughly  $18\Gamma$  or so, which is roughly what the splitting between the highest and lowest X states in the slowing manifold is (see Fig. 60).

Finally, I looked at how much we could stand to gain if we did have higher repump intensity. This is shown in Fig. 64. Clearly, more repump intensity would help a lot, but we'd need to either buy some kind of fiber laser or else shrink the slowing laser a bit. We may be able to afford to do the latter since there should be less pluming of the

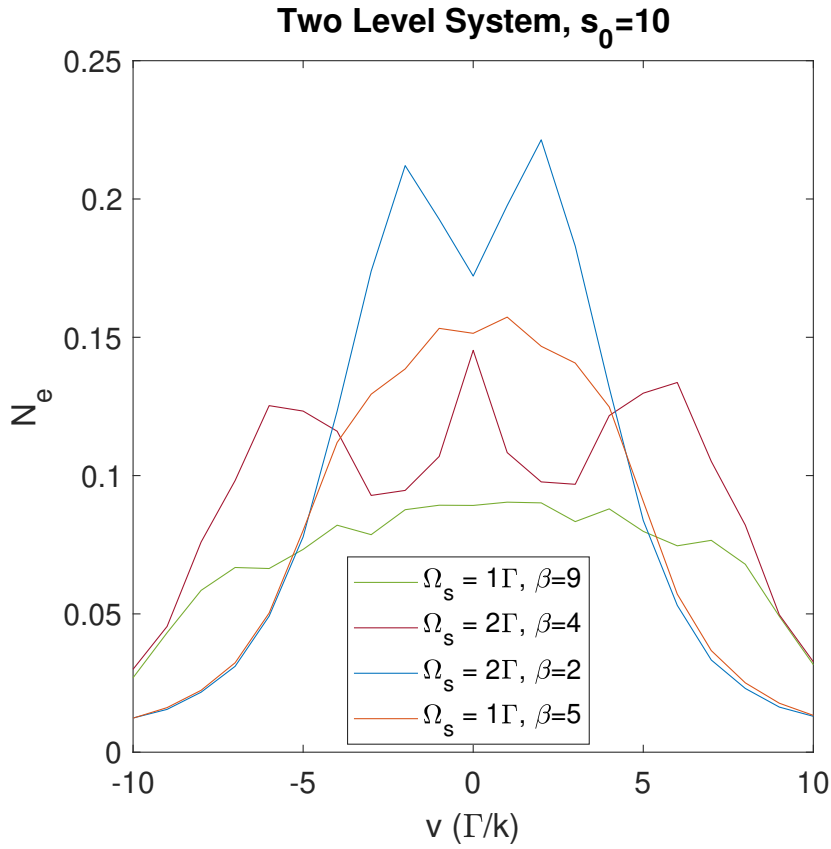


Figure 63: Excitation spectrum ( $B = 0, \Delta_s = 0$ ) for a two level system driven at various  $\Omega, \beta$ . We see that the width of the spectrum is similar for  $\{\Omega = 2, \beta = 4\}$  and  $\{\Omega = 1, \beta = 9\}$ , which are two of the configurations that led to the optimum slowing in Fig. 62.

SrF beam due to undesirable scattering events in a Zeeman slower. Also, some sort of 2D collimator could be used before the slowing region to further reduce pluming.

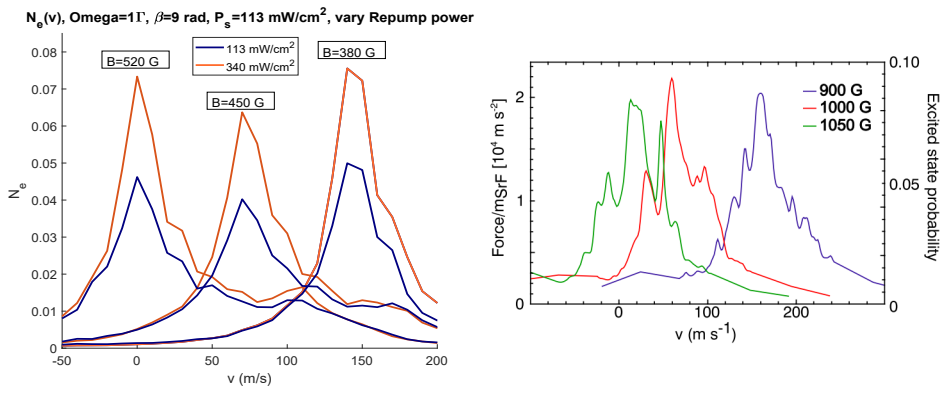


Figure 64: Effect of increased repump intensity (left). With an increase of 3x in repump intensity, we can get roughly a factor of 2 improvement in zeeman slowing force. This brings us to the same magnitude of force observed by the Ospelkaus group in their simulations (right).

**Adding repumping: Try repumping through B state** In the Ospelkaus paper, they suggest repumping from X,v=1 through the B,v=0 state. The B state has a lifetime very similar to the A state, so I'll just use the same value for  $\Gamma$  here. Unfortunately, the branching ratio for this transition is 1/260, making it fairly difficult to repump out of due to the low oscillator strength (linewidth is 25 kHz). It will require a lot of power to repump effectively over the range of Doppler+Zeeman shifts that need to be covered, especially with such a weak transition.

Luckily, though, the Zeeman shifts between the X and B state largely cancel out (the  $g_J$  in the B state should be basically 2.176 I think. I infer this because, for CaF, the  $g_j$  for the B state is 2.044 (see [this paper](#)), while for the A state it is -0.044, which implies to me that the B state g factor is modified by whatever the  $g_J$  factor is in the A state. This makes sense to me since the non-zero  $g_J$  factor arises from coupling between the A and B manifolds according to [this paper](#)). So, the relative Zeeman shift doesn't change too much over the magnetic fields achieved in the Zeeman slower (for the X→B transition, it works out that the positive magnetic moment states in each manifold primarily 'connect' to each other and vice-versa for the negative magnetic moment states).

The other difference is that, in the B state, the hyperfine structure is resolved (the  $F = 0$  state is  $2.3\Gamma$  below the  $F = 1$  manifold).

All told, we find that:

- $B = 380 \text{ G}$ ,  $v = 150 \text{ m/s}$  requires  $\Delta_{v=1\text{repump}} = -53\Gamma$  to hit the most red-detuned required transition
- $B = 520 \text{ G}$ ,  $v = 0 \text{ m/s}$  requires  $\Delta_{v=1\text{repump}} = +19\Gamma$  to hit the most blue-detuned required transition

The simplest approach to this task is to consider the repump 'sub-system' consisting of the 12 X,v=1 states and the 4 B,v=0 states as its own subsystem, and simulate it exactly the same was as I simulated the 'main' X→A Zeeman slowing system in the previous section. The only changes one makes to the code are:

- add a factor of  $\sqrt{1/260}$  to all the  $C_p$  matrices. This winds up having the correct effect on both the  $-\langle \vec{D} \cdot \vec{E} \rangle$  term and the 'decay term'.
- change the  $C_p$  matrices to reflect the fact that we are coupling from  $X$  to  $B$  not  $X$  to  $A$  (see the appendix for how I calculate  $C_p$  for this  $X\Sigma$  to  $B\Sigma$  transition).
- change the wavelength (used in calculating doppler shift) to 596 nm
- add an additional 'ground' state which is not coupled to the excited states by any lasers. The decay rate into this state is  $\Gamma$ . This state simulates the  $X, v = 0$  manifold, and how quickly it 'fills' due to repumping. Alternatively you could just extrapolate from the excited state population what the repump rate is.

- change the excited state  $g_J$  factor and add in the excited state hyperfine structure

A little bit of care needs to be taken when determining what  $s_0$  actually means in this simulation. When calculating  $\langle \vec{D} \cdot \vec{E} \rangle$ , all steps are basically the same ( $C_p$  calcs are different, see appendix) up to Eq.17, reproduced below:

$$\langle \vec{D} \cdot \vec{E} \rangle_{norm} = \frac{\mathcal{E}_0 d_\perp}{\hbar \Gamma} \sum_p \tilde{E}_p C_p \quad (80)$$

To keep everything consistent, I am still normalizing all energies, times, etc. by the  $\Gamma$  that corresponds to the  $v = 0 \rightarrow v = 0$  system (e.g. 6.63 MHz, not 25 kHz) and now  $d_\perp$  refers to the dipole element between X,v=1 and B,v=0. From atomic physics theory, we know that:

$$\Gamma_{X,v=1 \rightarrow B,v=0} = \frac{4}{3\hbar} \frac{1}{4\pi\epsilon_0} \frac{\omega^3}{c^3} d_\perp^2 \quad (81)$$

and so, ultimately, we get:

$$\left( \frac{\mathcal{E}_0 d_\perp}{\hbar \Gamma} \right)^2 = \frac{3\hbar}{4} 4\pi\epsilon_0 \frac{c^3}{\omega^3} \Gamma_{X,v=1 \rightarrow B,v=0} \frac{\mathcal{E}_0^2}{\hbar^2 \Gamma^2} \quad (82)$$

Expressing  $\mathcal{E}_0^2 = I/(2c\epsilon_0)$  and defining  $I_{sat} = \hbar c \Gamma \omega^3 / (4\pi \times 3c^3)$  (**NOTE the usage of the ‘normal’  $\Gamma$  here**), we then find

$$\left( \frac{\mathcal{E}_0 d_\perp}{\hbar \Gamma} \right) = \sqrt{\frac{I}{8I_{sat}}} \sqrt{\frac{\Gamma_{X,v=1 \rightarrow B,v=0}}{\Gamma}} \quad (83)$$

This last factor is just the factor of  $\sqrt{1/260}$  which I wrap into the  $C_p$  matrices. Thus, we have  $I_{sat} = 4 \text{ mW/cm}^2$  (it’s 2.9 mW/cm<sup>2</sup> for the X to A transition, the increase here results from changing to  $\lambda = 596 \text{ nm}$  from  $\lambda = 663 \text{ nm}$ ) for the way that I have written this simulation.

I ran this simulation at a few different  $s_0$  values. In Fig. 65, I plot the ratio of the repump rate (determined by how quickly the X, $v = 0$  state fills up in the simulation) to the rate at which X $v = 1$  fills up ( $R_{fill} = R_{sc}/50$ , where I use  $R_{sc} = 0.05\Gamma$  (see Fig. 64).

**Important points:** The scattering force seen in Fig. 64 will be reduced by a factor of  $R_{fill}/(R_{fill} + R_{Repump})$ . So, we would like  $R_{Repump}$  to be at least a couple of times bigger than  $R_{fill}$ . This will require a few Watts of power (at least for the beam sizes considered here). This kind of puts this in the ‘realistic but expensive’ category I think, as opposed to the ‘easy and very practical’ ( $\leq 100 \text{ mW}$ ) or obviously ludicrous ( $\geq 10 \text{ W}$ ).

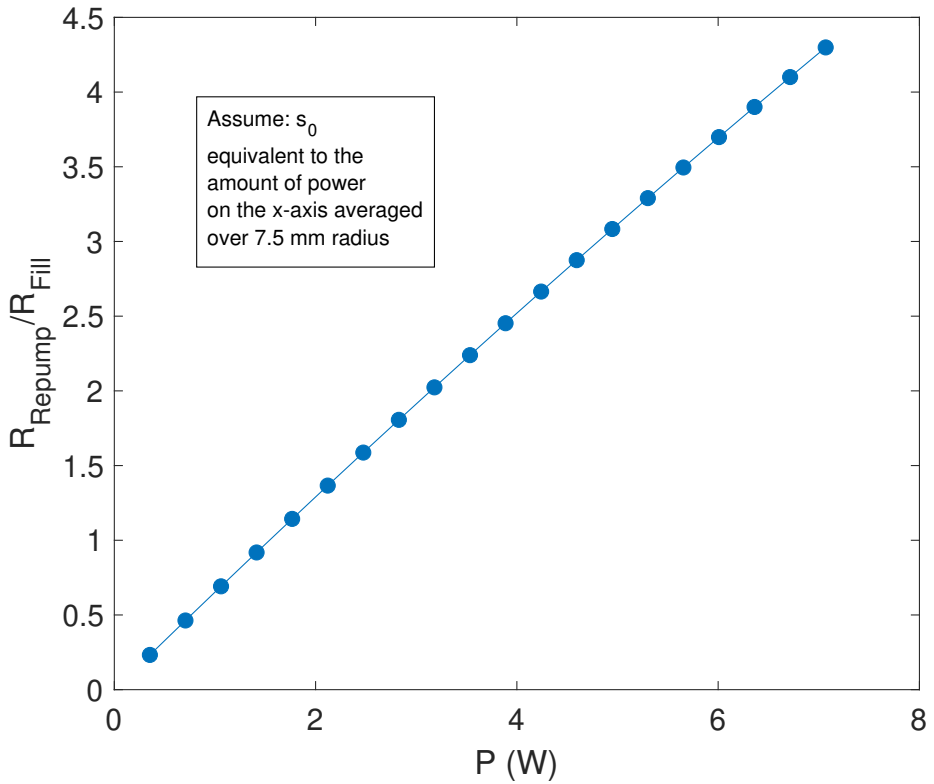


Figure 65: Ratio of repump rate vs ‘filling rate’ (assumes  $R_{sc} = 0.05$  and a 1/50 branching ratio into  $v = 1$  due to scattering from the  $A, v = 0$  state). This simulation was done for  $B = 380$  G and  $v = 150$  m/s but I get similar results for other combos like  $B = 450$  G  $v = 75$  m/s and  $B = 520$  G  $v = 0$  m/s.

## 5. Revised $\mathbf{X} \rightarrow \mathbf{A}$ $C_p$ matrices

After working through the SrF zeeman slower, I discovered an error in the coupling matrix calculation, and thus in the branching ratios from  $\Lambda\Pi$  to  $\Lambda\Sigma$ . The corrected matrices are listed below.

$$C_{-1} = \begin{pmatrix} 0 & 0 & 0 & 0 & 0 & 0 & 0 & 0 & 0 & 0 & 0 & 0 & -.495 & 0 & 0 \\ 0 & 0 & 0 & 0 & 0 & 0 & 0 & 0 & 0 & 0 & 0 & 0 & 0 & -.495 & 0 \\ 0 & 0 & 0 & 0 & 0 & 0 & 0 & 0 & 0 & 0 & 0 & 0 & 0 & 0 & 0 \\ 0 & 0 & 0 & 0 & 0 & 0 & 0 & 0 & 0 & 0 & 0 & 0 & 0 & \frac{\sqrt{2}}{3} & 0 \\ 0 & 0 & 0 & 0 & 0 & 0 & 0 & 0 & 0 & 0 & 0 & 0 & -.069 & 0 & -.513 \\ 0 & 0 & 0 & 0 & 0 & 0 & 0 & 0 & 0 & 0 & 0 & 0 & 0 & -.069 & 0 \\ 0 & 0 & 0 & 0 & 0 & 0 & 0 & 0 & 0 & 0 & 0 & 0 & 0 & 0 & 0 \\ 0 & 0 & 0 & 0 & 0 & 0 & 0 & 0 & 0 & 0 & 0 & 0 & 0 & 0 & 0 \\ 0 & 0 & 0 & 0 & 0 & 0 & 0 & 0 & 0 & 0 & 0 & 0 & -\frac{1}{\sqrt{6}} & 0 & 0 \\ 0 & 0 & 0 & 0 & 0 & 0 & 0 & 0 & 0 & 0 & 0 & 0 & 0 & -\frac{1}{2\sqrt{3}} & 0 \\ 0 & 0 & 0 & 0 & 0 & 0 & 0 & 0 & 0 & 0 & 0 & 0 & 0 & 0 & 0 \\ 0 & 0 & 0 & 0 & 0 & 0 & 0 & 0 & 0 & 0 & 0 & 0 & 0 & -\frac{1}{6} & 0 \\ 0 & 0 & 0 & 0 & 0 & 0 & 0 & 0 & 0 & 0 & 0 & 0 & 0 & 0 & 0 \\ 0 & 0 & 0 & 0 & 0 & 0 & 0 & 0 & 0 & 0 & 0 & 0 & 0 & 0 & 0 \\ 0 & 0 & 0 & 0 & 0 & 0 & 0 & 0 & 0 & 0 & 0 & 0 & 0 & 0 & 0 \\ -.495 & 0 & 0 & 0 & -.069 & 0 & 0 & 0 & -\frac{1}{2\sqrt{3}} & 0 & 0 & 0 & 0 & 0 & 0 \\ 0 & -.495 & 0 & \frac{\sqrt{2}}{3} & 0 & -.069 & 0 & 0 & 0 & -\frac{1}{6} & 0 & 0 & 0 & 0 & 0 \\ -.265 & 0 & 0 & 0 & -.513 & 0 & 0 & 0 & 0 & 0 & 0 & 0 & 0 & 0 & 0 \end{pmatrix} \quad (84)$$

$$C_0 = \begin{pmatrix} 0 & 0 & 0 & 0 & 0 & 0 & 0 & 0 & 0 & 0 & 0 & .495 & 0 & 0 \\ 0 & 0 & 0 & 0 & 0 & 0 & 0 & 0 & 0 & 0 & 0 & 0 & 0 & 0 & 0 \\ 0 & 0 & 0 & 0 & 0 & 0 & 0 & 0 & 0 & 0 & 0 & 0 & 0 & 0 & -.495 \\ 0 & 0 & 0 & 0 & 0 & 0 & 0 & 0 & 0 & 0 & 0 & 0 & 0 & -\frac{\sqrt{2}}{3} & 0 \\ 0 & 0 & 0 & 0 & 0 & 0 & 0 & 0 & 0 & 0 & 0 & 0 & .069 & 0 & 0 \\ 0 & 0 & 0 & 0 & 0 & 0 & 0 & 0 & 0 & 0 & 0 & 0 & 0 & 0 & 0 \\ 0 & 0 & 0 & 0 & 0 & 0 & 0 & 0 & 0 & 0 & 0 & 0 & 0 & 0 & -.069 \\ 0 & 0 & 0 & 0 & 0 & 0 & 0 & 0 & 0 & 0 & 0 & 0 & 0 & 0 & 0 \\ 0 & 0 & 0 & 0 & 0 & 0 & 0 & 0 & 0 & 0 & 0 & 0 & 0 & -\frac{1}{2\sqrt{3}} & 0 \\ 0 & 0 & 0 & 0 & 0 & 0 & 0 & 0 & 0 & 0 & 0 & 0 & 0 & 0 & -\frac{1}{3} \\ 0 & 0 & 0 & 0 & 0 & 0 & 0 & 0 & 0 & 0 & 0 & 0 & 0 & 0 & -\frac{1}{2\sqrt{3}} \\ 0 & 0 & 0 & 0 & 0 & 0 & 0 & 0 & 0 & 0 & 0 & 0 & 0 & 0 & 0 \\ .495 & 0 & 0 & 0 & .069 & 0 & 0 & 0 & -\frac{1}{2\sqrt{3}} & 0 & 0 & 0 & 0 & 0 & 0 \\ 0 & 0 & 0 & -\frac{\sqrt{2}}{3} & 0 & 0 & 0 & 0 & 0 & -\frac{1}{3} & 0 & 0 & 0 & 0 & 0 \\ 0 & 0 & -.495 & 0 & 0 & 0 & -.069 & 0 & 0 & -\frac{1}{2\sqrt{3}} & 0 & 0 & 0 & 0 & 0 \\ 0 & -.265 & 0 & 0 & 0 & -.513 & 0 & 0 & 0 & 0 & 0 & 0 & 0 & 0 & 0 \end{pmatrix} \quad (85)$$

$$C_1 = \begin{pmatrix} 0 & 0 & 0 & 0 & 0 & 0 & 0 & 0 & 0 & 0 & 0 & 0 & 0 & 0 & 0 \\ 0 & 0 & 0 & 0 & 0 & 0 & 0 & 0 & 0 & 0 & 0 & .495 & 0 & 0 & 0 \\ 0 & 0 & 0 & 0 & 0 & 0 & 0 & 0 & 0 & 0 & 0 & 0 & .495 & 0 & -.265 \\ 0 & 0 & 0 & 0 & 0 & 0 & 0 & 0 & 0 & 0 & 0 & \frac{\sqrt{2}}{3} & 0 & 0 & 0 \\ 0 & 0 & 0 & 0 & 0 & 0 & 0 & 0 & 0 & 0 & 0 & 0 & 0 & 0 & 0 \\ 0 & 0 & 0 & 0 & 0 & 0 & 0 & 0 & 0 & 0 & 0 & 0 & 0 & 0 & 0 \\ 0 & 0 & 0 & 0 & 0 & 0 & 0 & 0 & 0 & 0 & 0 & 0 & .069 & 0 & 0 \\ 0 & 0 & 0 & 0 & 0 & 0 & 0 & 0 & 0 & 0 & 0 & 0 & 0 & .069 & 0 \\ 0 & 0 & 0 & 0 & 0 & 0 & 0 & 0 & 0 & 0 & 0 & 0 & 0 & 0 & -.512 \\ 0 & 0 & 0 & 0 & 0 & 0 & 0 & 0 & 0 & 0 & 0 & 0 & 0 & 0 & 0 \\ 0 & 0 & 0 & 0 & 0 & 0 & 0 & 0 & 0 & 0 & 0 & 0 & 0 & 0 & 0 \\ 0 & 0 & 0 & 0 & 0 & 0 & 0 & 0 & 0 & 0 & 0 & -\frac{1}{6} & 0 & 0 & 0 \\ 0 & 0 & 0 & 0 & 0 & 0 & 0 & 0 & 0 & 0 & 0 & 0 & -\frac{1}{2\sqrt{3}} & 0 & 0 \\ 0 & 0 & 0 & 0 & 0 & 0 & 0 & 0 & 0 & 0 & 0 & 0 & 0 & 0 & -\frac{1}{\sqrt{6}} \\ 0 & .495 & 0 & \frac{\sqrt{2}}{3} & 0 & .069 & 0 & 0 & 0 & -\frac{1}{6} & 0 & 0 & 0 & 0 & 0 \\ 0 & 0 & .495 & 0 & 0 & 0 & .069 & 0 & 0 & 0 & -\frac{1}{2\sqrt{3}} & 0 & 0 & 0 & 0 \\ 0 & 0 & 0 & 0 & 0 & 0 & 0 & 0 & 0 & 0 & 0 & -\frac{1}{\sqrt{6}} & 0 & 0 & 0 \\ 0 & 0 & -.265 & 0 & 0 & 0 & -.513 & 0 & 0 & 0 & 0 & 0 & 0 & 0 & 0 \end{pmatrix} \quad (86)$$

### 5.1. Impact on Zeeman Slower simulations

In the previous section, I made the claim that all  $|X\Sigma, m_S = +1/2\rangle$  states can be coupled to  $|A\Pi, m_J = +1/2\rangle$  states as long as you irradiate the molecules with light containing all polarization components. This contradicted claims made by the other groups that have proposed Type II Zeeman slowers. It turns out that they were correct: two of the  $|X\Sigma\rangle$  states, specifically the  $|m_S = 1/2\rangle|m_N = 0\rangle|m_I = \pm 1/2\rangle$  states only couple effectively to the corresponding  $|m_J = -1/2\rangle$  state. The corrected transition probabilities are shown in Fig. 66

This may make the slowing slightly less effective, as now there will be a (slight) difference in the changes in frequency required to couple some  $|X\Sigma\rangle$  states to the appropriate  $|A\Pi\rangle$  state (e.g. increasing  $B$  will separate 1bX and 0+A by more than 1aX and 0-A).

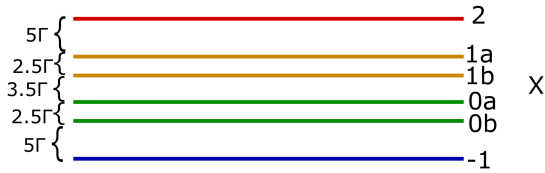
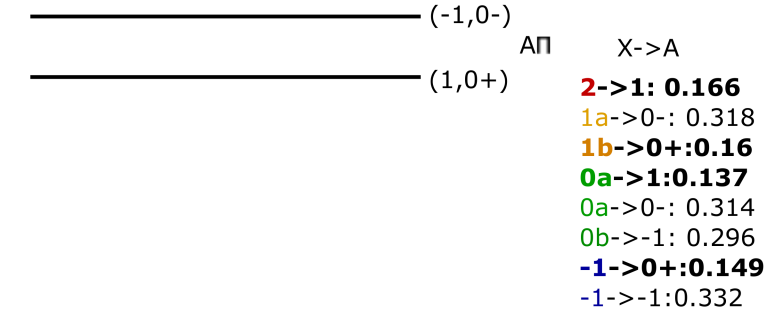


Figure 66: Upper state ( $m_S = 1/2$ )  $X$  manifold coupling to the two  $\text{A}\Pi$  manifolds (listed splitting values in  $X$  manifold result from hyperfine splitting, so as long as the B-Field is large enough these values will remain approximately the same at all B-Fields. The splitting between the  $A$  states is unlisted because that does depend on B Field). States are labeled by their effective  $m_F$  number ( $A$  has unresolved hyperfine structure). The transition elements calculated by taking  $\langle \psi_{eigen,i} | C_p | \psi_{eigen,j} \rangle$  are listed on the right. The ones coupling from  $|m_S = 1/2\rangle$  to  $|m_J = 1/2\rangle$  (the lower of the  $A$  states given the negative  $g_J$  factor) are bolded : going through the list, it is clear that, to couple all  $X$  states to the  $\text{A}\Pi$  manifold, one needs to couple some to  $|m_J = +1/2\rangle$  only (2,1b) while others can only couple to  $|m_J = -1/2\rangle$  (1a,0b). The latter are the exact ones indicated in the Ospelkaus paper (see Fig. 59)

## A. Generalized $C_p$ matrices

In Eq. 12-14, I wrote the  $C_p$  matrices for the atom-light coupling Hamiltonian ( $p$  is polarization), where the quantum states corresponding to each entry are described in the paragraph above Eq. 12. The entries in that matrix are only valid for SrF, since I had already taken into account J-mixing (hence the numerical entries in the rows & columns with entries corresponding to the two  $|X\Sigma, F = 1\rangle$  states). It would be nice to generalize my code to any molecule with a similar level structure (CaF, BaF, BaH, etc.). Further, it would also be nice to generalize it to also include  $|X\Sigma\rangle$  to  $|B\Sigma\rangle$  transitions, as the  $|B\Sigma\rangle$  state has a non-trivial magnetic  $g$  factor, which may lead to enhanced trapping in some instances, particularly for dcMOTs. For the generalized case, I assume that the  $|X, F = 1\rangle$  states are written as:

- $|F = 1, \hat{J} = 3/2\rangle = s(a|F = 1, J = 3/2\rangle + b|F = 1, J = 1/2\rangle)$
- $|F = 1, \hat{J} = 1/2\rangle = -b|F = 1, J = 3/2\rangle + a|F = 1, J = 1/2\rangle$

For SrF,  $s = 1$   $a = .888$  and  $b = .4598$  (per John Barry's thesis, chapter 2). For CaF,  $a = .772496$  and  $b = .63502$

In the equations below, I only write down the terms corresponding to coupling the ground state  $X$  to the excited state  $A$  or  $B$ . These are the last 4 columns of the  $C_p$  matrices. Just remember that for the full  $C_p$  matrix you need to have identical terms on the last 4 rows of the matrix (e.g.  $C_p = C_p^T$ )

$$C_{-1, X \rightarrow A} = \begin{pmatrix} 0 & -\frac{\sqrt{2}}{3}a - \frac{b}{6} & 0 & -\frac{\sqrt{2}}{3}a + \frac{b}{3} \\ 0 & 0 & -\frac{\sqrt{2}}{3}a - \frac{b}{6} & 0 \\ 0 & 0 & 0 & 0 \\ 0 & 0 & \frac{\sqrt{2}}{3} & 0 \\ 0 & \left(\frac{a}{6} - \frac{\sqrt{2}}{3}b\right) & 0 & \left(-\frac{a}{3} - \frac{\sqrt{2}}{3}b\right) \\ 0 & 0 & \left(\frac{a}{6} - \frac{\sqrt{2}}{3}b\right) & 0 \\ 0 & 0 & 0 & 0 \\ -\frac{1}{\sqrt{6}} & 0 & 0 & 0 \\ 0 & -\frac{1}{2\sqrt{3}} & 0 & 0 \\ 0 & 0 & -\frac{1}{6} & 0 \\ 0 & 0 & 0 & 0 \\ 0 & 0 & 0 & 0 \\ 0 & 0 & 0 & 0 \\ 0 & 0 & 0 & 0 \\ 0 & 0 & 0 & 0 \end{pmatrix} \quad (87)$$

$$C_{0,X \rightarrow A} = \begin{pmatrix} \frac{\sqrt{2}}{3}a + \frac{b}{6} & 0 & 0 & 0 \\ 0 & 0 & 0 & -\frac{\sqrt{2}}{3}a + \frac{b}{3} \\ 0 & 0 & -\frac{\sqrt{2}}{3}a - \frac{b}{6} & 0 \\ 0 & -\frac{\sqrt{2}}{3} & 0 & 0 \\ (-\frac{a}{6} + \frac{\sqrt{2}}{3}b) & 0 & 0 & 0 \\ 0 & 0 & 0 & (-\frac{a}{3} - \frac{\sqrt{2}}{3}b) \\ 0 & 0 & (\frac{a}{6} - \frac{\sqrt{2}}{3}b) & 0 \\ 0 & 0 & 0 & 0 \\ -\frac{1}{2\sqrt{3}} & 0 & 0 & 0 \\ 0 & -\frac{1}{3} & 0 & 0 \\ 0 & 0 & -\frac{1}{2\sqrt{3}} & 0 \\ 0 & 0 & 0 & 0 \\ 0 & 0 & 0 & 0 \\ 0 & 0 & 0 & 0 \\ 0 & 0 & 0 & 0 \\ 0 & 0 & 0 & 0 \end{pmatrix} \quad (88)$$

$$C_{1,X \rightarrow A} = \begin{pmatrix} 0 & 0 & 0 & 0 \\ \frac{\sqrt{2}}{3}a + \frac{b}{6} & 0 & 0 & 0 \\ 0 & \frac{\sqrt{2}}{3}a + \frac{b}{6} & 0 & -\frac{\sqrt{2}}{3}a + \frac{b}{3} \\ \frac{\sqrt{2}}{3} & 0 & 0 & 0 \\ 0 & 0 & 0 & 0 \\ (-\frac{a}{6} + \frac{\sqrt{2}}{3}b) & 0 & 0 & 0 \\ 0 & (-\frac{a}{6} + \frac{\sqrt{2}}{3}b) & 0 & (-\frac{a}{3} - \frac{\sqrt{2}}{3}b) \\ 0 & 0 & 0 & 0 \\ 0 & 0 & 0 & 0 \\ -\frac{1}{6} & 0 & 0 & 0 \\ 0 & -\frac{1}{2\sqrt{3}} & 0 & 0 \\ 0 & 0 & -\frac{1}{\sqrt{6}} & 0 \\ 0 & 0 & 0 & 0 \\ 0 & 0 & 0 & 0 \\ 0 & 0 & 0 & 0 \end{pmatrix} \quad (89)$$

Next, to derive the transition matrix for  $X \rightarrow B$  transitions, we must get the rotational matrix element for coupling between two case  $b$  states  $|N, J, F, m_F\rangle$  ( $\Lambda = 0$ ). I won't work through the math here: just trust me that you wind up obtaining:

$$\langle D_{-pq}^1(\omega)^* \rangle = (-1)^{F-M_F+F'+J+3/2+J'+N+3/2+N} \sqrt{(2F+1)(2F'+1)(2J+1)(2J'+1)(2N+1)(2N'+1)} \\ \left( \begin{matrix} F & 1 & F' \\ -M_F & -p & M'_F \end{matrix} \right) \left\{ \begin{matrix} J' & F' & 1/2 \\ F & J & 1 \end{matrix} \right\} \left\{ \begin{matrix} N' & J' & 1/2 \\ J & N & 1 \end{matrix} \right\} \left( \begin{matrix} N & 1 & N' \\ -\Lambda & q & \Lambda' \end{matrix} \right) \quad (90)$$

For the states we are concerned with,  $\Lambda = \Lambda' = 0$  (and thus only  $q = 0$  is relevant),  $N' = 1$ ,  $N = 0$  (remember, per the notation in Sec. 1, the prime refers to the ground state), and  $J = 1/2$ . Calculating these elements between given  $\langle F, m_F | \dots | \hat{J}', F', m'_F \rangle$ , I find:

$$C_{-1,X \rightarrow B} = \left( \begin{array}{cccc} 0 & -\frac{a}{3} + \frac{b}{3\sqrt{2}} & 0 & -\frac{a}{3} - \frac{\sqrt{2}b}{3} \\ 0 & 0 & -\frac{a}{3} + \frac{b}{3\sqrt{2}} & 0 \\ 0 & 0 & 0 & 0 \\ 0 & 0 & \frac{1}{3} & 0 \\ 0 & \left(-\frac{a}{3\sqrt{2}} - \frac{b}{3}\right) & 0 & \left(\frac{\sqrt{2}a}{3} - \frac{b}{3}\right) \\ 0 & 0 & \left(-\frac{a}{3\sqrt{2}} - \frac{b}{3}\right) & 0 \\ 0 & 0 & 0 & 0 \\ \frac{1}{\sqrt{3}} & 0 & 0 & 0 \\ 0 & \frac{1}{\sqrt{6}} & 0 & 0 \\ 0 & 0 & \frac{1}{3\sqrt{2}} & 0 \\ 0 & 0 & 0 & 0 \\ 0 & 0 & 0 & 0 \\ 0 & 0 & 0 & 0 \\ 0 & 0 & 0 & 0 \\ 0 & 0 & 0 & 0 \end{array} \right) \quad (91)$$

$$C_{0,X \rightarrow B} = \begin{pmatrix} \frac{a}{3} - \frac{b}{3\sqrt{2}} & 0 & 0 & 0 \\ 0 & 0 & 0 & -\frac{a}{3} - \frac{\sqrt{2}b}{3} \\ 0 & 0 & -\frac{a}{3} + \frac{b}{3\sqrt{2}} & 0 \\ 0 & -\frac{1}{3} & 0 & 0 \\ (\frac{a}{3\sqrt{2}} + \frac{b}{3}) & 0 & 0 & 0 \\ 0 & 0 & 0 & (\frac{\sqrt{2}a}{3} - \frac{b}{3}) \\ 0 & 0 & (-\frac{a}{3\sqrt{2}} - \frac{b}{3}) & 0 \\ 0 & 0 & 0 & 0 \\ \frac{1}{\sqrt{6}} & 0 & 0 & 0 \\ 0 & \frac{\sqrt{2}}{3} & 0 & 0 \\ 0 & 0 & \frac{1}{\sqrt{6}} & 0 \\ 0 & 0 & 0 & 0 \\ 0 & 0 & 0 & 0 \\ 0 & 0 & 0 & 0 \\ 0 & 0 & 0 & 0 \\ 0 & 0 & 0 & 0 \end{pmatrix} \quad (92)$$

$$C_{1,X \rightarrow B} = \begin{pmatrix} 0 & 0 & 0 & 0 \\ \frac{a}{3} - \frac{b}{3\sqrt{2}} & 0 & 0 & 0 \\ 0 & \frac{a}{3} - \frac{b}{3\sqrt{2}} & 0 & -\frac{a}{3} - \frac{\sqrt{2}b}{3} \\ \frac{1}{3} & 0 & 0 & 0 \\ 0 & 0 & 0 & 0 \\ (\frac{a}{3\sqrt{2}} + \frac{b}{3}) & 0 & 0 & 0 \\ 0 & (\frac{a}{3\sqrt{2}} + \frac{b}{3}) & 0 & (\frac{\sqrt{2}a}{3} - \frac{b}{3}) \\ 0 & 0 & 0 & 0 \\ 0 & 0 & 0 & 0 \\ \frac{1}{3\sqrt{2}} & 0 & 0 & 0 \\ 0 & \frac{1}{\sqrt{6}} & 0 & 0 \\ 0 & 0 & \frac{1}{\sqrt{3}} & 0 \\ 0 & 0 & 0 & 0 \\ 0 & 0 & 0 & 0 \\ 0 & 0 & 0 & 0 \end{pmatrix} \quad (93)$$